



Università degli Studi di Messina

Dipartimento di Scienze Matematiche, Informatiche, Fisiche e
Scienze della Terra (MIFT)

Dottorato di Ricerca in Fisica

XXXI Ciclo

Drawing up, development and optimization of a Limited Area Model for meteorological forecasting in regions with complex orography

PhD Student

Dr. Giuseppe CASTORINA

Supervisor:

Chiar.^{mo} Prof. Salvatore Magazù

Academic Year 2017-2018



Amia Mamma...

Introduction

The global climate changes and their impact on global scale represent one of most important issues nowadays. In the recently years, the understanding of the climate changes, through the studies of ice ages and interglacial ages have intrigued many scientists and researchers. Studying the last million year, they found that with a periodicity ranging between 40 and 100 thousand of years, there was a average temperature fluctuation of 10 K. Assuming the average temperature of the earth as a fundamental variable and disregarding the contribution of the atmosphere, through the global energy balance theory, one has:

$$C \frac{dT}{dt} = P_{in} - \alpha P_{in} - P_{out}$$

where C is the heat capacity of the Earth, and P_{in} is the incoming radiation given by $P_{in} = \pi R^2 S$.

P_{in} it is independent on Earth's temperature but affected by the time as function of astronomical modulations. In the last relation, $S \approx 1370 \text{ Wm}^{-2}$, is the solar constant and πR^2 represents the surface perpendicular to the solar rays. P_{out} is the emitted radiation by the surface of the Earth estimated through the Stefan-Boltzmann law for the black body at T temperature: $P_{out} = 4\pi R^2 \sigma T^4$ ($\sigma \approx 5.67 \times 10^{-8} \text{ Wm}^{-2} \text{ K}^{-4}$ Stefan-Boltzmann constant). Finally, α is the average albedo of the Earth (typically of the order to 0.3).

The climatic fluctuations are related with the astronomical variations of the terrestrial orbit (cycles of Milankovitch), but at global level, the variations of insolation alone can not explain the variation of 10 K observed in climate data. Therefore, an amplification mechanism to move from small solar modulation to the great climate change, it is necessary. According to G. Parisi [1], this mechanism is governed by positive feedback induced in the albedo. A further amplification is due to stochastic resonance induced by the weather fluctuations. When treating with physical phenomena that involve variables with different time scales, it is possible to consider the faster ones as perturbations acting on the slower.

The study of the climate: climatic fluctuations

From the examination of several different elements, direct and indirect, it has been possible to form an indicative picture of what has been the climate of the earth in the last decades, in the centuries, in the millennia and in the geological epochs. During the last two million years there have been alternations between periods of glacial climate and less cold (interglacial) intervals with periods of ice ages of about one hundred thousand years. On the basis of these elements, it appears that the

climate is subject to variations that have different time scales, also highlighting that the evolutionary trend of the long-term climate is completely masked by relatively short period fluctuations and therefore imperceptible.

What are the physical causes of climatic fluctuations?

A first hypothesis is that they can occur within the same climate system without the intervention of external factors. In fact, there are many mechanisms that can give rise to an internal variability of the system. This derives from the non-linear interactions (called "feedback") that occur between the various parts of the complex, which have very different reaction times.

A typical mechanism of this kind, which binds together the snowpack, the reflection of the radiant energy of the sun and the temperature of the air, could be the following: suppose that a small decrease in temperature occurs, such as to favor the extension of the snow cover on the Earth, the increased reflection of solar radiation by the snowpack would further reduce the temperature, thus hindering the sun's warming of the earth's surface.

Other climate influences may result from changes in the amount of particulate matter in the upper atmosphere due to volcanic activity, or an increase in the carbon dioxide content in the air as a result of fossil fuel fires.

An example of the possible effects that volcanic eruptions could have on climate fluctuations occurred in 1816, the year following the eruption of the Tambora volcano, on the Sumbawa island of present-day Indonesia (then the Dutch Indies), which took place from 5 to 15 April 1815.

The summer of the 1816 is remembered as the coldest recorded in the previous 200 years, in various parts of Europe, in the American states of the northeast and in eastern Canada. The cause of this anomaly seems to lie precisely in the enormous quantity of powders poured into the high atmosphere of the volcanic eruption, greatly increasing the reflectivity of the atmosphere towards the incident solar radiation. In this regard, it should be recalled that recently two researchers from NCAR in Boulder in Colorado observed that changes in the amount of particulate matter in the upper atmosphere are a better indicator than the number of sunspots to determine temperature fluctuations.

Another question that fascinates the man is as follows:

Can human activities on Earth be the cause of current or future climate changes?

That the climate is affected by urban areas is, for example, a proven reality: "the heat island" at the cities is a well documented fact that affects areas of the order of one thousand square kilometers. These influences, however, are of a purely local character and are presumed to have no relevance to the general climate of the earth. The problem is another: the increase in the use of fossil fuels, from the end of the last century to the present, has led to an increase in atmospheric carbon dioxide (CO₂) by 10% and is such that if by one or two centuries all available fuel reserves were consumed, the

concentration of CO₂ in the atmosphere would increase considerably. It is presumed that this could give rise to a significant increase in the temperature of the earth with appreciable consequences on the other elements of the climate.

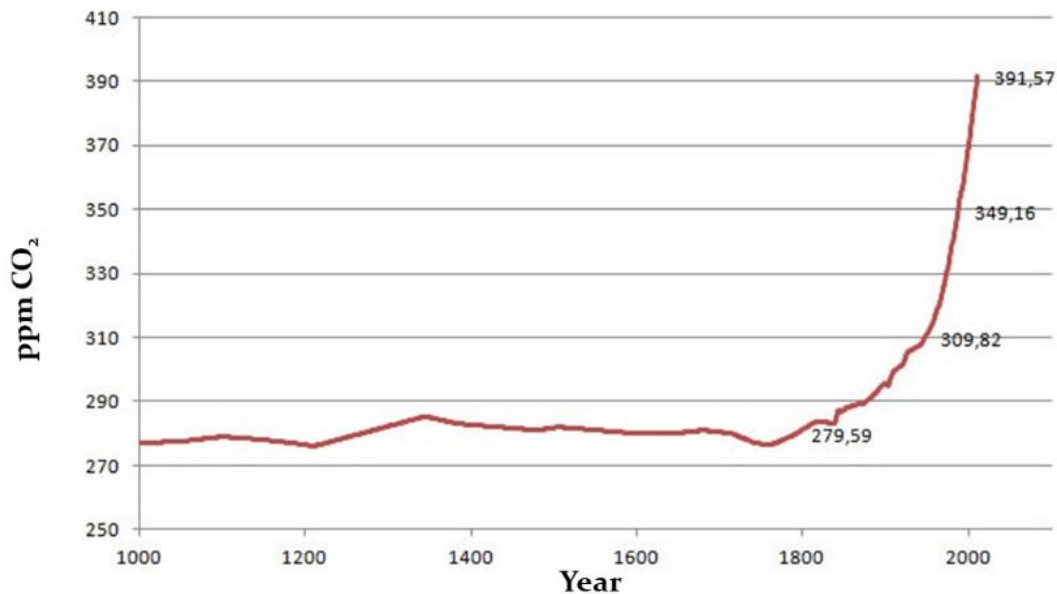


Fig. 1: Graph showing the increase in CO₂ over the years

Is it possible to make any predictions about the future evolution of the earth's climate?

Although much progress has been made in recent years towards the development of a quantitative climate theory, both through experimental and observational studies and through mathematical models, science is not yet able to provide a reliable answer. Some indications can be deduced with statistical methods taking into account the possible future implications of human activity. Climate fluctuations in the past seem to suggest that the interglacial warming of the last eight thousand years should be replaced by a cooling regime. The start of this turnaround could still be a few hundred years away, or even already in progress: the gradualness of the phenomenon would be such as to make the variation imperceptible for periods of the order of years. It should be kept in mind that the previous statement may not be valid if, as has already been mentioned, the increase of carbon dioxide in the atmosphere prevails, together with other effects. If this second hypothesis were to come about, there would be a considerable reduction of ice on the Arctic regions, with important consequences for the climate of the whole globe.

In conclusion, it seems necessary to make every effort to progress in the schematization and representation of all the factors and all the possible mechanisms of interaction between the various parts of the system, with particular reference to the atmosphere - ocean exchanges. These studies should be integrated with worldwide measures of several elements, including:

- Solar radiation (especially in the visible and ultraviolet);

- Average CO₂ content, nitrogen oxides, tropospheric aerosols, etc .;
- Reflective powers of the earth's surface, especially of snow and ice.

With these measures it will be possible to compare hypotheses and theoretical schemes with the observed experimental data.

Global warming and Extreme Meteorological Events in Sicily

Climate changes such as the global warming, are important not only from a scientific point of view. They can have implications also in social, economic and political environments. In fact, on December 2015 (Paris) at the United Nations conference on climate change (COP21) has been decided that before the end of century the global warming must be kept less of 2 °C.

During this meeting was discussed about the area known as “Stretto di Messina” which is one of most interesting area from climate point of view.

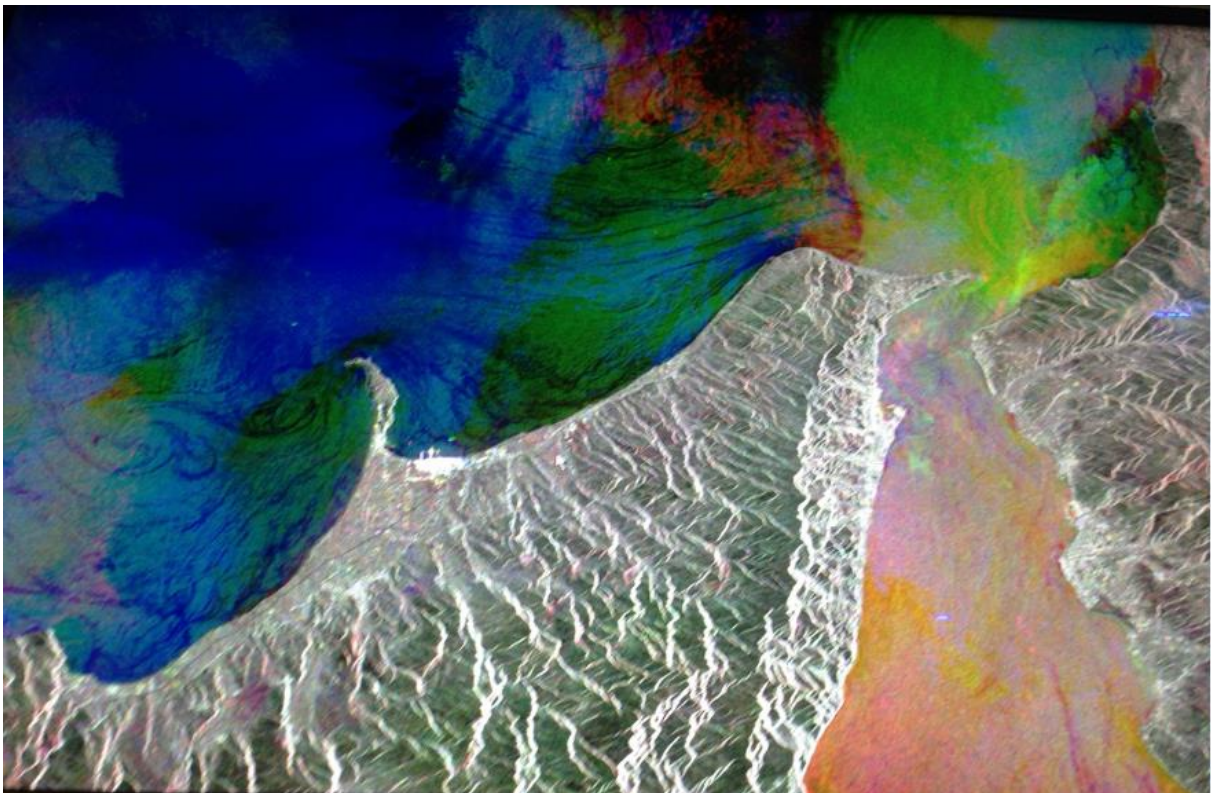


Fig. 2: The image shows the circulation of water masses in the Strait of Messina, between Calabria and Sicily. The strait has the reputation of being among the most unstable seas in the world

Its complex orography, the clash between the Ionian and Tyrrhenian seas, which have completely different kinds of salinity, temperature and density but also the exposure to winds both from northern quadrants and southeast, make this area among the most unstable of the world. Further, statistically

this area is interested by extreme weather events which often produce considerable property damage and sometimes loss of human lives.

The year of 2016 has been registered a new negative record. In particular, this year results as the most warm ever registered (NOAA: National Oceanic and Atmospheric Administration).

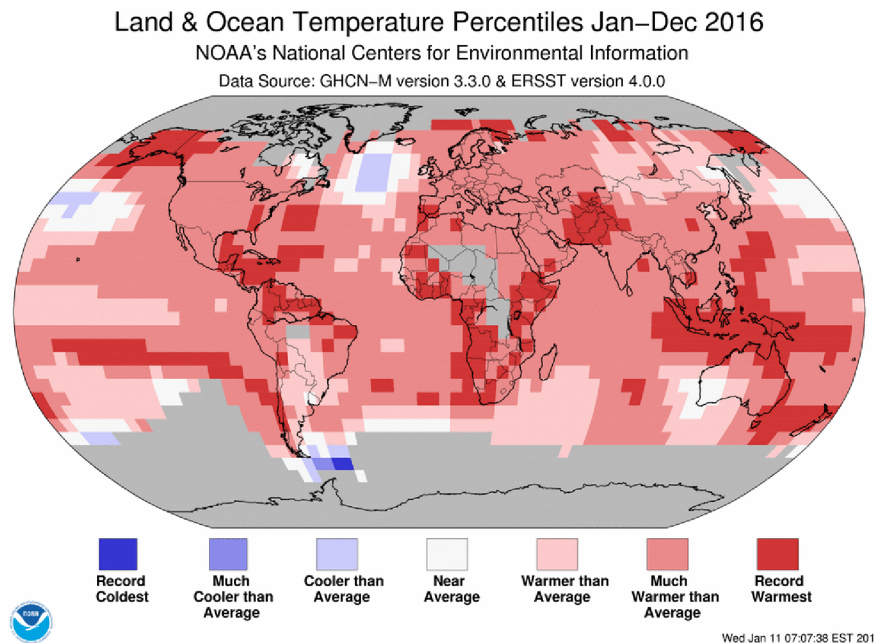


Fig. 3: Temperature anomalies of 2016 (source NOAA)

But the significant increase in planetary temperature has led to an increase in the frequency of extreme events in the “local area”?

In recent years, a growing attention has been addressed to environmental issues due to the significant increase registered, both in the number and intensity, of extreme weather events. The attention of stakeholders on phenomena as flash floods, strong winds and heavy seas has grown also as a result of the impact on daily life caused by landslides, damage to buildings and to agriculture and, in the most tragic circumstances, to the loss of lives. It clearly emerges, therefore, how important is the prevention of these phenomena. This can be performed only through an accurate study of the physical causes which determine such events. It clearly emerges the necessity to invest resources in the field of meteorology, to implement and improve the performance of forecasting bulletins, to broaden the detection network making it as dense as possible, to boost research in the field of weather numerical modeling, and to set up a sufficient number of operation unities connected with weather civil services. From a general point of view, heavy rainfall events in the Mediterranean can be divided into two types: floods and flash floods. The “Floods” are due to intense and long lasting precipitations (often

of several days) caused by the decrease of atmospheric circulation on a given area. The “Flash floods” are phenomena which consist in heavy and short precipitations (e.g. 60 mm/hour), where, even in 3 - 4 hours, pluviometric accumulations that are usually detected in an entire season can be recorded [2]. On the other hand, from the specific analysis of the extreme precipitation in Sicily, it emerges that the precipitations are nearly always connected to the action of particularly intense storm cells. These systems are usually divided into single cell storms and multi-cell storms [3]. The single cell is characterized by the presence of a single cumulonimbus (cloud with a pronounced vertical development), that has an average life time of 15 - 20 minutes and, therefore, has a low probability of initiation of flash floods. Furthermore, in the single cell storms, it's easy to determine the direction of motion, characterized by a displacement which follows exactly the level guides, the wind at 500-hPa level.

The mechanism that regulates the structure of a multi-cell system is quite different and more complex; in fact, the multi-cell is characterized by a regeneration process triggered by the cold downdraft (gust front) of the mature cell. This can lead to the development of a cluster of 3 - 4 cells that, therefore, would have a mean lifetime of about 60 minutes. In this case the displacement of the system does not follow the level guide but its direction is obtained from the sum between the average wind speed at 850 - 700-500 and 300 hPa and the vector opposite to the flow at 850 hPa that with the gust front will generate new cells.

By taking into account the length of the time-window that these weather perturbations can achieve, they can become cause of storms.

Among the mesoscale convective systems which can result in flash floods, one can distinguish:

- MCS (Mesoscale Convective System), in linear form if produced by cold front or circular in the case of cold drop;
- MCC (Mesoscale Convective Complex) which is a set of MCS or a MCS very wide. This system, characterized by a temperature of the convective core less than -52°C of at least 50,000 km², and by a surrounding crown with temperatures lower than -32°C for at least 100,000 km² [4].

However, the thunderstorm system potentially dangerous for the Mediterranean, and in particular on Sicily, is the so called "V Shaped" storm. Analyzing the causes that lead to its formation is equivalent to predict, in advance, favorable conditions to the manifestation of extreme events, such as those that occurred in eastern Sicily. The origin that give rise to the formation of very intense storms are to be linked to the presence of "deep instability" conditions that are to be found in the temperature and

humidity profiles in the air column of the arrival mass and in the existing site as well as the interaction between air masses of different nature thermo-hygrometer [5]. In the analyzed cases very often at the same time were observed:

- high amount of water vapor provided by the "warm conveyor belt" (a kind of river of warm and humid air flowing in the lower level troposphere in correspondence with the warm sector, namely between the rear of a warm front and the front of the cold front which follows) estimated by ThetaE (equivalent potential temperature or pseudopotential, namely the final temperature of a particle flow rate from a reference dimension, in this case 850 hPa, the conventional 1000 hPa) values that quantify the contribution of moist air;
- extensive resources of thermal energy (latent and sensible heat supplied from the sea) for strengthening updraft (hot running upward) [6];
- diffluence of jet stream flowing between the isobaric surfaces of 500 hPa and 300 hPa or - alternatively - jet streak (jet "core", which is the maximum speed of the jet stream) transit;
- diffluence in the high troposphere level (the rate of the change of the direction of the flow in the direction transverse to the motion); convergence lines to low level (often for the presence of a minimum baric secondary), nuclei of positive vorticity;(2ω , with ω the fluid angular velocity, it is positive in case of counterclockwise rotation (cyclonic));
- strong vertical wind shear (evidenced by the presence of a sub-tropical jet stream at 300-hPa level ;
- strong veering of the wind with height, with southeasterly low flow underlying southwesterly flow aloft;
- high values of Convective Available Potential Energy: CAPE
- high thermodynamic indices such as LI, K, TT, PWAT, SREH;
- orographic forcing that can generate dynamic feedback to persistent thunderstorms produced by the self-regenerating convective cell along the coast (cold air, after the precipitation, slides down the slope can generate a mini cold front (gust-front) on marine waters overlooking the mountain range, triggering a new convective activity)
- in some cases "dry intrusion", i.e. the intervention of a corridor of very dry air at the isobar of 500 hPa surface (the cold and dry air is heavier than warm and moist, therefore, if present at high altitude, is destined to sink to the ground which allows to trigger, animate, or possibly, intensify the convection)

Although a thorough analysis of these conditions can help estimate the likelihood of an extreme phenomenon and its location, it is appropriate to careful monitoring and forecasting very short-term

(nowcasting through satellite and radar) after the formation of the same, in order to identify the trajectory and, therefore, the areas that will be invested, in addition to his stage of development (next attenuation or intensification, evaluated on the basis on the energy of the system) [7].

In order to evaluate the probability of the genesis of storms it has been calculated the thermodynamic index CAPE [8], which measures the energy gained from the floating air mass until, during the ascent, remains warmer environment air. In other words, the CAPE measure the work done by the buoyancy and its unit of measurement is J / kg. For example, the CAPE of 1500 J / kg implies that a package of air of 1 kg has received, during the rise, a total energy of 1500 J. Under certain conditions and in the absence of interactions with the external environment and / or turbulence, (assuming that the parcel ascends without mixing with the environment) this potential energy is converted entirely into kinetic energy, going to animate intense updrafts. It's precisely the maximum kinetic energy available to convective systems which determines the intensity of the vertical speeds of the air mass and, hence, in the case of values of relative humidity near to 100%, the precipitation.

Extreme weather events are characteristics of the Mediterranean coastal areas and often cause flash floods. During these episodes, the precipitations that occur in a few hours often exceed the rain accumulations that normally occur in several months [9].

Usually, these extreme precipitations are in conjunction with intense and quasi-stationary mesoscale convective phenomena that insist on the same area for several hours [10]. Local factors such as the presence of orographic reliefs along to the coastline often determine their intensity. The geographical position and the complex orography of Sicily often cause extreme weather events [11-12]. Positioned at the center of the Mediterranean Sea, the island is placed in the transition zone between the arid and dry climate of North Africa; the more temperate and humid climate of central Europe. Hence, the phenomena trigger the interactions between processes typical of middle latitudes and the tropics.

In early autumn, the Mediterranean cyclones that originate from the contrast between air masses with very different temperatures and humidity interacting with seawater high temperature (Sea Surface Temperature, SST), affect the seas surrounding Sicily. These conditions can cause extreme weather events characterized by sudden and heavy rainfalls and dangerous flash floods [13].

From the geographic point of view, Sicily is characterized by an orography distributed in the direction of the parallel, especially in the Northern area, which is strongly exposed to the atmospheric perturbations that come from the South. In such cases, the warm and moist air coming from the Libyan Sea is often lifted over the orographic barriers, losing its humidity because of the cooling, and these modifications can cause heavy rains [14-15]. This occurs especially in the autumn seasons when the

sea around the island is still warm and able to transfer large amounts of humidity into the atmosphere [16-17].

It clearly emerges that the island complex orography plays a key role in the portion of the Ionian coastline between the towns of Catania and Messina.

Recently, extreme weather conditions have affected the eastern coast of Sicily, in particular the area between Catania and Messina. For example, from the tragic sequence of severe meteorological events that occurred between 2007 and 2011 in the below towns:

- 25 October 2007, which took place at Santa Margherita, Giampileri and Scaletta (Messina), with flash flood and precipitations of 175 mm in 2 hours, against an annual average amount of 800-1000 mm;
- 01 October 2009 at Giampileri, a tragic and disastrous event with 37 victims.
- 22 November 2011 at Barcellona and Saponara (Messina) with precipitations of 351 mm in 10 hours (recorded by the Castoreale weather station);

Referencing these three events, the recovery costs of the disaster damages were estimated at about 900 million euros (Source: DRPC Sicily – Stato dei rischi del territorio Siciliano – Rischio idrogeologico: raccolta dati storici – Sicilian Territory State of Risk – Hydrogeological Risk: Historical data Record).

Analysis of pluviometric accumulations in Sicily from 2002 to 2014

A study conducted by Sias (Servizio Informativo Agrometeorologico Siciliano) in 2010 showed [18] that rainfall accumulations of the Sicilian Region, in the period from 1921 to 2001, showed a downward trend average of about 19mm / decade.

But this trend appears to be confirmed? The increasing of the extreme weather events should not lead to a significant increasing of rainfall?

Province	2002	2003	2004	2005	2006	2007	2008	2009	2010	2011	2012	2013	2014	Climate
AG	360,09	639,87	703,07	650,80	533,22	549,91	424,80	739,11	659,04	602,76	596,53	734,11	558,78	556
CL	335,51	626,94	477,48	648,97	516,97	457,23	445,20	694,66	614,71	583,03	503,57	605,00	483,54	468
CT	534,25	1002,29	710,00	770,62	846,18	825,65	652,20	867,85	799,30	935,25	688,32	640,88	667,85	650
EN	426,57	895,20	706,87	808,80	503,00	611,53	664,23	744,37	644,93	662,57	593,87	674,47	564,73	566
ME	836,15	1028,47	918,37	901,06	799,35	1051,66	864,81	1305,16	1028,98	959,97	729,01	885,86	901,59	843
PA	597,55	785,18	719,69	761,63	553,68	717,92	530,73	1002,72	741,65	628,21	623,80	810,60	699,71	679
RG	303,03	707,43	683,46	571,69	648,40	618,91	430,80	598,60	717,60	836,03	576,23	611,91	432,94	476
SR	272,51	813,40	677,66	711,26	742,06	727,91	475,20	625,86	661,46	927,31	633,83	542,89	503,31	575
TP	499,15	774,80	888,73	752,33	571,91	765,87	447,64	951,11	702,60	610,51	561,10	776,38	611,14	535
Sicilian Average	462,76	808,18	720,59	730,79	634,98	702,95	548,40	836,60	730,03	749,51	611,81	698,01	602,62	594,22

Table 1: Values of annual precipitation collected by agrometeorological Sias stations. NB: Red cells highlight the data below the average temperatures expected. The column " Climate " is the average value of the rainfall of the last thirty years;

The row " Sicilian average" was calculated by averaging arithmetic value precipitation of the individual years of nine Sicilian provinces: Trapani (TP), Palermo (PA), Messina (ME), Caltanissetta (CL), Agrigento (AG), Catania (CT), Enna(EN), Ragusa (RG), Siracusa (SR).

In the Table 1 the values of annual precipitation observed at 107 agrometeorological stations of Sias located throughout the region Sicily, are reported [19]. The source data has been provided by Sias and the meteorological parameter investigated is the "daily precipitation total - monthly total" (in mm).

The table has been realized as follows:

1. After having cataloged stations for provinces of belonging, it is calculated for each station the "sum of annual precipitation values" registered a monthly basis;
2. It has been estimated the average annual rainfall of the stations belonging to each province, resulting in the "average annual rainfall provincial" in the table.

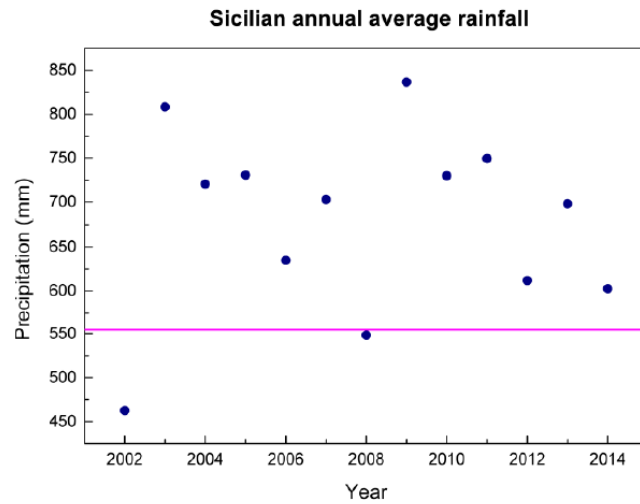


Fig. 4: Sicilian annual average rainfall obtained through provinces average.

Blue dots: values of annual average precipitation in Sicily; magenta continuous line: Sicilian climate average of the last thirty years

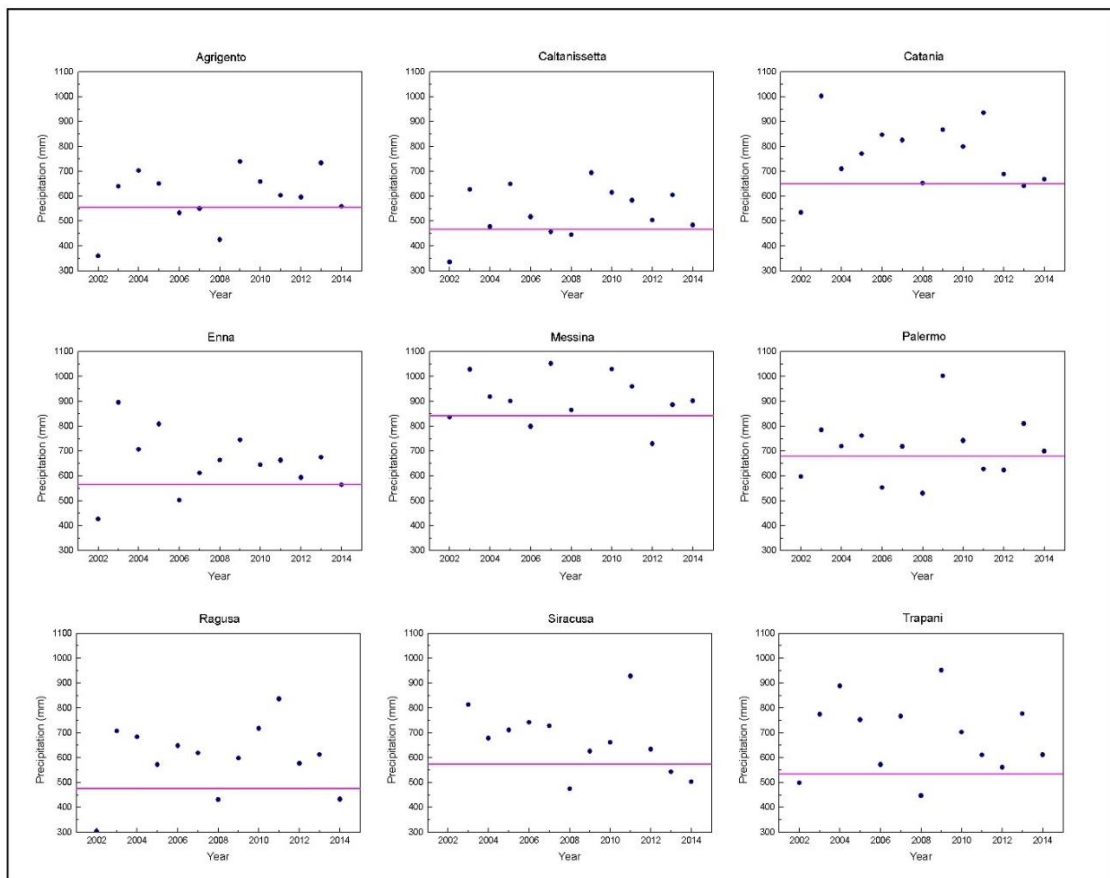


Fig. 5: Province annual average rainfall.

Blue dots: values of annual average precipitation in each Sicilian province; magenta continuous line: climate average of the last thirty years of each Sicilian province.

By the analysis performed, it emerges that, as shown in the Fig. 4, for the year 2002 an average Sicilian below the climatic averages has been registered; from 2003 to 2014, except the year 2008, it emerges a substantial increase in average rainfall in Sicily. In Trapani, Messina, Catania, Ragusa and Siracusa have been registered the largest increases, as reported in the Fig. 5.

The increase in global temperature and the surface of seas raises the probability of generation of extreme weather events such as heavy rainfall: this leads to the reversal of the trend of rainfall which is therefore growing [20-22].

The intensity of the convective systems can be increased by high resources of thermal energy in the lower layers [23].

In the last 150 years the average temperature on earth has been a gradual increase; the Global Warming has reported a sudden acceleration since 1980.

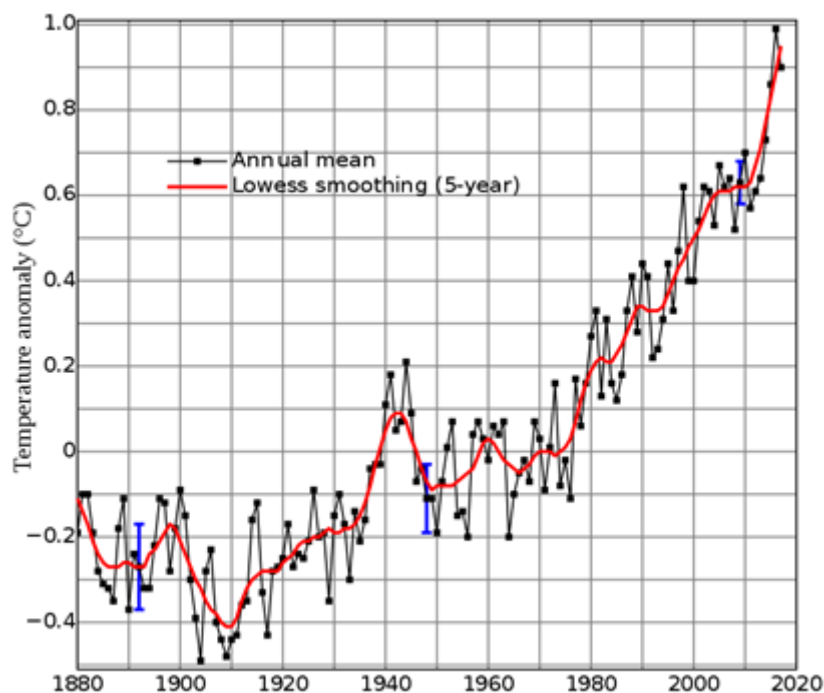


Fig. 6: Global land – ocean temperature index

Nowadays a great debate about the causes, whether natural or man-made, which have led to an increase in the average temperature of the Earth, of about 0.8°C in the last thirty years, is in progress [24]. It is clear that the two hypotheses should not be in close antithesis since the effects of the two causes may overlap. Increased concentrations of greenhouse gases, caused by the action of human activities (CO_2 in the atmosphere up to 386ppm against the value of 270 of the pre-industrial period), would have resulted in a substantial overheating. Such gas, in fact, is retained in atmosphere: soil

heating by radiation shortwave, cooling for reintroduction long-wave (infrared) inhibited by the presence of gas called - precisely - "greenhouse"[25].

Another hypothesis invoked to justify the rising temperatures in our planet, formulated by researchers of the Earth Institute at Columbia University (<http://earth.columbia.edu/news/2003/story03-20-03.html>) deals with a significant variation in solar activity, that has been gradually increasing in recent years.

Beyond the actual cause of Global Warming, the significant increase of the planetary temperature, has led to an increase in the resources of thermal energy available for convective phenomena, and, hence to an increase of the evaporative potential of seas and, consequently, to a rise in the frequency of extreme events.

The increasing of the global temperature and of the surface of our seas determines raises probability of generation of severe weather events such as heavy rainfall: this leads to the reversal of the trend of rainfall which is therefore growing.

This, in theory, would favor an increasing of the rainfall. The analyzed data confirm this trend: in Sicily, from 2003 to 2014, with the exception of 2008, there were accumulations rainfall higher than average weather.

Weather Station-Arduino Interfacing for a Weather Monitoring System Programmed for Emergency Weather Conditions

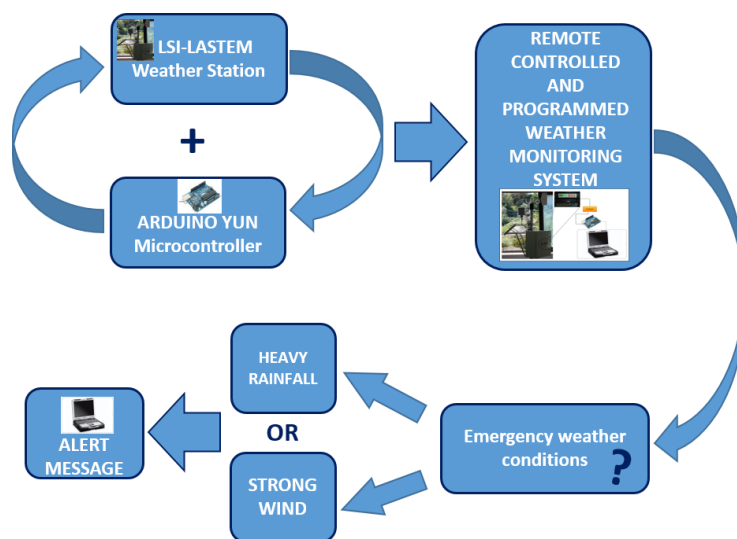


Fig. 7: Monitoring system composed of a meteorological station and an Arduino board

The significant increase of extreme weather conditions generates more and more concern. In fact, it is full-blown, that phenomena such as flash floods, strong winds and storm surges cause relevant impact on everyday life: landslides, mudslides, and damage to buildings and agriculture and, in the most tragic cases, loss of life. As a rule, the predictability degree of the emergency weather conditions can be often quite low because it is very difficult to go into the exact space-time location of particularly heavy rainfall of limited extent. Weather conditions [26], which can raise the risk level of extreme events, are well known by the operators that know local orography and have experience about territory response to a particular type of “stress”. This often requires a depth and careful study of the physical causes (analysis of thermodynamic variables and atmosphere’s dynamics) that are involved in the genesis of these events. It is equally important, indeed essential, to strengthen the networks of detection in the area of interest, making them more capillary as possible and equipping each station with the necessary technology for real-time data transmission for 24 hours on 24 now-casting (immediate future forecasts, until a few hours). An accurate short-term weather forecasting system for a preventive warning, that uses a network detection of high spatial resolution, can be very useful. A recent example of extreme weather condition in Sicily is that of 10th October 2015.

The highest rainfall accumulations were recorded on the Ionian sector of the province of Messina. The SIAS station in Antillo (not equipped with alarm systems) recorded 223 mm in a few hours; an extremely high amount of rain in the unit of time that was directly responsible for the flood wave of the Mela Torrent, whose overflowing gave rise to the flooding registered in the territory of Milazzo and Barcellona Pozzo di Gotto. In these municipalities, small rainfall accumulations were recorded (about 10 - 20mm). For this reason critical hydrogeological situations were not expected.

Such extreme events occur in the presence of Mediterranean cyclones, in the pre - frontal phase and in the hot sector of the depression system. Especially in the first phase of the autumn season we often witness the transit to a large series of cyclonic vortexes that, in rapid succession, often in formation due to orographic causes on North Africa (leeward to the Atlas range) or in the Balearics (leeward to the Pyrenees) and then pushed on the central Mediterranean by the ascending branch of the Sub-Tropical Stream, they reach our region. Having entered the Mare Nostrum, characterized by much higher surface temperatures than the oceanic ones, these cyclonic vortexes, fed from below, acquire the huge resources of thermal energy (water vapor and sensitive heat).

In this case, on the night between October 9th and 10th 2015, the low pressure center, moving between Tunisia and our region, activated an intense flow of southern currents, recalling from the Libyan coasts a rather hot air mass (even 25 ° C in the isobaric surface of 850 hPa, or at an altitude of 1520 m elevation). The strong winds of Scirocco in the low strata, in contact with the sea surface, in the stretch of sea between Libya and Sicily, caused an increase in the relative humidity of the air mass of

North African origin, accompanied, therefore, by very high values of the equivalent potential temperature in the lower layers. The "potential energy available for convection" (CAPE) reached peaks even higher than 4000 J / kg on the seas south of Sicily. This heat reservoir, ready to be converted into kinetic energy, or in strong upward currents, was triggered by the initial, apparently mechanical lifting of the hot air layer next to the ground. The reliefs exposed to the Scirocco winds, ie the eastern ones, and in particular the Etna and the Peloritani, favored the forced ascent of the hot and humid air mass directed towards Sicily. During the morning of October 10, our region was affected by a remarkable cumuliform activity that, thanks to a marked vertical "wind shear", due to the strong Scirocco on the ground and the south-western currents in the immediately overlying layers, generated storm cells also particularly intense in the area between Messinese Ionian and the eastern side of Etna. The mathematical models on a global scale, on that occasion, did not propose values worthy of note in the field of precipitation.

It is clear, therefore, because the storm cells are often of an extremely limited extension, only the real-time weather station data transmission can provide an alert system on a very precise location. In this way, weather stations, specifically programmed, located in strategic risk areas, such as streams' sources, where are recording critical meteorological parameters (such as severe rainfall amounts, wind storm, etc.), can send an alert message to the weather experts and/or authorities in order to be able to set up and carry promptly procedures to alert population.

Weather station/Arduino monitoring system

The data acquisition system is composed by a LSI LASTEM weather station, integrated by an Arduino YUN for the remote connection, able to capture typical meteorological parameters such as rainfall, wind speed, wind direction, temperature, relative humidity, solar radiation and barometric pressure [27].



Fig. 8: Weather station-Arduino Monitoring System

The employed weather station consists of a 12 inputs data logger, a sensors kit and a software for acquisition programming and data transfer and an Arduino YUN for the remote connection. In addition, weather sensors, such as:

- DNA202 sensor is a speed wind meter, characterized by compact size and a robust structure and of rotor and it is suitable to acquire low and high speeds up to 75 m/s. The sensing element is a high efficiency and durability relay-reed. The sensor body is made of anodized aluminum, while the rotor is made of carbon fiber reinforced;
- DNA212 sensor is a direction wind meter; it is very compact, sturdy and suitable both in very low and strong wind conditions; it is up to durability applications without maintenance. The measuring element is a Hall Effect transducer and the sensor body is composed of anodized aluminum. The above two sensors are completed of a cable L= 3m with connector IP65;
- temperature and relative humidity sensor is a thermos-hygrometer. It is specifically dedicated to meteorological applications where there may be rapid thermo-hygrometric variations and there may be long periods of hygrometric saturation. An anti-radiation shield protects the sensor from solar radiation by ensuring the best accuracy of the temperature measurement;
- barometric pressure sensor has an accuracy of 1hPa; it is housed in the IP65 box, where the data logger is fit;
- solar radiation measurement sensor obeys the requirements of Class 2 of the standard ISO9060 and specific WMO No. 8; it is lightweight and compact;
- rain gauge is characterized by an exterior part of anodized aluminum. The measurement system consists of a collector cone and a teeter connected to a magnet, which activates a reed relay, each teeter corresponds to 0.2 mm of rain. The rain gauge is mounted on a base positioned on a flat surface.

Power supply is a key component of this system, because a continuous power supply is necessary to make the system work continuously. A rechargeable battery is connected with a solar panel. The heart of the system is the data logger in which the values are stored. The E-Log data logger, allows the signals acquisition from the meteorological sensors, the processing and the storing of statistical values and the typical calculations of the weather applications with a particularly low power consumption. The Arduino YUN board is connected to the weather station with the E-log.. It is a microcontroller board based on the ATmega32u4 and the Atheros AR9331. The Atheros processor supports a Linux distribution based on OpenWrt named Linino OS.

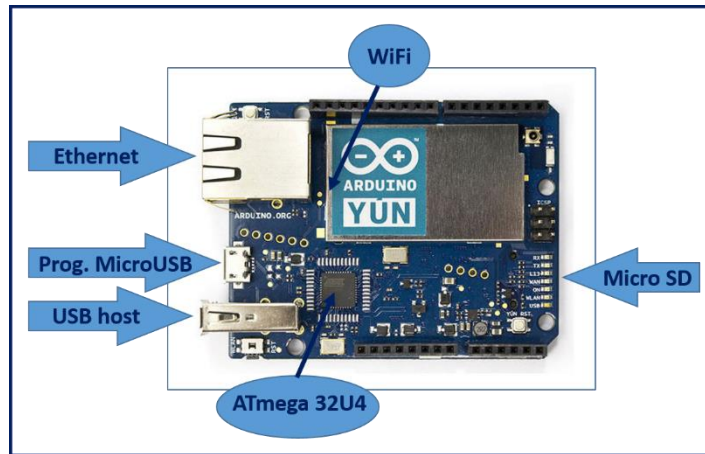


Fig. 9: Arduino YUN board.

LSI-lastem weather-station and Arduino YUN interfacing

Arduino YUN board connects the LSI-Lastem weather station to E-log sending real-time data weather at a control center to emergency weather conditions monitoring. The RS232 cable of the weather station E-log is connected through an USB/RS232 adapter to the YUN MicroUSB port. The measures taken by the weather station sensors are sent from E-log through the USB port to the Arduino board, which then sends the measurements via Internet to the Cloud. The YUN distinguishes itself from other Arduino boards in that it can communicate with the Linux distribution onboard, offering a powerful-networked computer with the ease of Arduino. In addition to Linux commands like cURL, it is possible can write your own shell and python scripts for robust interactions.

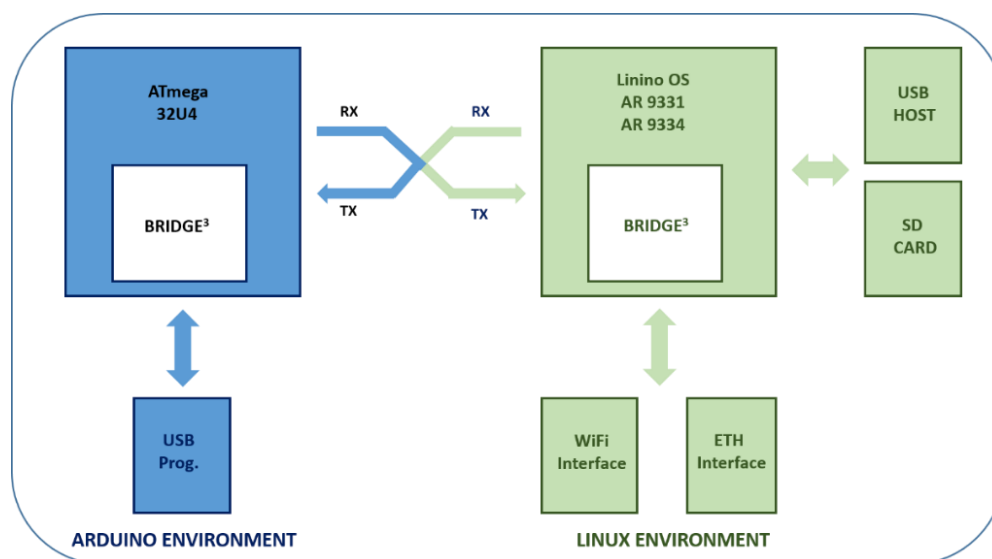


Fig. 10: Arduino YUN and LINUX environment

The Bridge library facilitates communication between the two processors, giving Arduino sketches the ability to run shell scripts, communicate with network interfaces, and receive information from the AR9331 processor. The USB host, network interfaces and SD card are not connected to the 32U4, but to the AR9331, and the Bridge library enables the Arduino to interface with those peripherals.

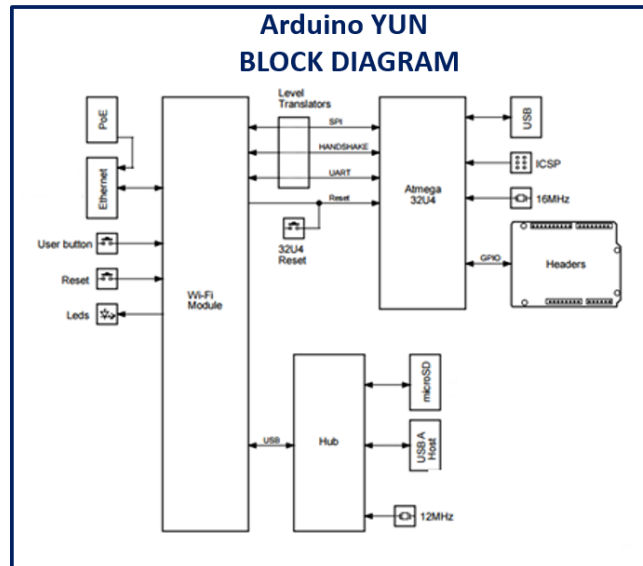


Fig. 11: Arduino YUN Block Diagram.

In terms of Communication, Arduino YUN has a number of facilities for communicating with a computer, another Arduino, or other microcontrollers. The ATmega32U4 provides a dedicated UART TTL (5V) serial communication. The 32U4 also allows for serial (CDC) communication over USB and appears as a virtual com port to software on the computer. The chip also acts as a full speed USB 2.0 device, using standard USB COM drivers. The Arduino software includes a serial monitor, which allows simple textual data to be sent to and from the Arduino board. The RX and TX LEDs on the board will flash when data is being transmitted via the USB connection to the computer. Digital pins '0' and '1' are used for serial communication between 32U4 and AR9331. The communication between the processors is handled by the Bridge library. A Serial library Software allows serial communication on any of the YUN's digital pins. Pins '0' and '1' should be avoided as they are used by the Bridge library. The ATmega32U4 also supports I2C (TWI) and SPI communication.

On the SD card of the board, the Node.js (a JavaScript environment that allows user to write web server programs), is installed. Below, it will be used to connect a microcontroller to a web browser using the node.js-programming environment, i.e. HTML, and JavaScript. Node Serial port Library to communicate with serial port of E-log is installed. It allows serial communication on any YUN's digital pins. Pins '0' and '1' should be avoided as they are used by the Bridge library. In the JavaScript

file (named serial.js) the parameters and protocol communication, send/receive commands controls are specified. “A1I\r\n” command is sent to E-log, as a string, in TTY communication protocol, E-log responds by sending a string containing all the measurements of the sensors of the weather station. Making a parsing of the string, is possible to get the weather station measures.

Communication parameters are:

- Baudrate = 9600 bps;
- DataBits = 8;
- Parity = ‘none’;
- StopBits = 1;
- FlowControl = false.

The program code of serial.js is:

```
/*
  serial.js
*/
var serialport = require("serialport");
var serialPort = new serialport.SerialPort("/dev/ttyUSB0",
    {baudrate: 9600,
    dataBits:8,
    parity:'none',
    stopBits: 1,
    flowControl: false,
    parser: serialport.parsers.readline("\n")
    });
serialPort.open(function (error)
{
  if ( error )
  {
    console.log('failed to open: '+error);
  }
  else
  {
    //open connection
    serialPort.write("A1I\r\n", function(err,result)
    {
      console.log('error: '+err);
    });
    var interval = setInterval(function()
    {
```

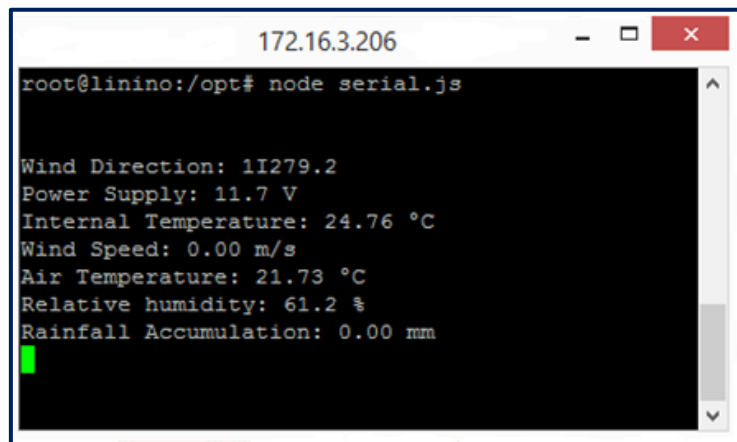
```

        serialPort.write("A11\r\n", function(err,result)
    {
        console.log('error: '+err);
    });
},10000);
serialPort.on('data', function(data)
{
    //console.log(data.toString());
    console.log("\n");
    try
    {
        var values=data.split(";");
        console.log('Wind Direction: '+values[0].toString());
        console.log('Power Supply: '+values[1].toString()+ ' V ');
            console.log('Internal Temperature: '+values[2].toString()+ ' \u00B0C ');
        console.log('Wind Speed: '+values[3].toString()+ ' m/s ');
        console.log('Air Temperature: '+values[4].toString()+ ' \u00B0C ');
            console.log('Relative humidity: '+values[5].toString()+ ' %');
            console.log('Rainfall Accumulation: '+values[6].toString()+ ' mm/h');

        if (values[3]>25.0)
        {
            console.log('ALERT WIND');
        }
        if (values[1]<11.0)
        {
            console.log('ALERT POWER SUPPLY');
        }
        if (values[6]>30.0)
        {
            console.log('ALERT RAIN');
        }
    }
    catch(err){
        console.log('waiting...');
    }
});
}
});

```

Typing “node serial.js” into Linux shell will appear as the result shown in the Fig. 12:

A screenshot of a Linux terminal window. The window title bar shows the IP address '172.16.3.206' and standard window control buttons. The terminal prompt is 'root@linino:/opt#'. The command 'node serial.js' has been executed, resulting in the following output:

```
Wind Direction: 11279.2  
Power Supply: 11.7 V  
Internal Temperature: 24.76 °C  
Wind Speed: 0.00 m/s  
Air Temperature: 21.73 °C  
Relative humidity: 61.2 %  
Rainfall Accumulation: 0.00 mm
```

A green cursor is visible on the line following the last output line.

Fig. 12: Typing “node serial.js” into Linux result window.

The program sends weather warnings (in the case in which the measure Rainfall Accumulation is greater than 30 mm/h or in the presence of strong wind with wind speed greater than 25 m/s) and a warning message relating to an insufficient power supply.

The WRF model

The Numerical Weather Prediction

The Numerical Weather Prediction (NWP) represents one of the most complex challenges of Atmospheric Physics. The objective of knowing in advance the evolution of time with a reasonable degree of reliability can now be pursued thanks to the development achieved by modern computers. The parallel development of the computer networks and the internet has made the weather forecast available at a capillary level thanks, for example, to the usability of specific applications on multiple communication devices. However, it should be stressed that the above-mentioned weather data diffusion, while meeting the sharing requirement, if not properly filtered, does not guarantee the correctness of the information itself.

Definition of model and of the main constituent equations (primitive equations)

From a general point of view, a meteorological model is nothing but a schematic and simplified representation of physical reality, described through a set of equations that simulate the behavior of the atmosphere. A particular software uses input data, executes a run using algorithms based on a set of coupled equations, and expresses the output result (output) in the form of a new set of data. In the case of meteorological forecasting, the calculation algorithms consist of the set of differential equations to partial derivatives, which describe the dynamics of the atmosphere. The main core of a calculation code aimed at solving this system of differential equations is normally formulated in FORTRAN language. Specific subroutines, such as those related to matrix processing, to standard mathematical functions and to graphic sections, can use other languages, usually C.

As input data of the model, the values of: ground pressure, wind speed in its spatial components, air temperature and humidity at different altitudes of the atmosphere (up to about 20 ÷ 50 km in height) are usually used. These variables, called A_p prognostic variables, are present in the model in the form of derivatives with respect to time $\frac{\partial A_p}{\partial t}$.

These variables play a key role within the model because they coincide with the variables object of the observations and because in the progress of the calculation they allow to derive also all the other variables that depend on them, called diagnostics. The goal of a forecast is to return, after the calculation, the mutated value of the above-mentioned variables (i.e wind speed, temperature, pressure, humidity at various heights from the ground). From these you can then derive all the other dependent quantities: precipitation, cloudiness, etc ...

The main equations, called primitives, which are used by the models are:

- Navier-Stokes (NS) equations for the definition of wind field components (also called momentum balance equations in a fluid);
- First Principle of thermodynamics (principle of conservation of energy);
- Equation of evolution of water vapor (takes into account all the processes that make up the water cycle and its state passages, ie evaporation, condensation, fusion, solidification and sublimation);
- Continuity equation (mass conservation law).

To these equations are added:

- Gas state equation, which binds pressure, density, temperature and volume of a mass of air.
- Hydrostatic equation, which concerns the approximate relationship between pressure variation with altitude and air density.

Global models and limited area models

There are two types of meteorological models: Global Models (GM) and Limited Area Models (LAM). It is intuitive that global models take into account the whole earth's atmosphere, while those with limited area operate on smaller volumes. Since there are no simple analytical solutions of the system of equations valid for all points of the atmosphere, it is necessary to resort to a partition of the portion of the atmosphere of interest, in a three-dimensional matrix identified by grid points, thus reformulating the problem in discrete terms, once the boundary conditions have been defined. The simplification adopted, which takes the name of discretization, implies that the derivatives are replaced by finite differences.

This substitution makes the original differential equation system suitable for numerical calculation. This approach involves the definition of a series of fixed points, selected in the domain of definition of the equation variables. Each variable is then completely identified by the values assumed on these points, the so-called grid points, while the spatial derivatives become finite differences evaluated between the grid points. It should be noted that at each grid point a portion of atmosphere is associated, whose characteristics are represented by the values assumed by the variables. Therefore, the forecast becomes a procedure for calculating the future values of the meteorological variables on all grid points. In the specific case, one imagines to completely dissect the atmosphere both horizontally and vertically by means of a three-dimensional grid of appropriate scale. There are no constraints on the total number of points (also called nodes) to be used, although it is evident that by

infilling the grid the interval between the points decreases and this results in a better precision of the numerical computation. In practice it is the computing power of the electronic instrument that limits the choice of points: either the whole globe is considered and therefore the distance between the nodes is kept wide, or one concentrates on an area by infilling the grid step, thus gaining in resolution. Since the automatic calculation capabilities are finished, the Global Models, having the largest grid pitch, introduce the most important simplifications, operating with resolutions between 10 and 50 km horizontally.

The LAM, reducing the area of interest, use a denser grid, with a typical pitch of $1 \div 10$ km. In vertical, the portion of the atmosphere considered can extend up to a height of $30 \div 70$ km, distributed on about fifty levels, in an uneven way (denser near the ground, where a better vertical definition is required). It is important to underline that the Global Models serve to initialize the LAM, that is, at the initial instant $t = 0$ relative to the beginning of the calculations, the LAMs use the GM outputs as initial values and then elaborate a prediction.

In addition, GMs provide LAM with side contour conditions throughout the forecast time. Obviously there will be some gaps, because the initial conditions and boundary on all

points of the thicker mesh are not known; it will therefore be necessary to interpolate these data with appropriate techniques. Although suffering from these uncertainties, the LAM allow to produce very detailed forecasts, but valid only from a few hours up to about two days.

The initialization of the meteorological models involves the definition of the initial values in all the grid points (both horizontal and vertical) for each of the diagnostic variables, as well as the boundary conditions. To achieve this, a long preparation work called a data assimilation process must be carried out beforehand, which in terms of time, calculation and processing is the heaviest part of a model, so much so that it is now developed autonomously, with dedicated techniques . It is known that there is an interconnected network of synoptic meteorological stations all over the globe, coordinated by the World Meteorological Organization, which continuously measure the physical variables of interest and transmit them to the data collection centers. Satellite data and measurement results on ocean vessels and buoys also contribute to this purpose. As you can imagine, the distribution of the measuring points is not homogeneous along the grid nodes and this represents the first problem. Moreover, especially on the oceans, right where cyclones are born that affect the mid-latitudes, the data are lacking or missing altogether. There are very few stations that make vertical reliefs in height using the probe flasks (about a thousand in the whole world, with considerable gaps above the oceans and in sparsely inhabited areas). Therefore, not only are the data deficient, but many of them can be

affected by error, so it is essential to carry out a strict quality control for every data (there are special automatic procedures suitable for the purpose that can filter out the wrong values) and this too it's a time-consuming operation. The optimal interpolation is to transport the data to the grid points at the desired time, correcting them for local conditions. Finally, the data must be made homogeneous and correct to avoid discontinuity with the previous measures. The result of all these operations results in data sets on numerical grids that are then translated into cards called analysis, ie graphical maps of the values of the variables of interest observed at a specific time of day.

A Local Area Model for Sicily

The limited area model Weather Research Forecast (WRF) [28] is a new generation system of numerical forecast designed for operational forecasting of atmospheric phenomena.

The WRF is the result of collaboration between the National Centre for Atmospheric Research (NCAR), the National Centre for Environmental Prediction (NCEP) and the Earth's System Research Laboratory (ESRL) of the National Oceanic and Atmospheric Administration (NOAA).

The structure of the model consists of a central nucleus, called the WRF Software Framework (WSF), which is formed of several assimilation and parameterization schemes of the physicochemical variables to which pre and post processing modules are connected.

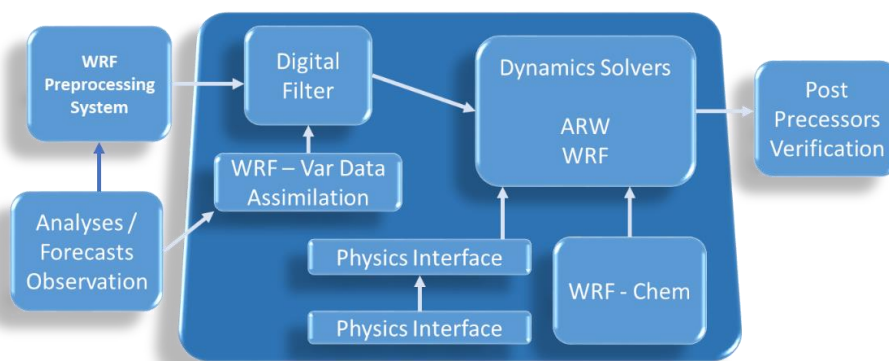


Fig. 13: Block diagram of WRF Software Framework (WSF)

The pre-processing phase (WPS) includes three calculation routines, Geogrid, Ungrib, and Metgrid that sequentially take care to elaborate the data that drive the model. Geogrid creates static data that includes geographic data and soil use data; Ungrib assimilates the GRIB data collected by the global

computing centers, while Metgrid intercepts the horizontal weather data, scaling them to the domain originally defined.

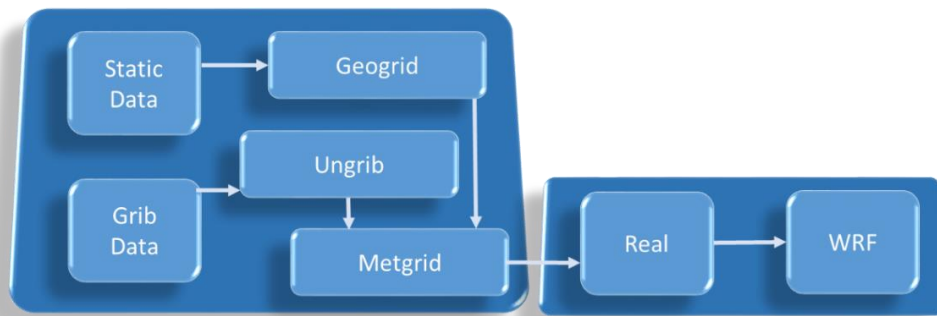


Fig. 14: Block diagram of Pre-processing System (left) and Real Data ARW System (right)

The pre-processed data are passed to other routines, in this case the WRF-REAL that interpolates the data in the spatial coordinates of the model.

The final step of process regards the production of output data and graphic post processing.

The WRF has two dynamical cores:

- the Advanced Research WRF (ARW), supported and developed by National Center of Atmospheric Research (NCAR), able to simulate different typologies of meteorological events with different spatial resolutions;
- the Non-hydrostatic Mesoscale Model (NMM), developed by National Center for Environmental Prediction (NCEP), able to work both in hydrostatic and in non-hydrostatic way.

The research activity aims to optimize the model for the Sicilian territory, characterized by a complex orography. The improvements made concern, first of all, the increase in the resolution of the initial static geographical data (DEM 20x20 m), the optimization of local land use parameters and vegetative coverage (CORINE data), the acquisition of data from sea temperatures in dynamic mode. In the following images shows some of the parameters that have been reviewed and updated.

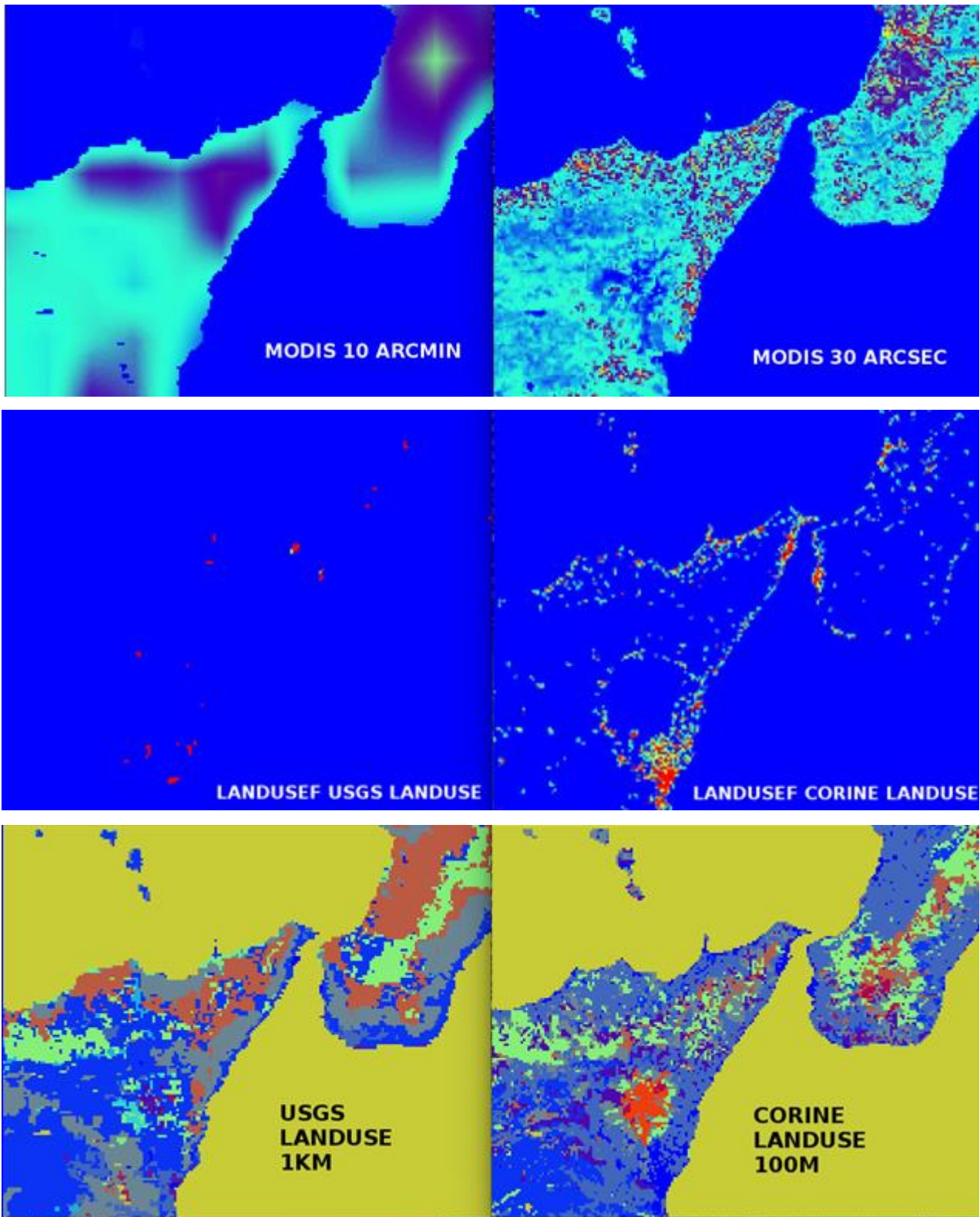


Fig. 15: Orography improvements. In particular, the increase in the resolution of the initial static geographical data (DEM 20x20 m), the optimization of the local land use parameters and the vegetation cover (CORINE data) is shown.

The model WRF results to be very versatile and it allows the use different typologies of parameterizations as it regards, for instance, the microphysics of the clouds, the convection, the turbulent flows inside the Planetary Boundary Layer, the radiative and diffusive processes.

The prognostic equations of the model

Limited area models are mostly non-hydrostatic. Under these conditions the vertical equation does not follow the hydrostatic approximation:

$$dp = -p \rho dz \quad 1)$$

Therefore the vertical speed turns out to be an unknown factor of the system. To overcome this problem it is possible to use the terrain-following coordinates η as a vertical coordinate [29].

$$\eta = \frac{p_h - p_{ht}}{\mu} \quad 2)$$

where:

$\mu = p_{hs} - p_{ht}$ it is directly associated with the mass of the air column per surface unit;

p_h it is the hydrostatic component of pressure;

p_{ht} it is the pressure at the upper (fictitious) edge of the atmosphere;

p_{hs} it is the pressure at the surface.

The WRF model integrates differential equations to the nonlinear partial derivatives defined [30] as follows. Introducing the appropriate flux form variables:

$$V = \mu v = (U, V, W); v = (u, v, w); \Omega = \mu \dot{\eta}; \Theta = \mu \theta \quad 3)$$

where:

$v = (u, v, w)$ it is the covariant velocities in the two horizontal and vertical directions, respectively;

$\omega = \dot{\eta}$ is the contra variant vertical velocity;

θ it is the potential temperature, that is the temperature of an air particle that is adiabatically brought to the altitude of 1000 hPa.

Considering the following variables:

$\phi = gz$ is the geo-potential, that is the work necessary to overcome the force of gravity and move upwards, at a given height, a unitary mass of air,

$\alpha = \frac{1}{\rho}$ is the inverse of the density,

$p = p_0(R_d\theta/p_0\alpha)^\gamma$ is the equation of state with R_d constant of the dry air gases, $\gamma = c_p / c_v = 1,4$ and p_0 the pressure reference, typically 10^5 Pa,

$\partial_\eta\phi = -\alpha\mu$ it is the diagnostic relationship for density,

it is possible to derive the differential equations to the partial, non-linear, fundamental derivatives of the model:

$$\partial_t U + (\nabla \cdot \mathbf{V}u) - \partial_x p + \partial_\eta(p\phi_x) = F_U \quad 4)$$

$$\partial_t V + (\nabla \cdot \mathbf{V}v) - \partial_y(p\phi_\eta) + \partial_\eta(p\phi_y) = F_V \quad 5)$$

$$\partial_t W + (\nabla \cdot \mathbf{V}w) - g(\partial_\eta p - \mu) = F_W \quad 6)$$

$$\partial_t \theta + (\nabla \cdot \mathbf{V}\theta) = F_\theta \quad 7)$$

$$\partial_t \mu + (\nabla \cdot \mathbf{V}) = 0 \quad 8)$$

$$\partial_t \phi + \mu^{-1}[(\mathbf{V} \cdot \nabla \phi) - gW] = 0 \quad 9)$$

F_U, F_V, F_W, F_θ represent forcing terms arising from model physics, turbulent mixing, spherical projections, and the earth's rotation.

The eqns. 4-9, has been calculated not taking into account a fundamental parameter from the meteorological point of view, the moisture. In fact it is responsible for the most important effects on atmospheric dynamics to which the release of latent heat is associated. Furthermore, water vapor and clouds play a fundamental role in the reflection, absorption and emission of both solar and terrestrial radiation. Therefore, it is necessary to reformulate the previous equations taking into account the effect of moisture, but keeping the prognostic variables and the vertical coordinate coupled with the mass of dry air.

The appropriate flux form variables considering the terms of dry air (subscript d) can be written as follows

$$V = \mu_d v; \Omega = \mu_d \dot{\eta}; \Theta = \mu_d \theta; \eta = \frac{p_{ah} - p_{dht}}{\mu_d}; \mu_d = p_{dhs} - p_{dht} \quad (10)$$

Adding an additional conservation equation to include water mixing ratios in all of its phases:

$$\partial_t Q_m + (\nabla \cdot \mathbf{V} q_m) = F_{Q_m} \quad (11)$$

where:

$$Q_m = \mu_d q_m \quad (12)$$

and

$$q_m = q_v, q_c, q_i, q_r, q_s \quad (13)$$

are the mixing ratio of water vapor (q_v), liquid water of the cloud (q_c), ice (q_i) and of all the hydrometeors that the model considers.

Finally, it is possible to rewrite the modified fundamental equations of model, taking into account the moisture, as follows:

$$\partial_t U + (\nabla \cdot \mathbf{V} u) + \mu_d \alpha \partial_x p + (\alpha/\alpha_d) \partial_\eta p \partial_x \phi = F_U \quad (14)$$

$$\partial_t V + (\nabla \cdot \mathbf{V} v) + \mu_d \alpha \partial_y p + (\alpha/\alpha_d) \partial_\eta p \partial_y \phi = F_V \quad (15)$$

$$\partial_t W + (\nabla \cdot \mathbf{V} w) - g \left[\left((\alpha/\alpha_d) \partial_\eta p - \mu_d \right) \right] = F_W \quad (16)$$

$$\partial_t \Theta + (\nabla \cdot \mathbf{V} \theta) = F_\Theta \quad (17)$$

$$\partial_t \mu_d + (\nabla \cdot \mathbf{V}) = 0 \quad (18)$$

$$\partial_t \phi + \mu_d^{-1} [(\mathbf{V} \cdot \nabla) \phi] - gW = 0 \quad (19)$$

$$\partial_t Q_m + (\nabla \cdot \mathbf{V} q_m) = F_{Q_m} \quad (20)$$

where:

$\alpha_d = \frac{1}{\rho_d}$ is the inverse of the density of dry air,

α is the inverse of density, and takes into account the mixing ratios of the various entities present in the volume of air considered. Analytically we have that:

$$\alpha = \alpha_d(1 + q_v + q_c + q_i + q_r + q_s + \dots) \quad 21)$$

$\partial_\eta \phi = -\alpha_d \mu_d$ it is the diagnostic relationship for density

$p = p_0(R_d \theta_m / p_0 \alpha_d)^\gamma$ is the diagnostic equation for total pressure (vapor plus dry air)

In eqn. 20, which represents the diagnostic equation for total pressure (vapor plus dry air), the potential temperature θ_m is given by:

$$\theta_m = \theta(1 + (R_v/R_d)q_v) \approx \theta(1 + 1.61 q_v) \quad 22)$$

Such systems of non-linear equations to partial derivatives can not be solved analytically. The solution is obtained by numerical calculation methods in which the equations are discretized and resolved on a grid. There are numerous numerical techniques but most LAM models use finite difference schemes. This technique approximates the spatial and time derivatives by means of a series development of Taylor appropriately truncated, in which the increments are represented by the spatial and time grid pitch.

Physical parameterizations

The presence of sources and wells energy associated with flows heat, water vapour and momentum, near the Earth's surface, in the Planetary Boundary Layer (PBL), and finally in the free atmosphere above PBL, are physical aspects that must be considered and schematized in the structure of a numerical model for meteorological simulation. Furthermore, radiative effects and water phase changes must be schematised. Many of these physical processes occur on scales smaller than that defined by the spatial grid (subgrid scale processes). It is therefore necessary to treat them with a different methodology from that of explicit simulation, which goes by the name of "parametrization". The terms to be parameterized appear in the prognostic equations either as terms of source or well, or as terms with unresolved scale, or as terms of correlation between sub-grid variables. This is a direct consequence of the non-linearity of the equations integrated by the model. In order for the equation system to be "closed" in the unknowns it is necessary that the terms of sub-grid correlation are expressed as a function of the unknowns themselves.

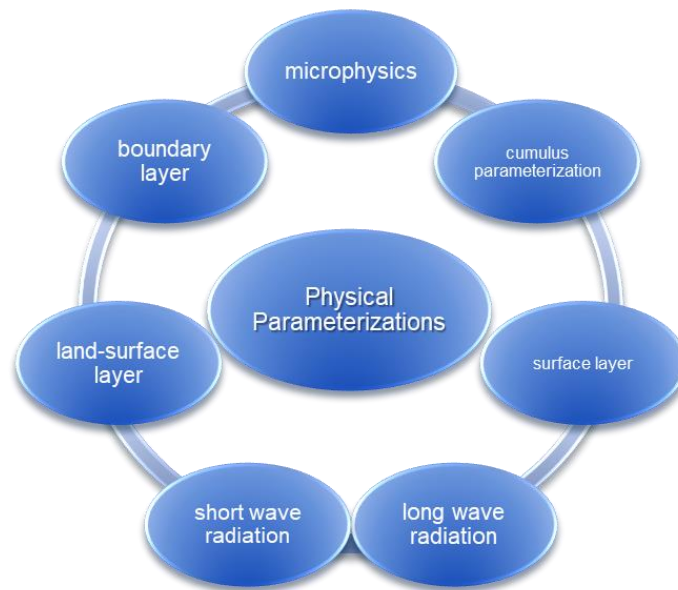


Fig. 16: Scheme of the physical parameterizations used in the limited area models

Microphysics

When a portion of moist air reaches the condensation level, the formation of the liquid phase takes place through an intermediate passage, called nucleation [31-41]. Nucleation can be homogeneous, or heterogeneous. In the first case (often negligible) there is the formation of droplets without the intervention of external elements. In the second case there is the intervention of an external element (atmospheric aerosol) that acts as an aggregator. Consider the case in which a sufficient quantity of water is deposited around a wettable aerosol, so as to form a film that envelopes it. From that point on, the aerosol is approximable to a drop of water. When the drop reaches the size of a few microns then come into play a series of processes that influence the subsequent evolution of these droplets. These processes are:

- Coalescence: process of growth of the droplets by impact and by aggregation, strongly dependent on the diameter of the drops and their relative speed.
- Breakup: fractionation of the drops; experimentally the probability of breaking a drop is an exponential function of the ray of the drop itself.
- Evaporation: happens when some drops are transported on unsaturated areas; it is a function of air humidity, saturation humidity and the content of drops in the air.

This is generally valid for liquid drops. We now introduce the main processes that take place inside the clouds when it extends below 273 Kelvin (cold cloud).

In case the temperature is below the freezing level, drops of liquid water can coexist with icy particles. This drop is in an unstable state but, in order to freeze it, similarly to the nucleation already seen, one must form within the drop an ice embryo large enough (with a radius greater than the critical ray) to grow. Because the number and size of these embryos grows as the temperature decreases, below a certain temperature, icing is a certain phenomenon. Also in this case, the heterogeneous nucleation is strongly advantageous compared to the homogeneous nucleation. The ice crystals formed, still too light to precipitate, can increase the size by diffusion or by aggregation. Based on the processes these particles undergo, various classes of solid hydrometeors are created. The residence time in the atmosphere of these liquid and solid particles is linked to the intensity of the ascension currents, to the state (solid / liquid), to the size of the particles, in turn related to the degree of over-saturation of the environment, as well as to the time of permanence in the atmosphere itself. It is also necessary keep in mind the heat fluxes coming from the outside of the cloud, both related to the state transitions that take place inside the cloud. It is therefore evident that it is not possible to accurately describe the various phenomena presented. For this purpose, in the numerical models of meteorological forecasting, the microphysical parameterization schemes were introduced, aimed at the representation of these processes.

The goodness of the adopted scheme is connected to the model's ability to describe atmospheric water in its various states: there are usually six classes of hydrometeor, two liquids (liquid water in the cloud and rain) and four solids (ice crystals, snow, hail and graupel).

The general approach in meteorological modelling is to define, for each hydrometeor class, m equations analogous to equation 11:

$$\partial_t Q_m + \partial_x(U q_m) + \partial_y(V q_m) = -\partial_\eta(\Omega_s q_m) + D_{q_m} + S_{q_m} \quad 23)$$

where the terms of sedimentation rate, Ω_s , and diffusion rate, D_{q_m} , are a function of the size of the particles and are calculated assuming a particular statistical distribution (generally gamma or exponential distribution) of the particle diameter. The source terms present in the eqn. 23, indicated collectively with S_{q_m} , describe each a particular microphysical process (nucleation, growth, fusion, etc ...) associated with the various classes of hydrometeors considered. Considering, for example, the diameters of a certain hydrometeora m distributed according to the exponential distribution function

$$N_m(D) = N_{0m} e^{(-\lambda_m D_m)} \quad 24)$$

to close the equation 23) it is necessary to write the terms Ω_s , D_{q_m} and S_{q_m} as a function of the mixing ratio (prognostic variable of the equation). If N_{0m} in eqn. 24 is known, for example from experimental

observations, integrating the distribution on all diameters, assuming the density ρ_m is known, it is possible to calculate the total mass M of each species in the volume considered, and therefore also the mixing ratio, as a function of λ_m :

$$M_m = \frac{\pi\rho_m}{6} \int_0^\infty D^3 N_m(D) dD = \frac{\pi\rho_m}{6} \int_0^\infty D^3 N_{0m} e^{(-\lambda_m D_m)} dD \quad (25)$$

Inverting the relation, λ_m can therefore be expressed as a function of the density (known quantity) and of the mixing ratio, and then obtain the distribution expressed in eqn. 24 as a function of the mixing ratio. The terms Ω_s , D_{qm} and S_{qm} can also be expressed as a function of Q_m .

Similar considerations can be made in the presence of an additional prognostic equation for the concentration (double moment diagram) [42].

The schemes of parameterizations of the microphysics of the clouds therefore play a key role in the refinement of forecast models.

Physical parameterization of convective phenomena:

In order to parametrize convective phenomena it is necessary to consider the statistical behavior of convective cloudy systems which are influenced by different large-scale conditions. Before tackling this problem it is important to introduce the potential temperature equation θ , defined as follows:

$$\theta = T \left(\frac{p_0}{p} \right)^{\frac{R}{c_p}} \quad (27)$$

where T is the temperature, p is the pressure, p_0 is ground pressure, R is the constant gas for dry air and c_p is the specific heat at constant pressure.

In formulating the collective effect of convective clouds systems, one should consider a "closure problem" in which a limited number of equations that govern the statistics of a huge system are searched.

The heart of the matter is then choosing the appropriate system closure conditions. A first classification of this conditions can be provided starting from the equilibrium equations of the potential temperature θ and the specific moisture q (where specific moisture q represents the ratio between water vapor mass and the fluid particle total mass) on large scale of pressure coordinates [43]:

$$c_p \left[\frac{\partial \bar{\theta}}{\partial t} + \bar{\mathbf{v}} \cdot \nabla_h \bar{\theta} + \bar{\omega} \frac{\partial \bar{\theta}}{\partial p} \right] = \left(\frac{p_0}{p} \right)^{\frac{R}{c_p}} Q_1 \quad (28)$$

$$L \left[\frac{\partial \bar{q}}{\partial t} + \bar{\mathbf{v}} \cdot \nabla_h \bar{q} + \bar{\omega} \frac{\partial \bar{q}}{\partial p} \right] = -Q_2$$

The marked variables indicate a large scale average and Q_1 and Q_2 are respectively the heat source and the moisture well. All the other symbols have the standard meaning assumed in literature. To simplify, these two equations can be rewritten respectively as:

$$\frac{\partial T}{\partial t} = \left(\frac{\partial \bar{T}}{\partial t} \right) + \frac{1}{c_p} Q_1 \quad (29)$$

$$\frac{\partial q}{\partial t} = \left(\frac{\partial \bar{q}}{\partial t} \right) - \frac{1}{L} Q_2$$

where:

$$\left(\frac{\partial \bar{T}}{\partial t} \right) = - \left(\frac{p_0}{p} \right)^{\frac{R}{c_p}} \left(\bar{\mathbf{v}} \cdot \nabla_h \bar{\theta} + \bar{\omega} \frac{\partial \bar{\theta}}{\partial p} \right) \quad ; \quad \left(\frac{\partial \bar{q}}{\partial t} \right) = - \left(\bar{\mathbf{v}} \cdot \nabla_h \bar{q} + \bar{\omega} \frac{\partial \bar{q}}{\partial p} \right) \quad (30)$$

To solve this two equation system:

$$\left(\bar{T}, \bar{q}, T' \equiv \frac{1}{c_p} Q_1, q' \equiv \frac{1}{L} Q_2 \right) \quad (31)$$

you must have at least two types of closing conditions among the three possible choices [44]:

- Coupling of terms $\frac{\partial T}{\partial t}$ e $\frac{\partial q}{\partial t}$
- Coupling of terms Q_1 e Q_2
- Coupling of terms Q_1 e Q_2 with the two terms $\partial \bar{T} / \partial t$ e/o $\partial \bar{q} / \partial t$

The first choice is equivalent to assume a condition on the variation time of the system state (on a large scale) and is usually achieved by imposing a balance state condition.

The coupling of source terms, on the other hand, is a condition for the humid-convective processes and is usually present in the form of a cloud parameterization model. The combination of these two types of closure represents the methodological basis for those parameterization schemes known as

'adjustment schemes', like Arakawa and Schubert [45] and Betts and Miller [46–47] schemes. The third type of choice requires a direct coupling between large-scale circulation and humid-convective processes. It represents the starting point for many schemes, such as the Kuo [48] and Anthes [49] schemes and, starting from the Fritsch and Chappel [50] scheme, the Kain Fritsch [51] [44] scheme.

Thermal convection

Thermal convection [52–54] is a process of energy transport through the combined action of conduction, energy storage and mixing. At the molecular level, the thermal exchange by conduction, in fact, is accompanied by a transport of internal energy due to the relative motion of the particles. It is the most important heat exchange mechanism between a solid surface and a fluid (liquid or gas).

A necessary condition for the phenomenon to happen is that the fluid is placed, or can be placed, in relative motion with respect to the other body with which it exchanges heat.

Therefore convection can occur between a solid and a liquid, between a solid and an aeriform, between a liquid and an aeriform, but also between two inescapable liquids. In general it can be said that convection occurs within the fluid in a limited space that begins at the interface between the fluid and the other body and end at a distance that depends on the case under examination, but which is however somewhat reduced.

The transmission of energy by convection, from a surface whose temperature is higher than that of the surrounding fluid, takes place in different stages: first the heat passes by conduction from the surface to the adjacent fluid particles and the energy thus transmitted increases the internal energy and particle temperature.

Since the flow of heat from the surface to the fluid generates variations in the density of the fluid layers closest to it, a movement of the lighter fluid is generated upwards which, when meeting regions of the fluid at lower temperature, mixes with it giving part of the its energy to other particles [55–57]. Therefore there is a flow of both matter and energy, as this is stored in the particles and removed from their motion. Finally, when the heated fluid particles reach a lower temperature region, again the heat is transmitted by conduction from the warmer fluid particles to the colder ones (Fig. 17).

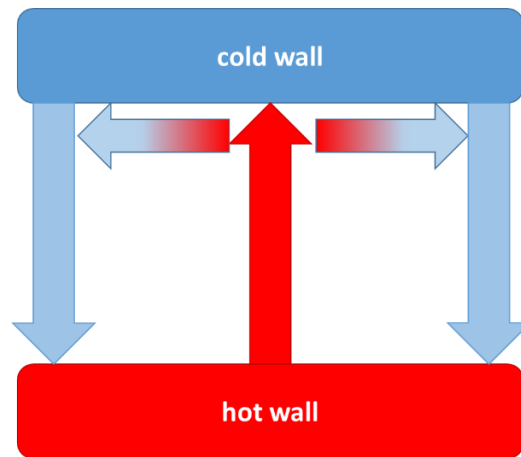


Fig. 17: Convection process scheme

Convection study

It is understandable that the fluid-dynamic phenomena are not independent from the thermal ones, the velocity field and that of the temperature in the fluid are closely connected and it follows that in the study of the convection the thermal and dynamic processes must be dealt with simultaneously. The thermofluidodynamic field is known when at any point the values of all the variables defining the kinematic and thermodynamic status of the fluid are known (possibly also as a function of time). In many cases, for the description of the thermo-fluid dynamics field five independent differential equations are required (two for the thermodynamic variables and three for the velocity components). Generally the five equations used are: the mass balance, the balance of the energy (each expressed by a scalar equation) and the equation of the momentum (which is a vector quantity) that is expressed through the three scalar equations of the components x , y , z . Given the complexity of the aforementioned equations and the difficulties in their solution even with numerical methods, experimental analysis of physical models is almost indispensable in the study of heat transfer by convection. The generalization of the experimental results occurs through the adimensional coefficients that characterize the studied physical configuration from the geometric and thermophysical point of view.

Dynamic limit layer

Consider the motion of a fluid along a flat plate. Assume that the motion is mainly in a direction parallel to the considered plate so as to be able to consider only the component of the parallel velocity precisely to the wall u . Sufficiently far from the wall we can consider $u = u_\infty$ (undisturbed current). Near the wall, the particles in contact with the surface itself assume zero speed.

These particles, due to the viscosity of the fluid, delay the motion of the adjacent particles up to a distance $y = \delta$ from the surface, distance at which the described effect becomes negligible. The different fluid particles moving at different speeds exert a tangential effort t , which acts along planes parallel to the plate. As the distance from the considered surface increases, the speed component parallel to the surface increases until the value of the undisturbed current u_∞ ; as the distance from the leading edge increases, the thickness d of the boundary layer increases, increasing the effects of viscosity in the flow. The region in which a significant velocity gradient is manifested is defined as a boundary layer, with a tangential effort proportional to the gradient itself; the local thickness d of the boundary layer is such that it results $u(\delta) = 0.99 u_\infty$. Fig. 18, highlights the development of the dynamic boundary layer on a flat plate. Assuming the Newtonian fluid, the tangential effort at the surface τ_s can be determined by:

$$\tau_s = \mu \left. \frac{\partial u}{\partial y} \right|_{x=0} \quad 32)$$

being μ [$kg / (m s)$] the dynamic viscosity.

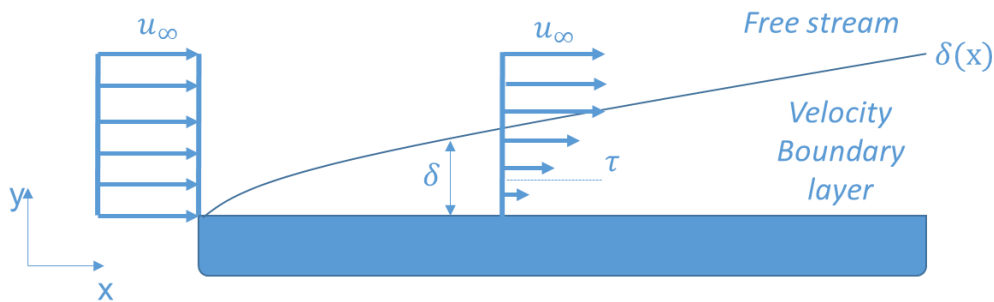


Fig. 18: Development of the dynamic boundary layer on a flat plate

Thermal limit layer

As for the dynamic boundary layer, in the vicinity of a wall touched by a fluid a thermal limit layer is manifested if there is a difference in temperature between the wall and the fluid. Consider a flat isothermal plate (at temperature T_w), lapped at the entrance by a fluid at temperature $T_\infty < T_w$. At the entrance the thermal profile is uniform, being $T(y) = T_\infty$. The fluid particles in contact with the plate assume the same temperature as that of the plate itself, thereby achieving thermal equilibrium. In turn, these particles exchange energy with the particles of the adjacent layers up to the thickness

δt beyond which it is verified that the temperature is equal to that of the undisturbed fluid T_∞ . In particular, the thickness of the thermal boundary layer is that for which it results:

$$\frac{(T_w - T)}{(T_w - T_\infty)} = 0,99 \quad (33)$$

As the distance from the leading edge increases, the thickness δt of the boundary layer increases, increasing the effects of heat exchange in the flow. It is interesting to note that, in the thermal limit layer, for a distance x any from the leading edge and for an infinitesimal surface dA , at distance $y = 0$ from the wall, the conductive heat exchange relation (calculated with the postulate of Fourier). Indicating with λ_f the thermal conductivity of the fluid [$W / (m \cdot K)$] we have:

$$q'' = -\lambda_f \left. \frac{\partial T}{\partial y} \right|_{y=0} \quad (34)$$

In truth, such a mechanism of energy transmission also takes place in the successive layers at a distance $y > 0$ from the wall when the fluid is in laminar motion. If the fluid is characterized by laminar motion, the heat exchange in a direction perpendicular to the fluid motion takes place by conduction only. A drastically different situation, on the other hand, is that relating to turbulent motion. In this case, the particle-to-particle heat conduction mechanism is enhanced by the establishment of innumerable vortices that favor the exchange of internal energy between the different fluid zones.

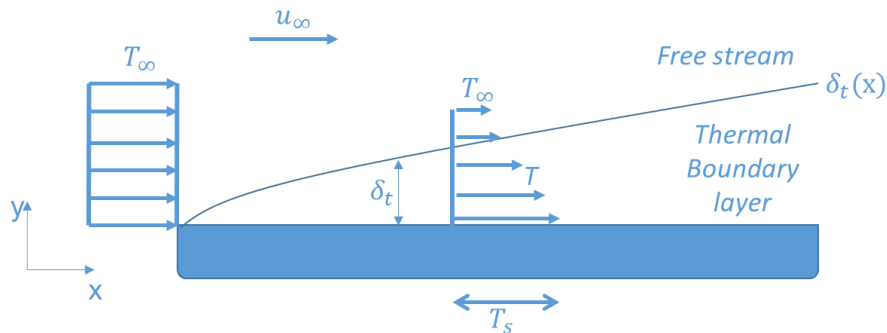


Fig 19: Development of the dynamic boundary layer on a flat plate

However, the practical cases in which the convection phenomenon is characterized only by laminar-type fluid motion are an exception. In fact, in most cases, both types of motion are present in the convection phenomenon: the laminar motion in fact distinguishes areas of fluid close to the wall while the turbulent motion characterizes areas of fluid that are a bit more distant from the wall. The transition from one type of motion to the other takes place gradually so that, in a fluid region

intermediate to the two preceding ones, a mixed type of motion is generated. It is clear then at this point how fluid motion and convection are intimately connected phenomena and therefore in examining any problem of convection it is first necessary to specify the motion regime.

The description of the convection

Consider a temperature fluid T_∞ moving at a velocity V along a surface of area A and an arbitrary shape. This surface has a uniform temperature T_w different from T_∞ . The thermal flux q'' exchanged by convection between surface and fluid at any point of the considered area can be expressed by the Newton relation:

$$q'' = h \cdot (T_w - T_\infty) \quad (35)$$

wherein h is the local heat transfer coefficient by convection, $[W / (m^2K)]$.

The thermal power exchanged q from the entire surface A , since the conditions of motion vary along the surface itself, will be obtained by:

$$q = \int_A q'' dA = (T_\infty - T_w) \cdot \int_A h \cdot dA \quad (36)$$

or, by defining a coefficient of heat exchange by mean convection \bar{h} as:

$$q = \bar{h} \cdot A \cdot (T_\infty - T_w) \quad (37)$$

Given the value of h it is possible to evaluate the flow of heat, so its determination is the fundamental problem of thermal convection. Unfortunately, giving a value to h is not easy since it depends both on the properties of the fluid (viscosity, density, thermal conductivity, specific heat) and on the geometrical configuration and on the motion conditions. In the thermal limit layer, at a general distance x from the leading edge and for an infinitesimal surface dA , at distance $y = 0$ from the wall, it is possible to apply the heat exchange relation. This relationship equals the convective and the conductive thermal flow (calculated with the Fourier postulate). Indicating with the thermal conductivity of the fluid $[W / (m \times K)]$, one has:

$$q'' = h \cdot (T_w - T_\infty) = -\lambda_f \left. \frac{\partial T}{\partial y} \right|_{y=0} \quad (38)$$

On the surface, since there is no fluid motion, the thermal energy is transferred by conduction. The convective exchange coefficient can therefore be expressed as follows:

$$h = \frac{-\lambda_f \left. \frac{\partial T}{\partial y} \right|_{y=0}}{(T_w - T_\infty)} \quad 39)$$

which indicates the strong influence of the temperature gradient on the fluid-wall separation surface on the convective heat exchange. If one relates to a length L characterizing the geometry of the system (pipe diameter, wall length) the previous equation becomes, after having multiplied both members by L:

$$q'' = L \cdot h \cdot (T_w - T_\infty) = -L \cdot \lambda \cdot \left. \frac{\delta T}{\delta y} \right|_{y=0} \Rightarrow L \frac{h}{\lambda} = -\frac{L}{(T_w - T_\infty)} \cdot \left. \frac{\delta T}{\delta y} \right|_{y=0} \quad 40)$$

The dimensionless grouping:

$$N_u = L \cdot \frac{h}{\lambda} \quad 41)$$

takes the name of the Nusselt number and represents the ratio between the heat that is exchanged by convection, between the surface and the fluid, and the heat that the same surface exchanges by conduction through a layer of stationary fluid of thickness L. The greater the value of the Nusselt number the greater the influence of mass transport in the heat exchange.

The method for the study of convection, dimensional analysis

In the study of convection the fundamental objective is the evaluation of the convection coefficient. Given the difficulty in solving analytically the constituent equations mentioned previously, in the study of convection it is almost essential to resort to experimental investigation on physical models, supported by dimensional analysis. This method makes it possible to generalize the experimental results by means of pure numbers, each of which constitutes a grouping of some of the physical quantities on which the convective phenomenon depends (which come into play in the description of the phenomenon). In practice, for similar geometrical situations and for boundary conditions of the same type, particular equations are obtained experimentally, which allow the calculation of h. These equations are equal to each other if each of the pure numbers assumes the same value in the different physical systems under examination. The pure numbers are derived on the basis of Buckingham's theorem. According to this theorem if an equation, which describes a physical phenomenon, is dimensionally homogeneous (if changing the units of measurement does not change the equation) it can be reduced to a relation between a complete set of dimensionless groups. By complete series we mean that each group is independent, it can not be obtained by a linear combination from the others. The starting equation must be of the type:

$$f(x_1, x_2, x_3, x_4, x_5, \dots, x_n) = 0 \quad (42)$$

in this case:

$$f(d, \omega, \rho, \mu, \lambda, c_p, h) = 0 \quad (43)$$

in explicit form with respect to the convective heat exchange coefficient h:

$$h = f(d, \omega, \rho, \mu, \lambda, c_p) \quad (44)$$

According to Buckingham's theorem, if n are the quantities in play and m the fundamental quantities involved (in our case: length, mass, time, temperature) the phenomenon can be treated in terms of $n - m$ adimensional groups linked together by a relationship of the type:

$$(\Pi_1, \Pi_2, \Pi_3, \dots, \Pi_{n-m}) = 0 \quad (45)$$

$$\Pi_1 = F(\Pi_2, \Pi_3, \dots, \Pi_{n-m-1}) = 0$$

The link between these dimensionless groups can be an experientially derived empirical relationship. Experiments are arranged in such a way as to vary the value of the groups one at a time and thus go back to an analytic relationship. Hence the opportunity that these groups, even if they are adimensional, represent groupings of quantities with a physical meaning, even if their dimensions mutually elide: as for example the Reynolds number represents the relationship between inertial forces and forces of friction.

If these groups contain quantities that represent the geometric (d) and thermophysical characteristics of the physical system, the solution, or the relationship between the dimensionless groups from which h is obtainable, can be generalized as a function of these characteristics.

We obtain relationships that link the following adimensional parameters to each other, from these relations, in particular from that which defines the Prandtl number, it is possible to derive the value of the convective exchange coefficient:

- Reynolds number: as already mentioned, it represents the relationship between inertial forces and friction forces:

$$Re = \frac{\rho dw}{\mu} \quad (46)$$

- Nusselt Number: Represents the real impact of convective mechanisms in the thermal exchange achieved:

$$Nu = \frac{h L}{\lambda_f} \quad (47)$$

- Prandtl Number: represents the relationship between the availability of the fluid to transport momentum and its availability to transport heat. It depends on the nature of the medium and its physical state. It is defined as follows:

$$Pr = \frac{c_p \mu}{\lambda_f} = \frac{v}{a} \quad (48)$$

- Grashof Number: represents the relationship between the floating inertia forces on one side and the friction forces squared on the other:

$$Gr = \frac{g \beta (T_s - T_\infty) L^3}{v^2} \quad (49)$$

The meaning of the symbols shown in the previous equations is as follows:

ρ = fluid density [kg / m^3];

w = average fluid velocity [m / s];

μ = dynamic viscosity [$kg / (m \cdot s)$];

v = kinematic viscosity [m^2 / s] = μ / ρ ;

a = thermal diffusivity [m^2 / s];

λ_f = thermal conductivity of the fluid [$W / (m K)$];

L = characteristic geometric size [m].

β = coefficient of thermal expansion, defined by:

$$\beta = -\frac{1}{\rho} \left(\frac{\partial \rho}{\partial T} \right)_p \quad \beta \approx -\frac{1}{\rho} \frac{\rho_\infty - \rho}{T_\infty - T} \quad \beta \approx \frac{1}{T} \quad (50)$$

The relationship that is found experimentally between the aforementioned pure numbers is generally of the type:

$$Nu = f(Re, Gr, Pr) \quad 51)$$

Or, with a relationship that interpolates the experimental data:

$$Nu = C \cdot Re^a \cdot Gr^b \cdot Pr^c \quad 52)$$

Experimentally determined the coefficient C and the exponents a, b, c it is possible to calculate with the relation obtained the value of h for physically similar situations. It is thus possible to perform measurements on models and extend their validity to real situations.

Forced convection

Many applications concern thermal exchanges with fluids whose motion is caused by the action of pumps, fans, etc. in this case we speak of forced convection and for a certain geometry, one has:

$$Nu = f(Re, Pr) \quad 53)$$

Inertia forces and viscous forces are important, while floating ones are neglected (so Grashof number does not appear). Ultimately, for a given geometry, the Nusselt number Nu must be a function of Re and Pr . Knowing this function from the experimental investigation, also for different fluids with different values of w and L , it is possible to determine that of h and, therefore, the heat flux exchanged by convection locally.

Obviously the type of function for the same system will be different depending on whether you are in conditions of laminar motion or turbulent motion (conditions identified by the value of the Reynolds number).

Natural convection

In natural convection, the motion of the fluid is due to the presence of floating forces, that is, to the simultaneous presence of a field of volume forces (eg gravitational forces) and to the density gradient of the fluid. Inertial and viscous forces remain important, but a more important role is played by floating forces.

Also for the natural convection, the number of Nusselt Nu can be determined as a function of other adimensional parameters, which, in this case, are Gr and Pr :

$$Nu = f(Gr, Pr) \quad 54)$$

Since the Rayleigh number (Ra) is equal to:

$$Ra = Gr \cdot Pr = \frac{g\beta(T_s - T_\infty)L^3}{\nu a} \quad (55)$$

it is possible to write also:

$$Nu = f(Ra) \quad (56)$$

Also for natural convection the type of function for the same system will be different depending on whether you are in laminar or turbulent motion conditions. The conditions of the motion can be identified by the value of the Rayleigh number. For flat and cylindrical vertical walls, the turbulent flow occurs at values of Ra equal to 10^9 .

The ratio Gr/Re^2 indicates the importance of the buoyancy forces with respect to those of inertia (forced convection effect), infact one has:

$$\frac{g\beta(T_s - T_\infty)L}{u_0^2} = \frac{Gr}{Re_L^2} \quad (57)$$

If $Gr \ll Re^2$ the effects of natural convection can be neglected.

If $Gr \gg Re^2$ the effects of forced convection are negligible compared to the importance of the floating forces.

If Gr and Re^2 are of the same order of magnitude it are in a mixed convection regime.

Tests of the model performance

The WRF model is configured to run with different resolution till 0.8 km of grid spacing. It run twice a day at 00 and 12 UTC. In Table 2 are shown the characteristics of the different run in use at Messina University:

RUN	Grid spacing	Forecast time	Time step	Initialization data	Number of daily run
ARW 10 km	10 km	120 h	1 h	GFS 0.25 °	2 (00,12z)
ARW 3.3 km	3.3 km	72 h	1 h	UNIME 10KM Nesting	2 (00,12z)
ARW 1.1 km	1.1 km	36 h	1 h	UNIME 3KM Nesting	2 (00,12z)

Table 2: Characteristics of the different run of the WRF model in use at Messina University

The configurations of the physics parameterizations are show in the Table 3:

CU parameterization	Betts-Miller-Janjic - Explicit
Microphysics parameterization	Thompson
Shortwave radiation option	RRTMG
Longwave radiation option	RRTMG
Surface layer option	Eta Similarity Scheme
Land surface option	Unified Noah Land Surface Model
Planetary Boundary Layer scheme	Mellor-Yamada-Janjic MYJ

Table 3: Configurations of the physics parameterizations of the WRF model in use at Messina University

Below are the main outputs produced by the WRF model, to which are added secondary outputs produced by post-production software such as UPP (Unified Post Processor, produced by NCEP), NCL (NCAR Command Language, produced by NCAR) and VAPOR (Visualization and Analysis Platform for Ocean, Atmosphere, and Solar Researchers, for 3D post-production):

LU_INDEX	LAND USE CATEGORY (-)
VAR_SSO	VARIANCE OF SUBGRID-SCALE OROGRAPHY (M2)
LAP_HGT	LAPLACIAN OF OROGRAPHY (M)
U	X-WIND COMPONENT (M S-1)
V	Y-WIND COMPONENT (M S-1)
W	Z-WIND COMPONENT (M S-1)
PH	PERTURBATION GEOPOTENTIAL (M2 S-2)
PHB	BASE-STATE GEOPOTENTIAL (M2 S-2)
T	PERTURBATION POTENTIAL TEMPERATURE (THETA-T0) (K)
MU	PERTURBATION DRY AIR MASS IN COLUMN (PA)
MUB	BASE STATE DRY AIR MASS IN COLUMN (PA)
P	PERTURBATION PRESSURE (PA)
PB	BASE STATE PRESSURE (PA)
P_HYD	HYDROSTATIC PRESSURE (PA)
Q2	QV AT 2 M (KG KG-1)

T2	TEMP AT 2 M (K)
TH2	POT TEMP AT 2 M (K)
PSFC	SFC PRESSURE (PA)
U10	U AT 10 M (M S-1)
V10	V AT 10 M (M S-1)
QVAPOR	WATER VAPOR MIXING RATIO (KG KG-1)
QCLOUD	CLOUD WATER MIXING RATIO (KG KG-1)
QRAIN	RAIN WATER MIXING RATIO (KG KG-1)
QSNOW	SNOW MIXING RATIO (KG KG-1)
CWM	TOTAL CONDENSATE MIXING RATIO (KG KG-1)
SHDMAX	ANNUAL MAX VEG FRACTION (-)
SHDMIN	ANNUAL MIN VEG FRACTION (-)
SNOALB	ANNUAL MAX SNOW ALBEDO IN FRACTION (-)
TSLB	SOIL TEMPERATURE (K)
SMOIS	SOIL MOISTURE (M3 M-3)
SH2O	SOIL LIQUID WATER (M3 M-3)
SMCREL	RELATIVE SOIL MOISTURE (-)
SEAICE	SEA ICE FLAG (-)
XICEM	SEA ICE FLAG (PREVIOUS STEP) (-)
SFROFF	SURFACE RUNOFF (MM)
UDROFF	UNDERGROUND RUNOFF (MM)
IVGTYP	DOMINANT VEGETATION CATEGORY (-)
ISLTYP	DOMINANT SOIL CATEGORY (-)
VEGFRA	VEGETATION FRACTION (-)
GRDFLX	GROUND HEAT FLUX (W M-2)
ACGRDFLX	ACCUMULATED GROUND HEAT FLUX (J M-2)
ACSNOM	ACCUMULATED MELTED SNOW (KG M-2)

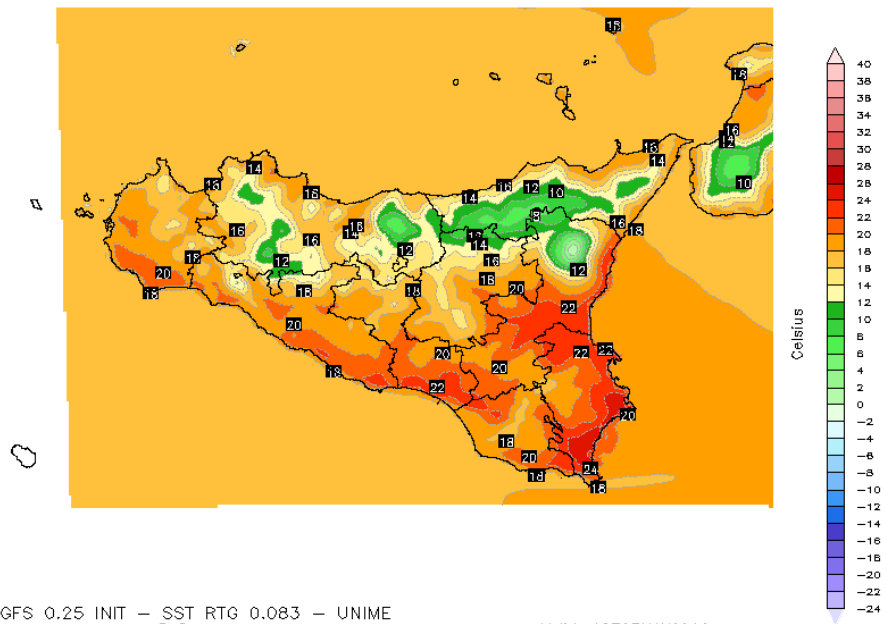
SNOW	SNOW WATER EQUIVALENT (KG M-2)
SNOWH	PHYSICAL SNOW DEPTH (M)
CANWAT	CANOPY WATER (KG M-2)
SSTSK	SKIN SEA SURFACE TEMPERATURE (K)
LAI	LEAF AREA INDEX (M-2/M-2)
VAR	OROGRAPHIC VARIANCE (-)
TKE_PBL	TKE FROM PBL (M2 S-2)
EL_PBL	LENGTH SCALE FROM PBL (M)
F_ICE_PHY	FRACTION OF ICE (-)
F_RAIN_PHY	FRACTION OF RAIN (-)
F_RIMEF_PH	MASS RATIO OF RIMED ICE (-)
HGT	TERRAIN HEIGHT (M)
TSK	SURFACE SKIN TEMPERATURE (K)
RAINC	ACCUMULATED TOTAL CUMULUS PRECIPITATION (MM)
RAINSH	ACCUMULATED SHALLOW CUMULUS PRECIPITATION (MM)
RAINNC	ACCUMULATED TOTAL GRID SCALE PRECIPITATION (MM)
SNOWNC	ACCUMULATED TOTAL GRID SCALE SNOW AND ICE (MM)
GRAUPELNC	ACCUMULATED TOTAL GRID SCALE GRAUPEL (MM)
HAILNC	ACCUMULATED TOTAL GRID SCALE HAIL (MM)
CLDFRA	CLOUD FRACTION (-)
SWDOWN	DOWNWARD SHORT WAVE FLUX AT GROUND SURFACE (W M-2)
GLW	DOWNWARD LONG WAVE FLUX AT GROUND SURFACE (W M-2)
SWNORM	NORMAL SHORT WAVE FLUX AT GROUND SURFACE (SLOPE-DEPENDENT) (W M-2)
OLR	TOA OUTGOING LONG WAVE (W M-2)
ALBEDO	ALBEDO (-)

ALBBCK	BACKGROUND ALBEDO (-)
EMISS	SURFACE EMISSIVITY (-)
NOAHRES	RESIDUAL OF THE NOAH SURFACE ENERGY BUDGET ($W M^{-2}$)
TMN	SOIL TEMPERATURE AT LOWER BOUNDARY (K)
XLAND	LAND MASK (1 FOR LAND, 2 FOR WATER) (-)
UST	U^* IN SIMILARITY THEORY ($M S^{-1}$)
PBLH	PBL HEIGHT (M)
HFX	UPWARD HEAT FLUX AT THE SURFACE ($W M^{-2}$)
QFX	UPWARD MOISTURE FLUX AT THE SURFACE ($KG M^{-2} S^{-1}$)
LH	LATENT HEAT FLUX AT THE SURFACE ($W M^{-2}$)
ACHFX	ACCUMULATED UPWARD HEAT FLUX AT THE SURFACE ($J M^{-2}$)
ACLHF	ACCUMULATED UPWARD LATENT HEAT FLUX AT THE SURFACE ($J M^{-2}$)
SNOWC	FLAG INDICATING SNOW COVERAGE (1 FOR SNOW COVER) (-)
SR	FRACTION OF FROZEN PRECIPITATION (-)
SST	SEA SURFACE TEMPERATURE (K)
PRESSURE	MODEL PRESSURE (HPA)
GEOPT	GEOPOTENTIAL (M^2/S^2)
HEIGHT	MODEL HEIGHT (KM)
TK	TEMPERATURE (K)
TC	TEMPERATURE (C)
THETA	POTENTIAL TEMPERATURE (K)
TD	DEWPOINT TEMPERATURE (C)
TD2	DEWPOINT TEMPERATURE AT 2M (C)
RH	RELATIVE HUMIDITY (%)
CLFLO	LOW CLOUD FRACTION (%)
CLFMI	MID CLOUD FRACTION (%)

CLFHI	HIGH CLOUD FRACTION (%)
RH2	RELATIVE HUMIDITY AT 2M (%)
WSPD	WIND SPEED (M S-1)
WDIR	WIND DIRECTION (DEGREES)
WS10	WIND SPEED AT 10 M (M S-1)
WD10	WIND DIRECTION AT 10 M (DEGREES)
UMET	ROTATED WIND COMPONENT (M S-1)
VMET	ROTATED WIND COMPONENT (M S-1)
U10M	ROTATED WIND COMPONENT (M S-1)
V10M	ROTATED WIND COMPONENT (M S-1)
SLP	SEA LEVEL PRESSURE (HPA)
DBZ	REFLECTIVITY (-)
MAX_DBZ	MAX REFLECTIVITY (-)
CAPE	CAPE (J/KG)
CIN	CIN (J/KG)
MCAPE	MCAPE (J/KG)
MCIN	MCIN (J/KG)
LCL	LCL (METERS AGL)
LFC	LFC (METERS AGL)

Operational production began on March 26, 2016. From this date, the model produces daily meteorological parameters maps, such as:

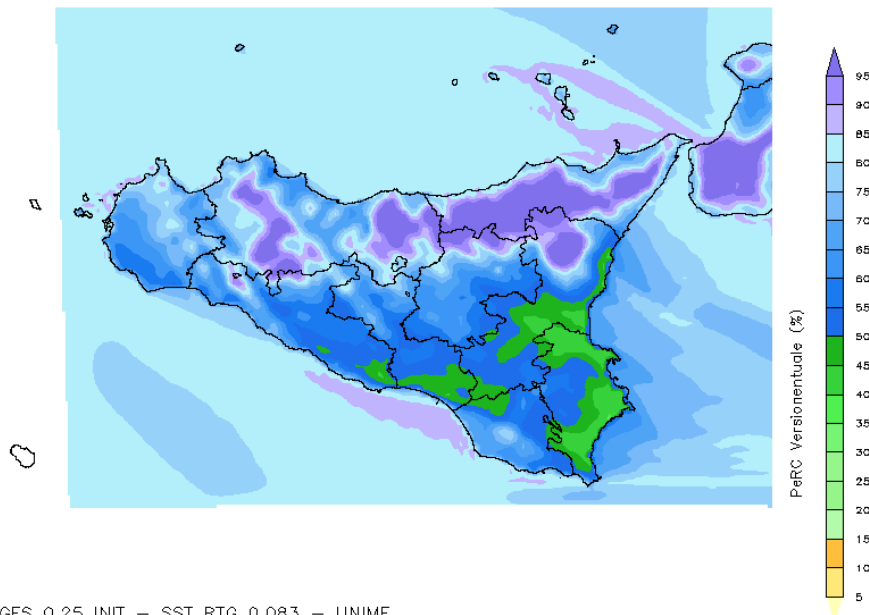
Ground temperature (2 meters)



GFS 0.25 INIT - SST RTG 0.083 - UNIME
Temperatura 2m [C]
WRF-ARW 3KM,run:00Z03MAY2016

Valid: 12Z03MAY2016
UNIME (C) 2016 / + 12H

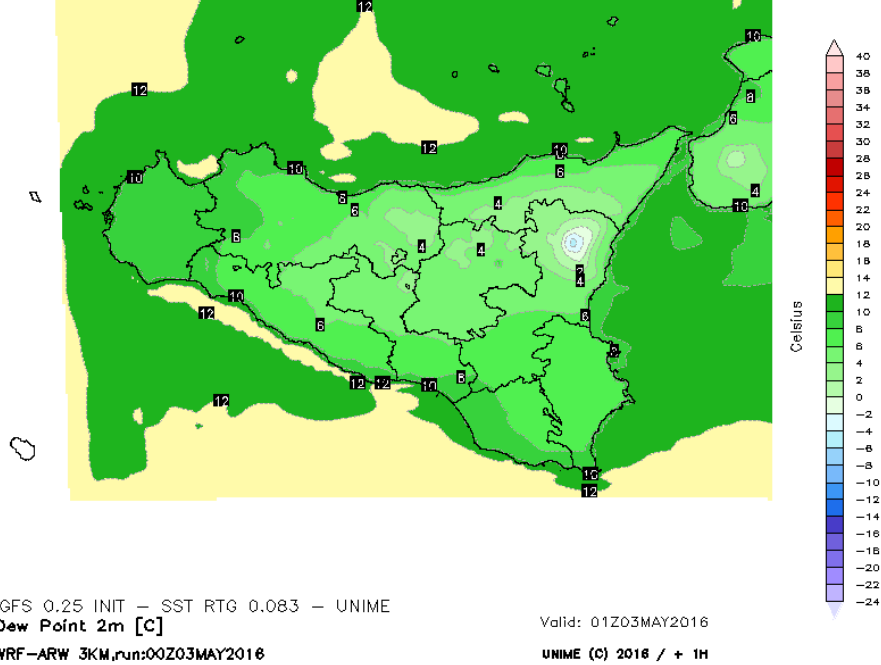
Relative moisture 2 meters:



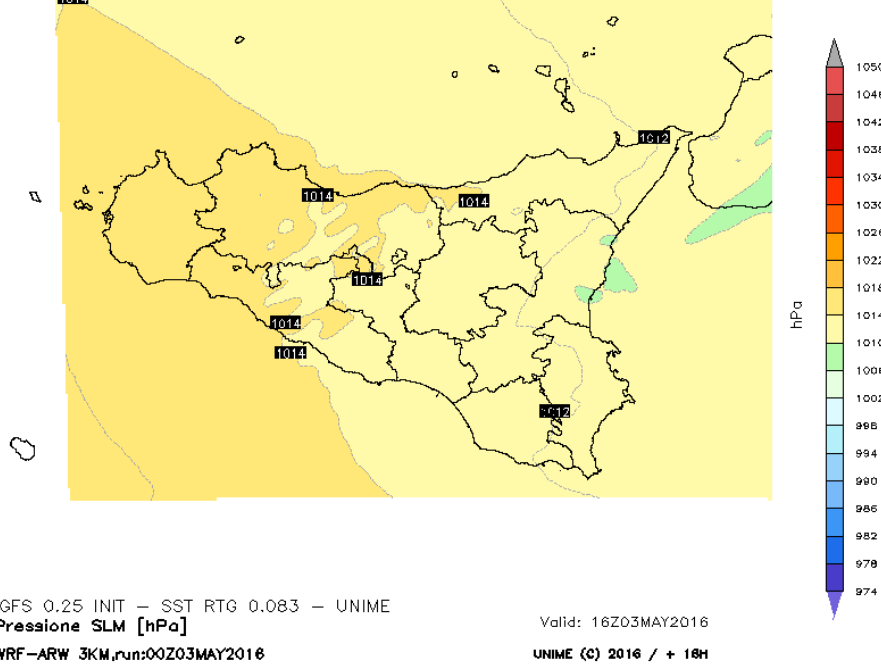
GFS 0.25 INIT - SST RTG 0.083 - UNIME
Umidita a 2 Metri (%)
WRF-ARW 3KM,run:00Z03MAY2016

Valid: 10Z03MAY2016
UNIME (C) 2016 / + 10H

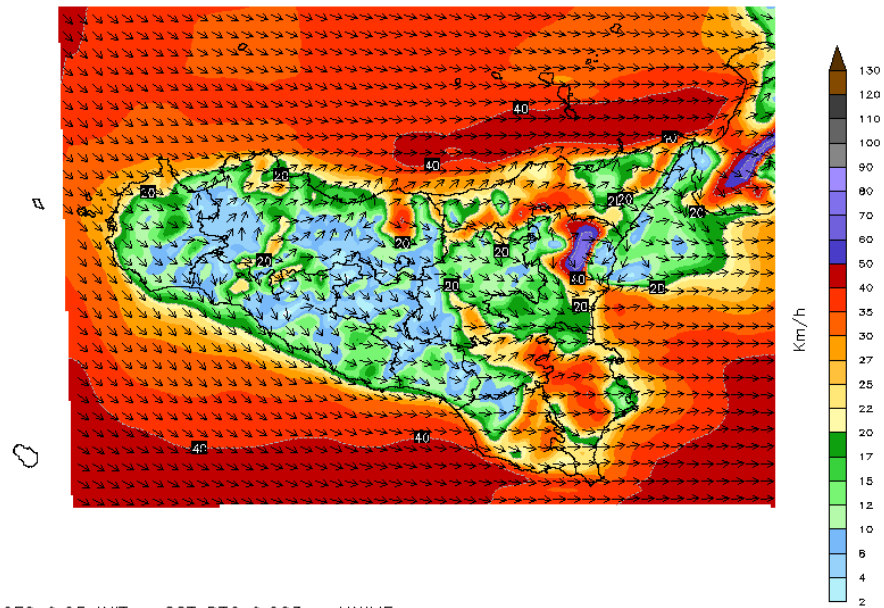
Dew Point 2 meters::



Pressure On sea level



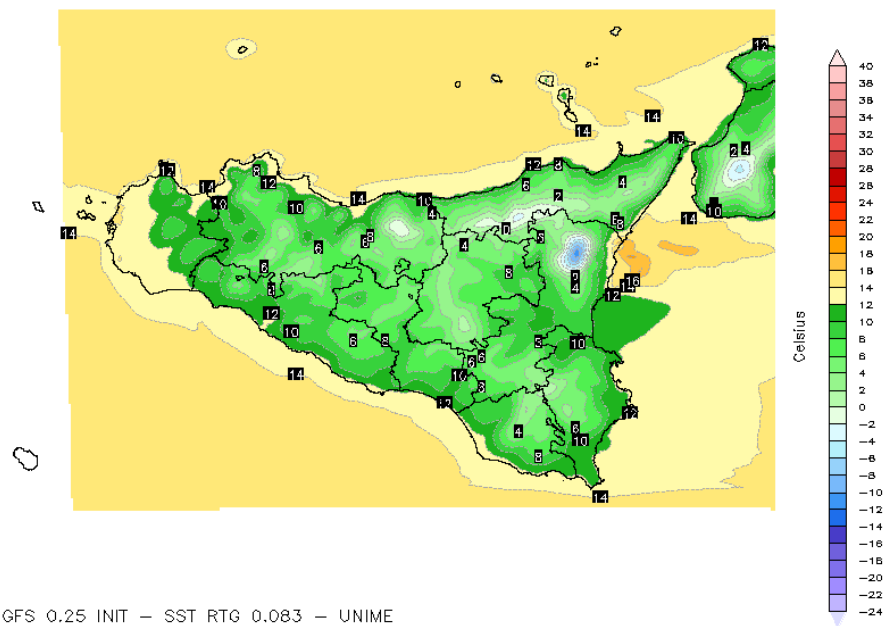
Wind 10 meters:



GFS 0.25 INIT - SST RTG 0.083 - UNIME
Venti a 10 m (Km/h)
WRF-ARW 3KM, run: 00Z03MAY2016

Valid: 01Z03MAY2016
UNIME (C) 2016 / + 1H

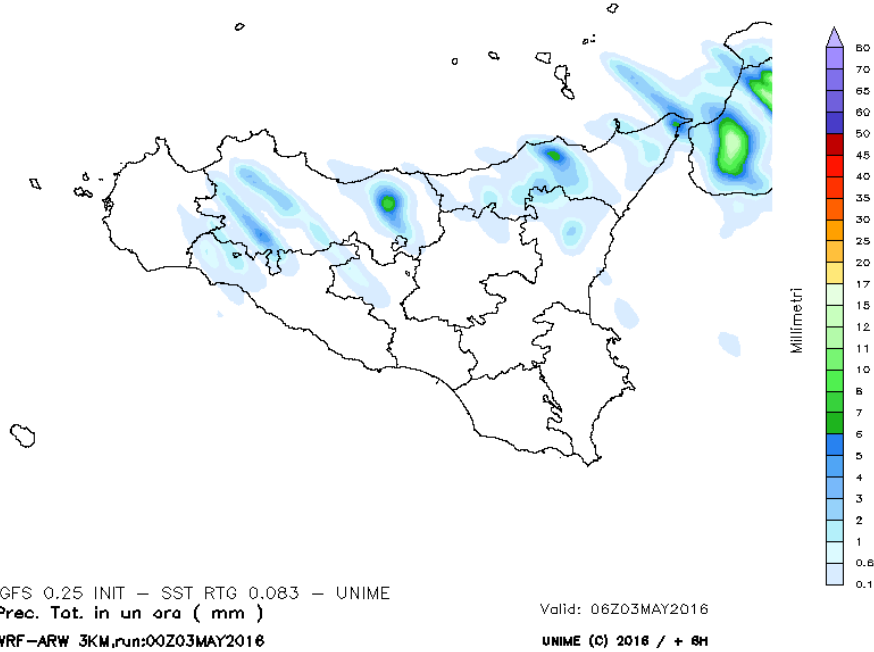
Wind Chill:



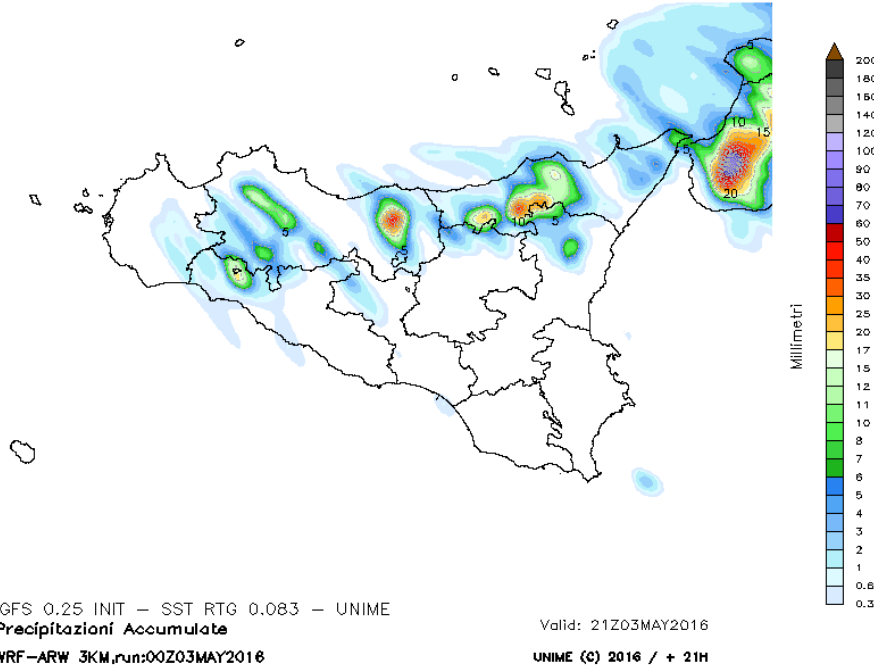
GFS 0.25 INIT - SST RTG 0.083 - UNIME
Wind Chill Index
WRF-ARW 3KM, run: 00Z03MAY2016

Valid: 05Z03MAY2016
UNIME (C) 2016 / + 5H

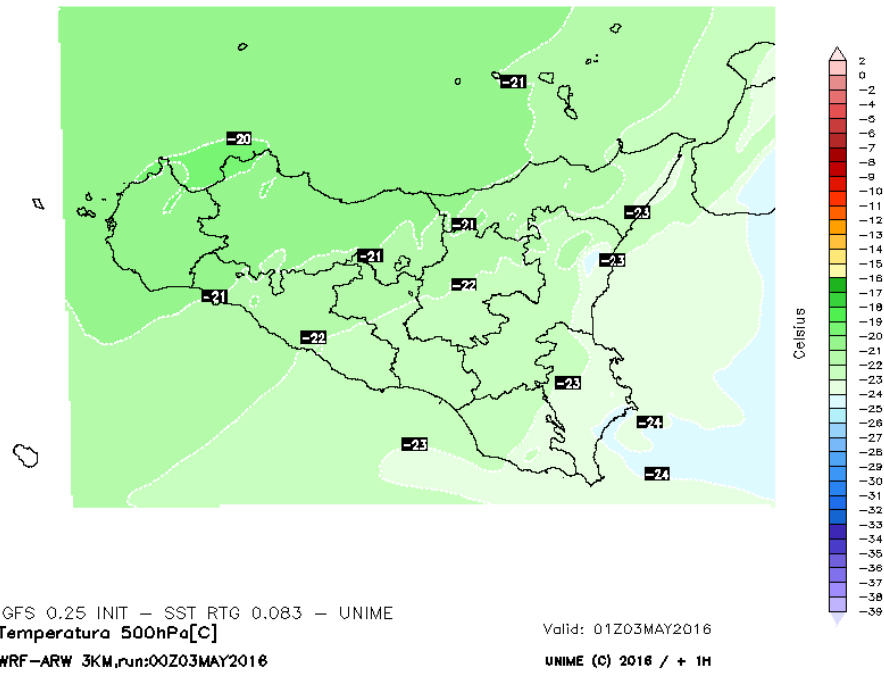
Rain 1 hour:



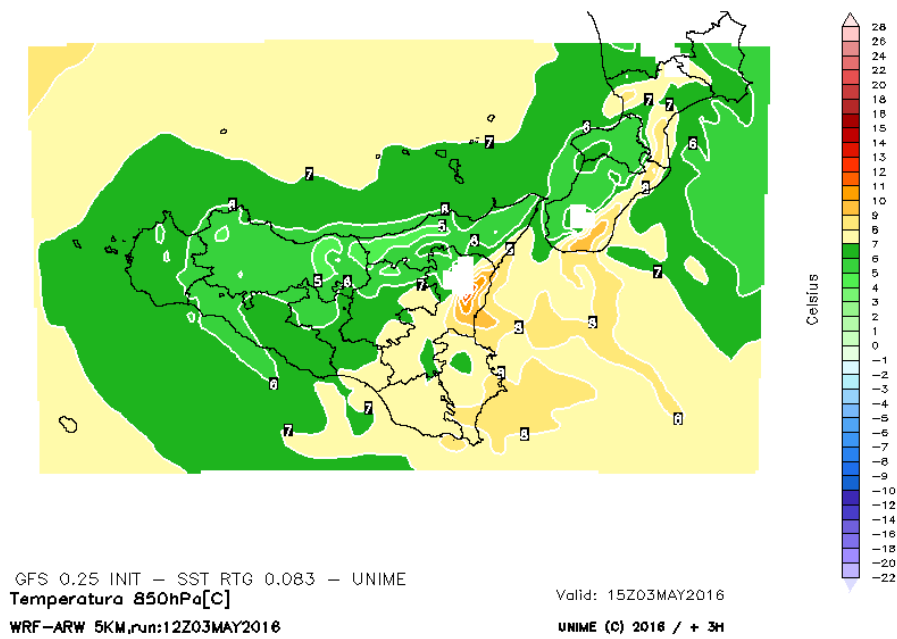
Rain accumulated:



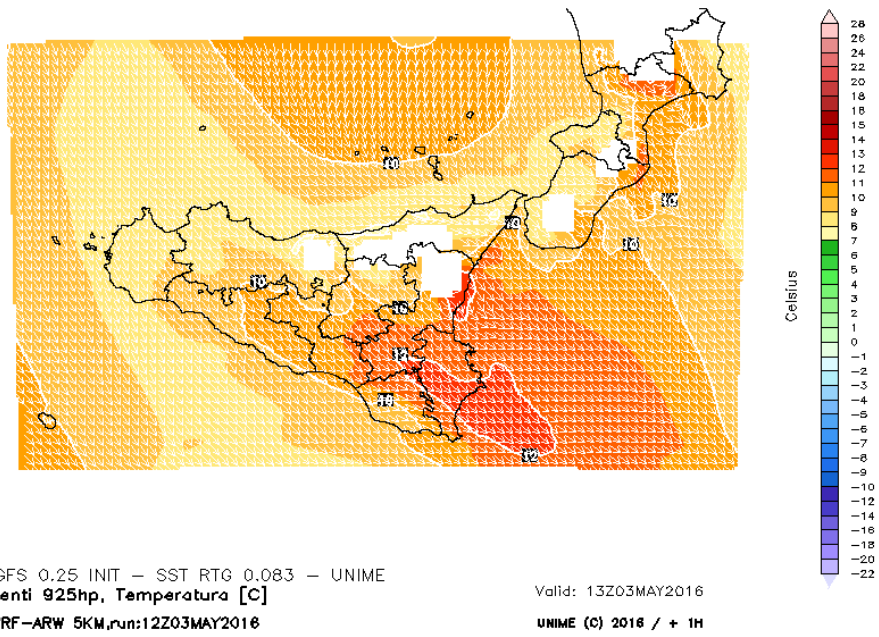
Temperatures at 500hPa:



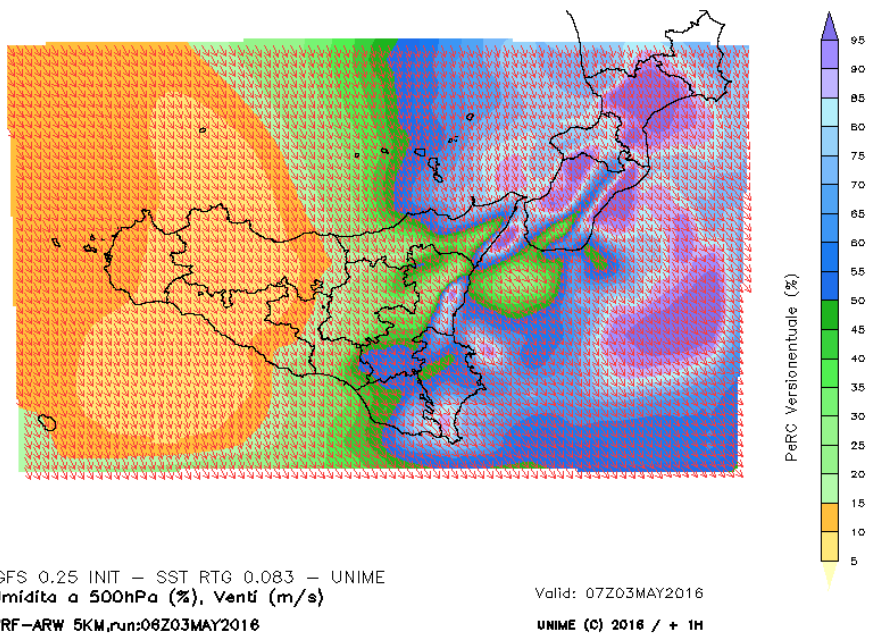
Temperatures at 850 hPa:



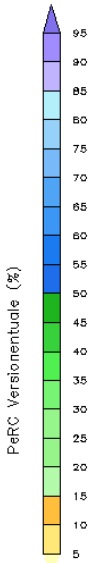
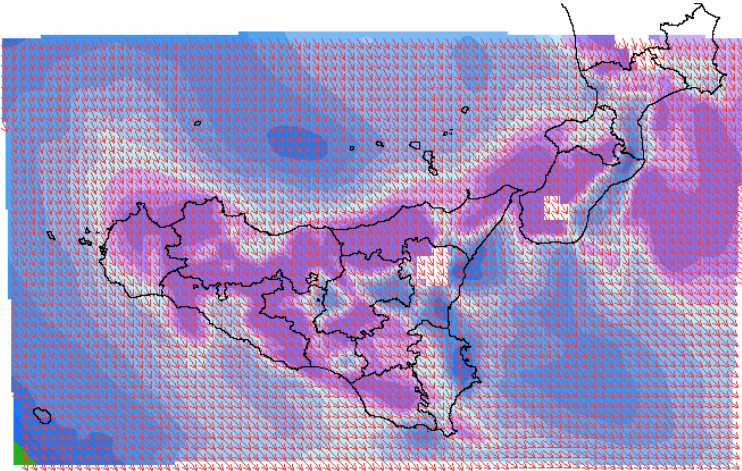
Temperature and winds at 925 hPa:



Moisture and Winds at 500hPa:



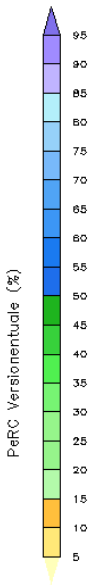
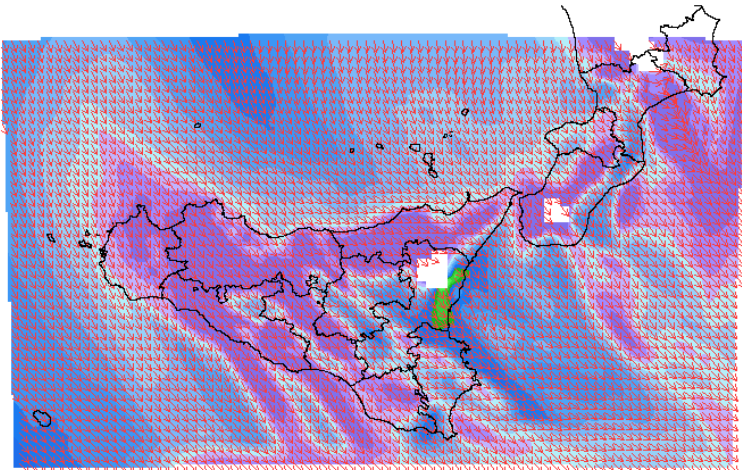
Moisture and Winds at 700hPa:



GFS 0.25 INIT - SST RTG 0.083 - UNIME
 Umidità a 700hPa (%), Venti (m/s)
 WRF-ARW 5KM,run:12Z03MAY2016

Valid: 13Z03MAY2016
 UNIME (C) 2016 / + 1H

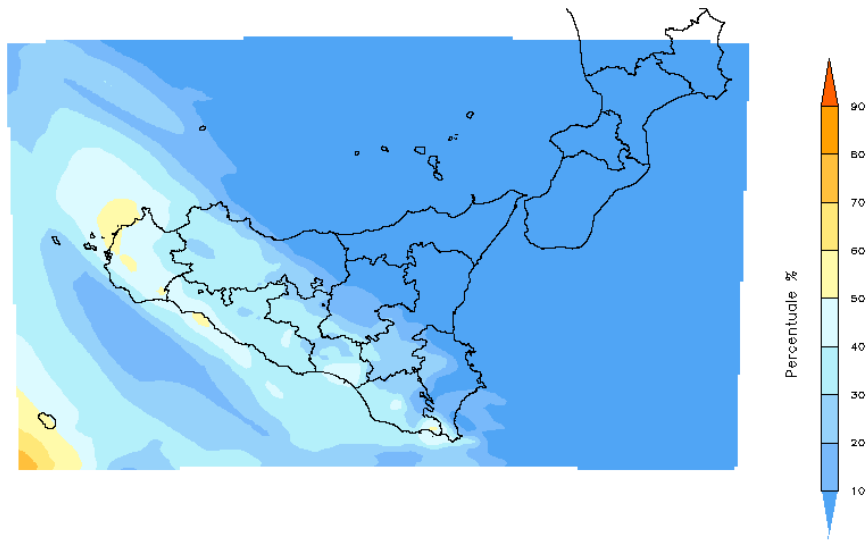
Moisture and Winds at 850hPa:



GFS 0.25 INIT - SST RTG 0.083 - UNIME
 Umidità a 850hPa (%), Venti (m/s)
 WRF-ARW 5KM,run:06Z03MAY2016

Valid: 12Z03MAY2016
 UNIME (C) 2016 / + 6H

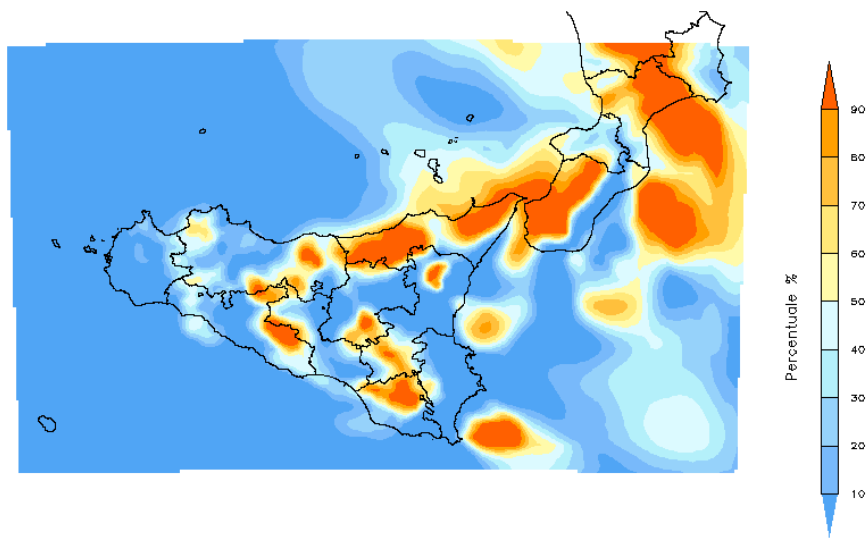
High clouds:



GFS 0.25 INIT - SST RTG 0.083 - UNIME
Nubi alte (%)
WRF-ARW 5KM,run:12Z03MAY2016

Valid: 12Z06MAY2016
UNIME (C) 2016 / + 72H

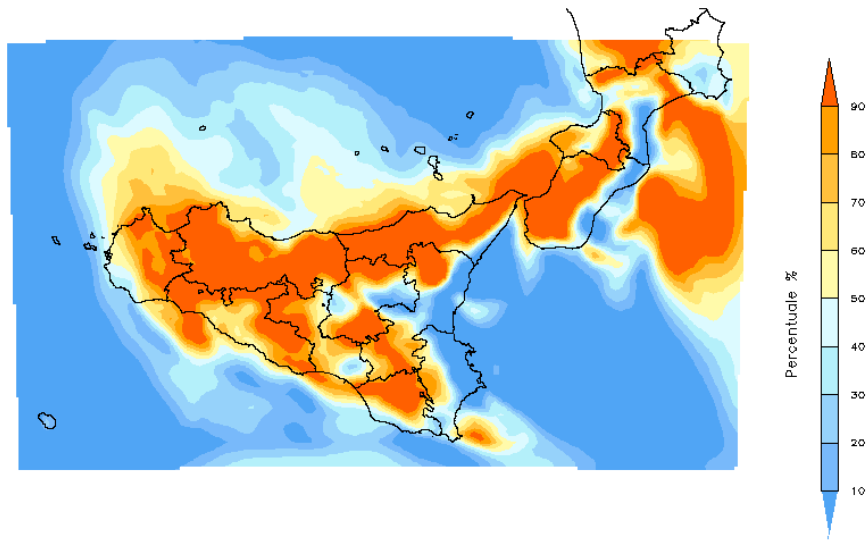
Medium clouds:



GFS 0.25 INIT - SST RTG 0.083 - UNIME
Nubi medie (%)
WRF-ARW 5KM,run:12Z03MAY2016

Valid: 13Z03MAY2016
UNIME (C) 2016 / + 1H

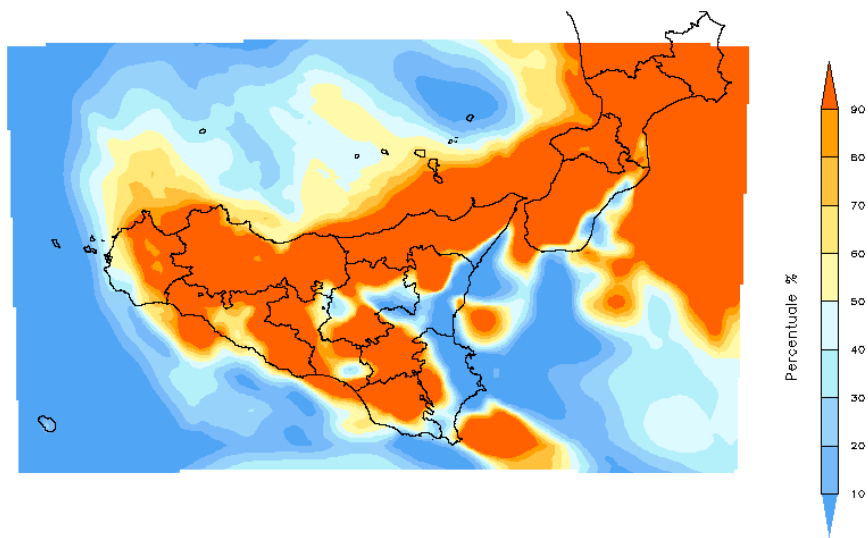
Low clouds:



GFS 0.25 INIT - SST RTG 0.083 - UNIME
Nubi basse (%)
WRF-ARW 5KM,run:12Z03MAY2016

Valid: 13Z03MAY2016
UNIME (C) 2016 / + 1H

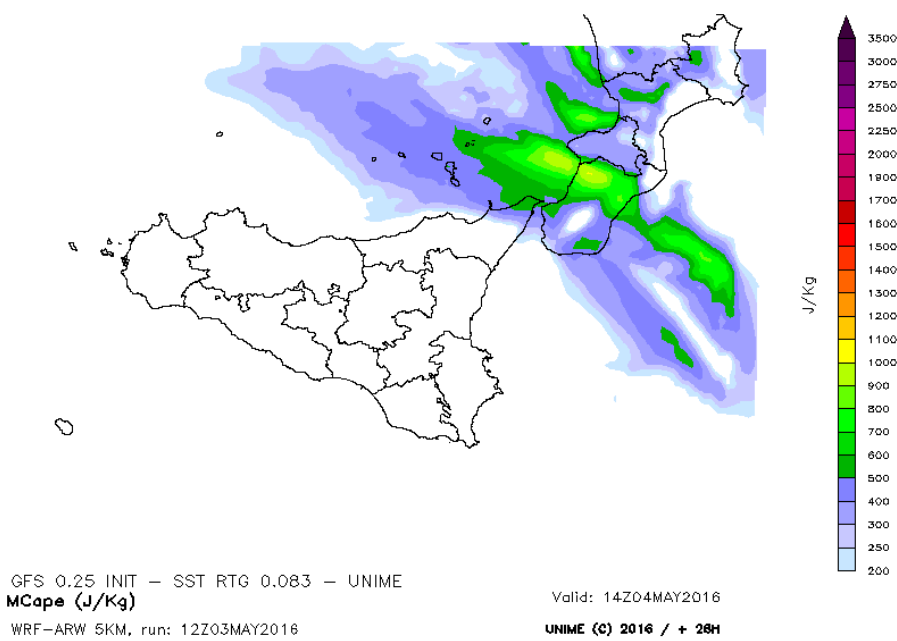
Total clouds:



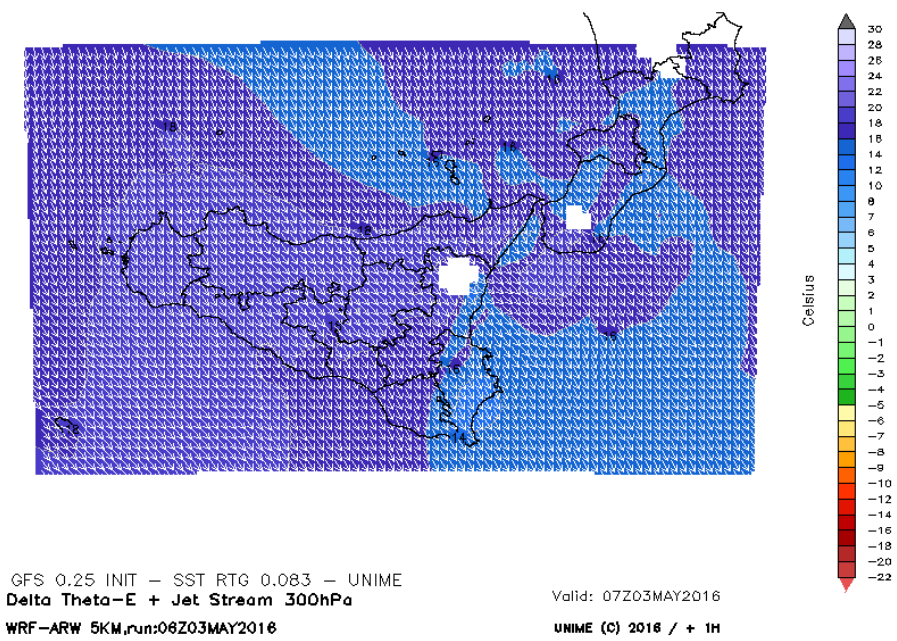
GFS 0.25 INIT - SST RTG 0.083 - UNIME
Nuvolosit totale (%)
WRF-ARW 5KM,run:12Z03MAY2016

Valid: 13Z03MAY2016
UNIME (C) 2016 / + 1H

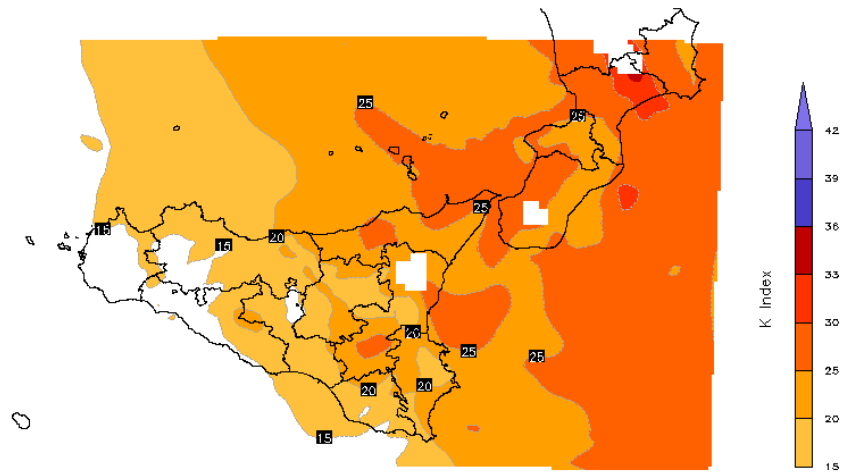
M CAPE:



ThetaE:



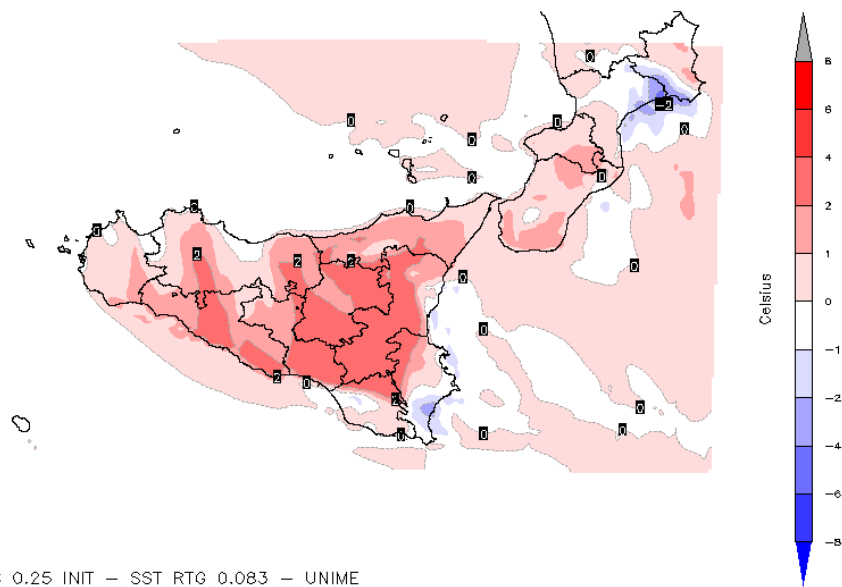
K index:



GFS 0.25 INIT - SST RTG 0.083 - UNIME
K Index
WRF-ARW 5KM, run: 12Z03MAY2016

Valid: 13Z03MAY2016
UNIME (C) 2016 / + 1H

Difference of temperatures to 2 meters in 24 hours:



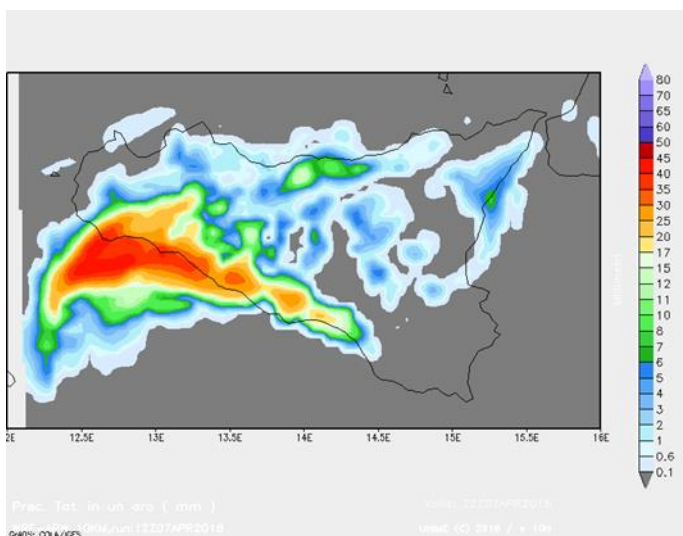
GFS 0.25 INIT - SST RTG 0.083 - UNIME
Diff. Temperatura 2m vs 24h prec.
WRF-ARW 5KM, run: 12Z03MAY2016

Valid: 16Z04MAY2016
UNIME (C) 2016 / + 28H

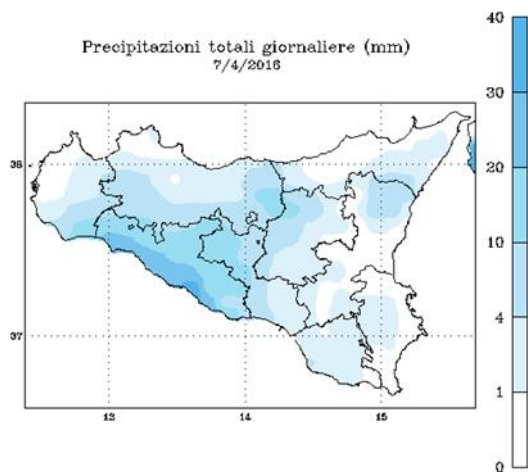
On the quality of the above products, first tests were carried out, the results of which are described:

- 7 April 2016:

Synoptic description: The day was characterized by the presence of a depression system located in the south-west of Sicily in slow movement towards the east. This situation has recalled a flow of hot and moisture currents from the southern quadrants, which has invested in particular the south-western coasts of the island, causing widespread rainfall on Agrigento and Trapani. Precipitations of an orographic nature also occurred on the slopes of the Peloritani mountains exposed to the flows.

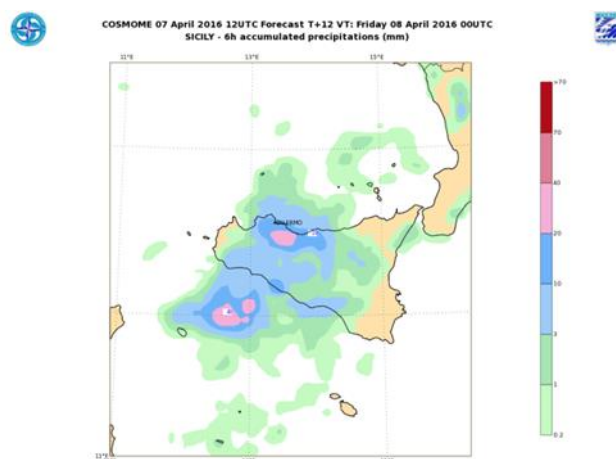
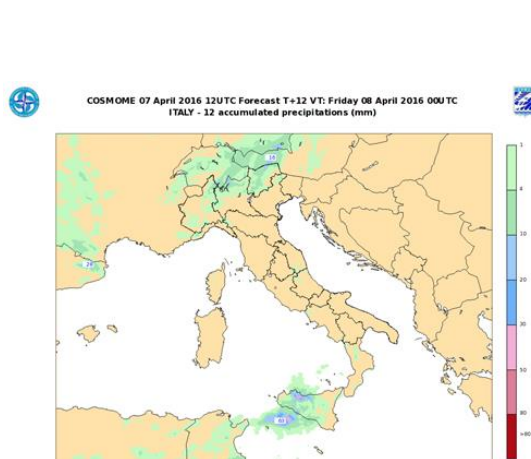


WRF model



Rain observed by SIAS network

As shown in the figure, the performances of the WRF model are in perfect agreement with the rains observed by the SIAS meteorological station network. The following maps show the prediction elaborated by the COSMO-ME model:



The meteorological forecast, elaborated by the COSMO-ME model, overestimates the rains on the Palermo and underestimates the rains of the Agrigento area.

Also on 7 April a run was performed with a spatial resolution of 1 km, centered on the area of the province of Messina that allowed to obtain the sequence of accumulated rains. Each image is obtained with time steps, i.e. with a sampling time of one hour.

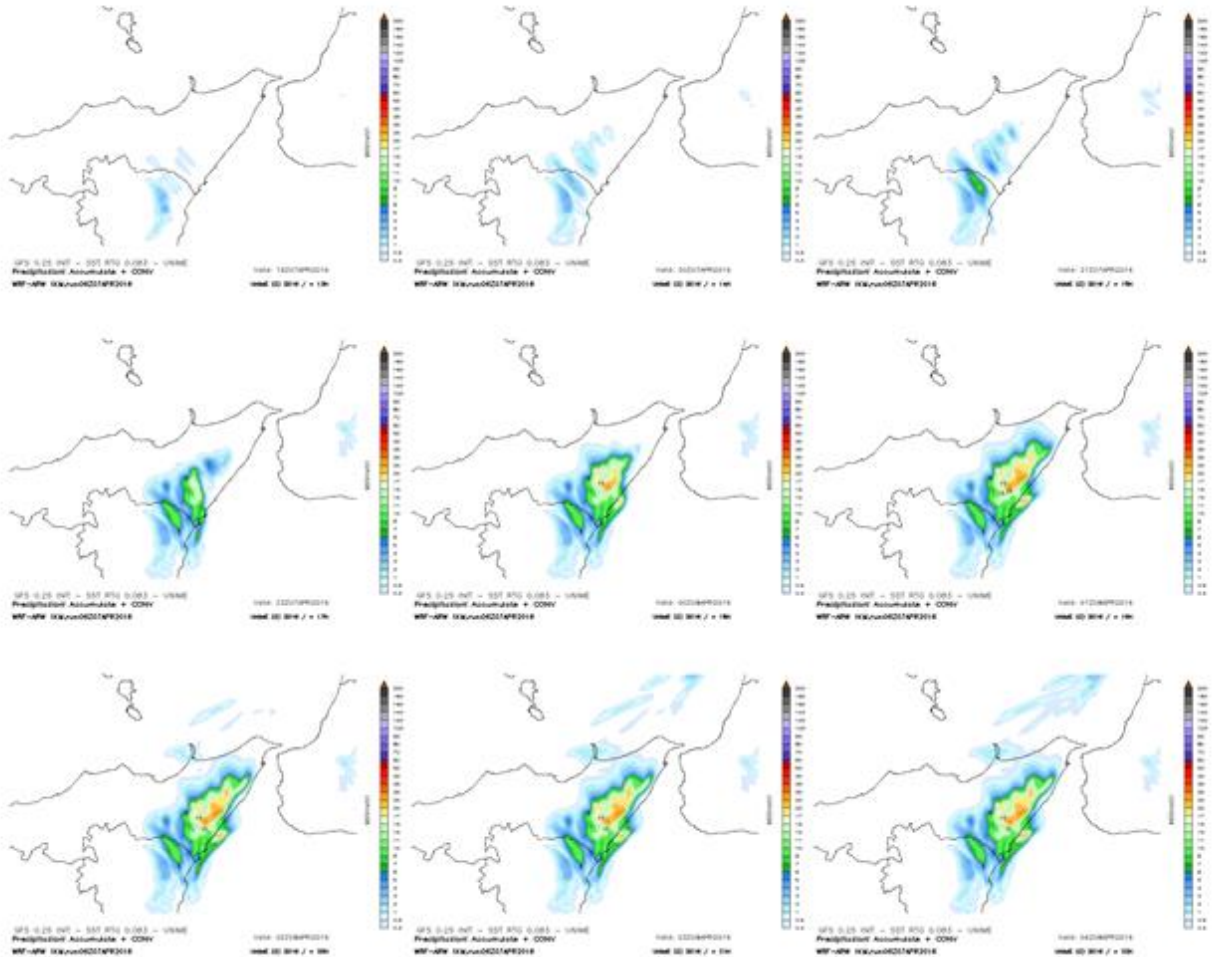


Fig. 20: Run with a spatial resolution of 1 km, centered on the area of the province of Messina. It allowed to obtain the sequence of accumulated rains. Each image is obtained with one hour time steps.

- 8 April 2016

Synoptic description: Southern flows continue to affect Sicily. The 10-meter wind forecast maps produced on the experimental sub-domain at 1 km on the area of the province of Messina are shown.

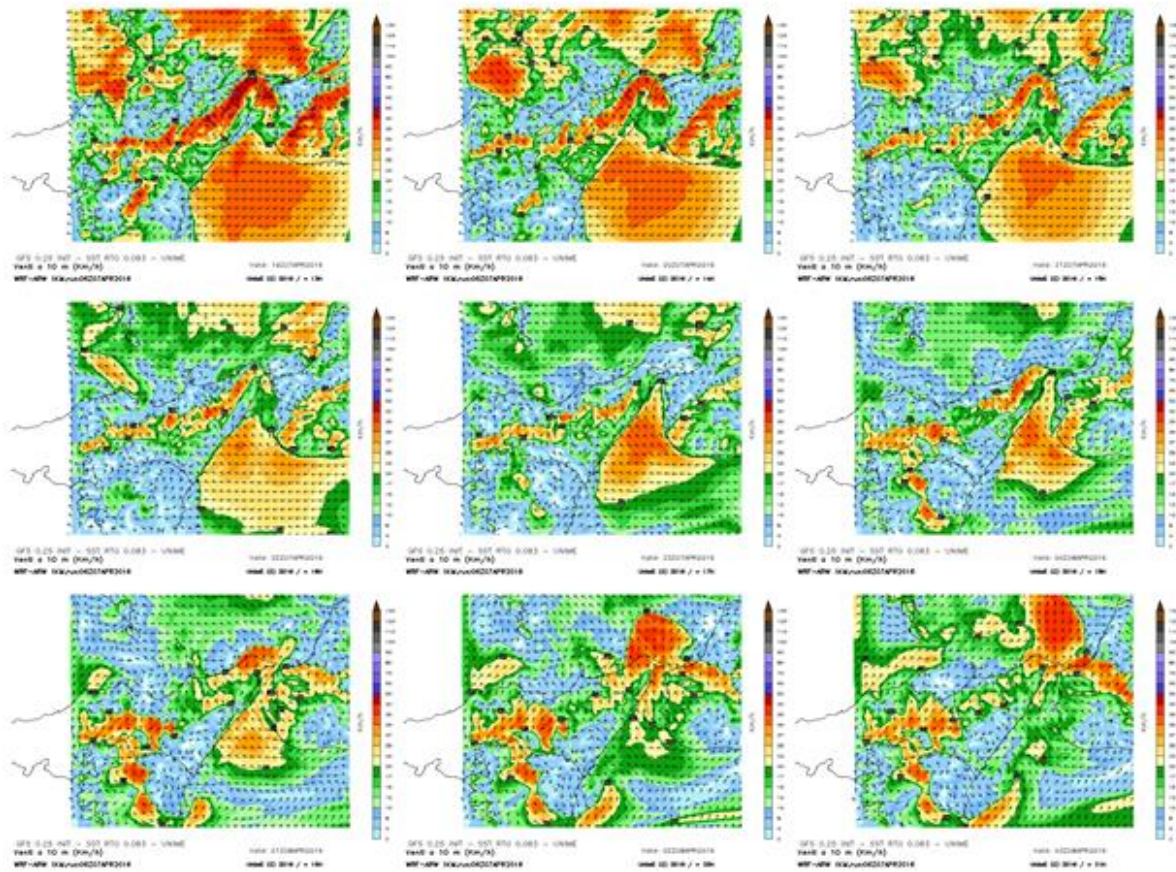


Fig. 21: The 10-meter wind forecast maps produced on the experimental sub-domain at 1 km on the area of the province of Messina are shown.

The maps also show the effect of channeling the flow operated by the Strait of Messina.

- 12 April 2016

Synoptic description: Sicily is hit by intense winds of hot air generated by the expansion of the North African subtropical anticyclone. Temperatures reach for the first time during the year high values, above 30 degrees with peaks of around 34 degrees on limited areas of Syracuse.

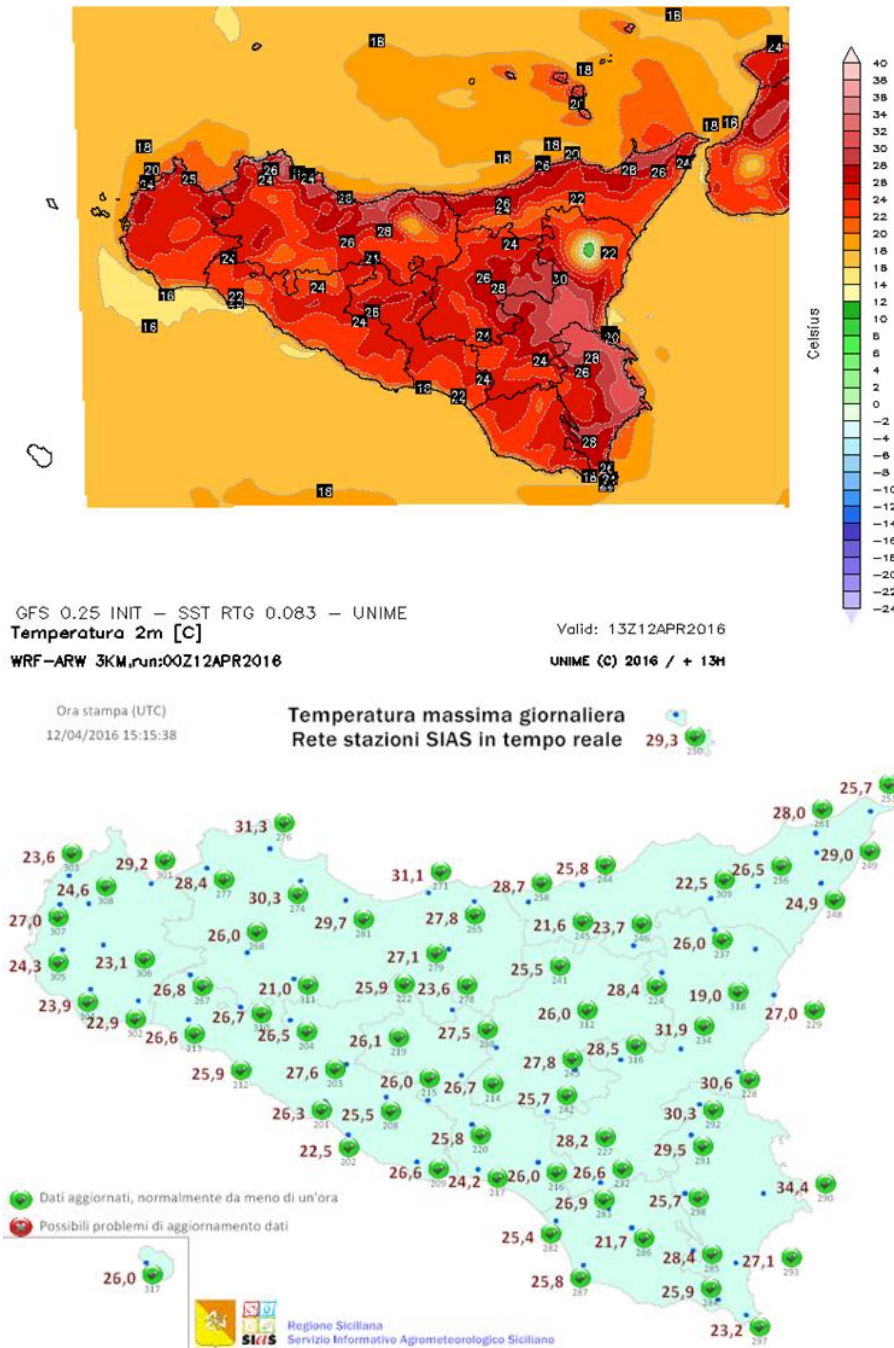


Fig. 22: Maps produced by the WRF-UNIME model run on 12 April 2016 00UTC (up) compared to the data collected by the SIAS observing network (down)

Case Study

- **10th October 2015**

The selected case study concerns a recent flood event that occurred in Messina in the early hours of 10 October 2015 [58]. In the case study, the Antillo meteorological station, which is a unit of a Dipartimento Regionale della Protezione Civile – Regional Civil Protection Department (DRPC) weather stations network, recorded, from 00 to 09 UTC, a maximum precipitation accumulation of 175,4 mm. The heavy rains occurred, were the results of a mesoscale convective system developed in the Ionian Sea and powered the low atmospheric layers by the very humid Southeastern streams [59-60]. Another important element that triggered the violent thunderstorm was the orographic lift induced by the barrier of Nebrodi and Peloritani Mountains, together with the one induced by Mt. Etna (Fig. 23).



Fig. 23: 3D Orography of the eastern coast of Sicily between Catania and Messina

The surface analysis chart at 00:00 UTC of 10 October 2015, shows a low-pressure system centered over the Central Mediterranean Sea, originating a Mediterranean cyclone, with its warm branch extended between the Southern coast of Sardinia and the Greek coast, while the cold branch was affecting the North to South, all over Tunisia. The winds on the Eastern Sicily reinforced maintaining

a S-S-E component. The air temperatures were a few degrees lower than the sea surface one. The weather station of Messina reported thunderstorms (Fig. 24a).

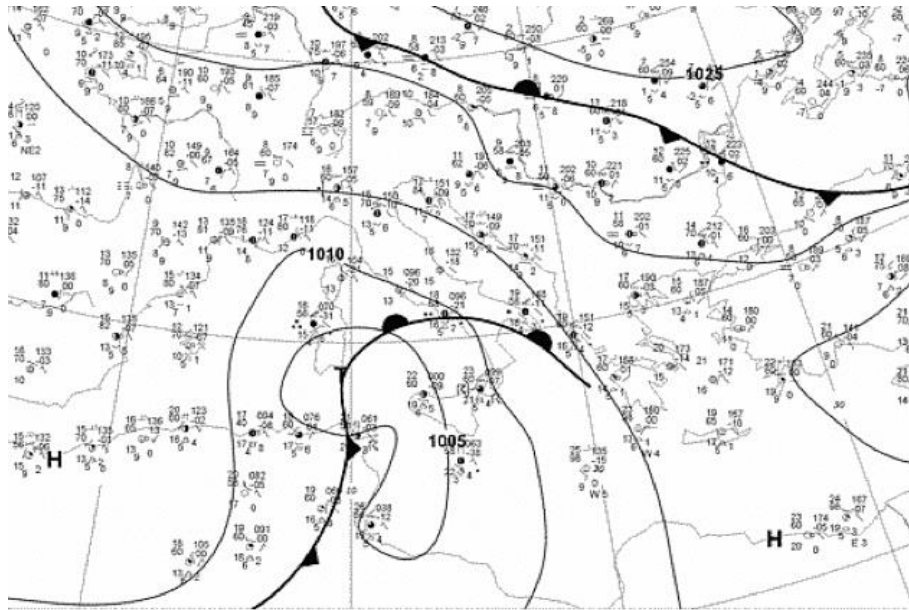


Fig. 24 a: Time shots of surface maps at 00:00 UTC on 10 October 2015.

At 06:00 UTC of 10 October 2015, the low-pressure over Southern Sardinia deepened reaching values below 1000 hPa. The cold air approached the Western coast of Sicily reduced the temperature by 6-8 degrees. The winds along the eastern coast of Sicily maintained a southern component, while all the Sicilian weather stations have registered thunderstorms (Fig. 24 b).

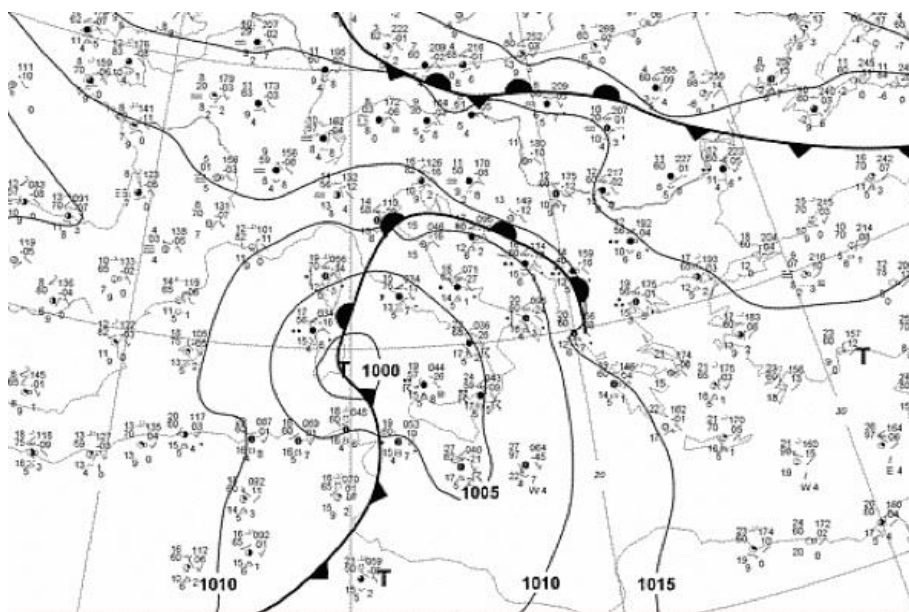


Fig. 24 b: Time shots of surface maps at 06:00 UTC on 10 October 2015.

At 12:00 UTC of 10 October 2015, the low pressure moved to the central Tyrrhenian sea, maintaining pressure values below 1000 hPa. The cold front crosses all of Sicily, also affecting the Central Tyrrhenian Sea and Malta (Fig. 24 c).

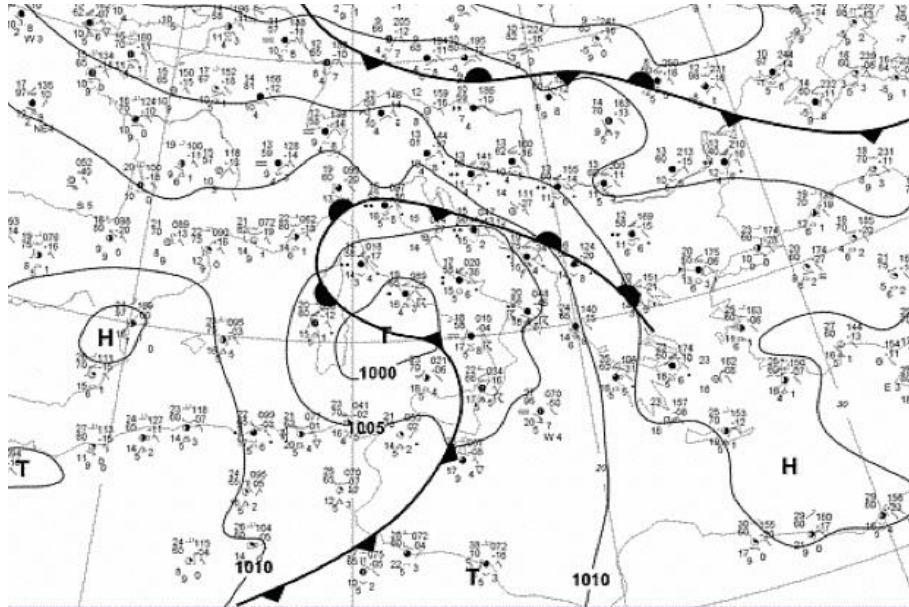


Fig. 24 c: Time shots of surface maps at 12:00 UTC on 10 October 2015.

The synoptic analysis allowed us to formulate the following hypotheses about the causes that led to the event:

1. The intense S-E flux, affected the Ionian coast throughout the whole event interval and it funneled huge volumes of warm air from Libya to the central Tyrrhenian Sea. In addition to the heat content, this air mass was self-enriched with water vapor, largely drawn from the Gulf of Sirte, where SST ranged between 25°C and 26° C, as registered by the Italian Air Force Weather Service. These circumstances allowed the air masses with high values of equivalent potential temperature to rise in the lower atmosphere layers. Then, the potential energy available for convection (CAPE), reached peak values higher than 4000 J/kg on the Southern seas of Sicily (GFS model analysis data). Under such circumstances, both the Alcantara Valley and the side valleys of the Peloritani chain played a key role in conveying high volumes of *warm and moist air* to advance for several tens of kilometers inland;
2. The forced lifting due to the Peloritani Chain, which turns almost perpendicularly to the ground flow, facilitated the warm and moist air mass initial lift, and the same occurred to the SE air streams due to Mt. Etna;

3. The arrival of a little pulse of cool air, probably connected to the action of a convective cell in Western Sicily made it possible for the development of the entire cluster of storms, according to the well known "multicell cluster storm" scheme.

The outcome of the above-mentioned factors was the development of two convective cells, visible in the 03.00 UTC infrared image (Fig. 25), which affected the entire Ionian coast of Sicily with heavy rainfalls and severe thunderstorms [61].

In other words, it can be inferred that the trigger of this event was an initial lift of a layer of warm air next to the surface, supported in its upward movement by the high altitude flow perturbation produced by Mt. Etna, due to strong upper-air southwesterly wind streams.

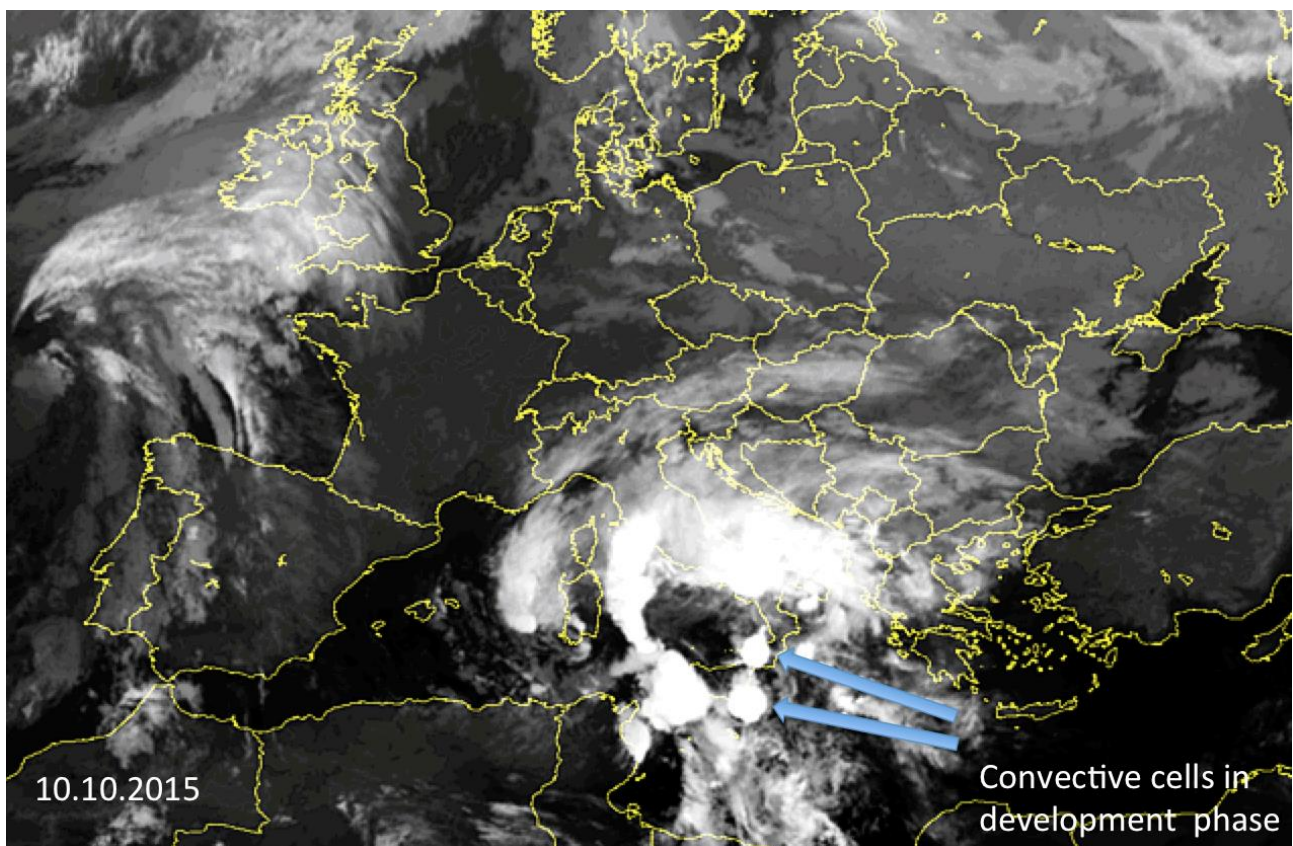


Fig. 25: Thermal infrared MSG image at 03.00 UTC of 10 October 2015.

Despite the short duration, these phenomena were powerful enough to produce a greater accumulation of rain of 175 mm, as recorded by Antillo weather station (Fig. 26). This quantity of rain was sufficient to determine the Mela creek overflow and the flash flood that occurred in Milazzo and Barcellona Pozzo di Gotto, both located on the Tyrrhenian coastline.

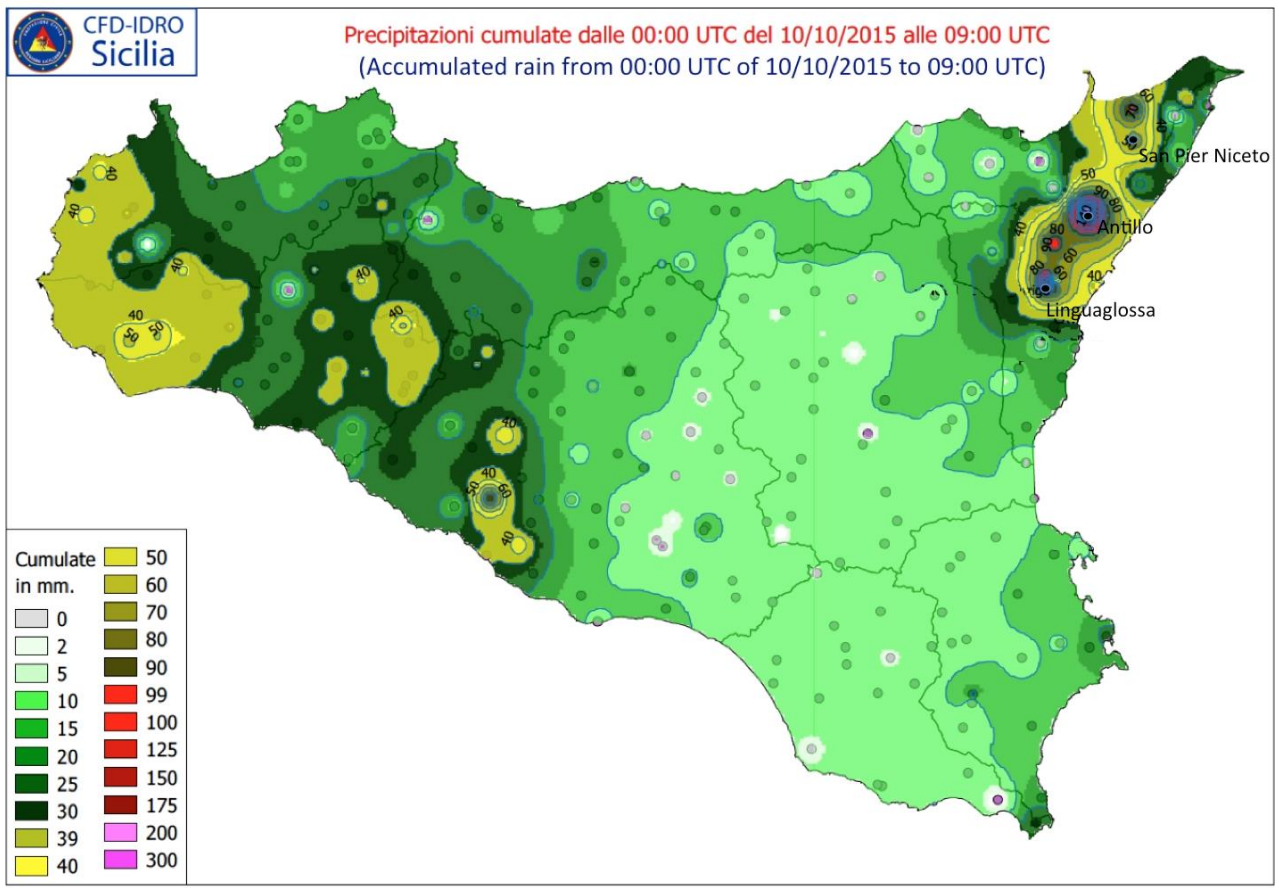


Fig. 26: Precipitation observed by the monitoring network of the Regional Department of Civil Protection

Impact of horizontal resolution for the forecasting of mesoscale thunderstorm events

A mountain barrier determines a considerable effect on atmospheric circulation and may significantly influence the weather forecast. In fact, the discontinuities of the earth's surface, i.e. a complex orography, may affect the motion of atmospheric circulation at all scales, determining sometimes a strong change in wind direction and intensity [62]. Therefore a detailed analysis of both boundary conditions and orography is often a crucial element in the development of an effective meteorological model [63].

In the presence of orographic forcing, such as those generated by very high reliefs - in our case Mt. Etna and Peloritani Mountains – an increased spatial resolution may allow to explore relevant scales of air motions which otherwise should not have been taken into account in the simulation.

This case study presents a comparison of the findings obtained by numerical simulations performed at different spatial resolutions together with the employment of different approaches for the model initialization process [64].

More specifically, in this study compares the simulation results obtained by using an initial configuration run characterized by a horizontal grid spacing of 10 km and those obtained by using a Nesting Two Way configuration with a subdomain horizontal grid spacing of 0.8 km and a parent domain with a horizontal grid spacing of 4 km.

This study mentions all configurations developed using the WRF-ARW, together with non-standard geographic data. The GTOPO30 digital elevation model developed by USGS working at 30 arcsec resolution has been replaced by the ASTER GDEM V2 model, as a result of the collaboration established in 2011 between METI (Ministry of Economy, Trade, and Industry of Japan) and NASA, characterized by a 1 arcsec resolution.

The USGS data (Landuse) at a 30 arcsec resolution were replaced by Corine Land Cover 2006 data, developed by EEA (European Environment Agency) characterized by a 3 arcsec resolution, reclassified on 24 classes of Landuse [65].

The global model NCEP FNL at 0.25 degrees with a time interval resolution of 3h, processed for the 00Z run relative to the 10 October 2015 have generated the initial and boundary conditions. Were used the RTG sea surface temperature data with a resolution of 0.083 degrees. For long-wave radiations the RRTM (Rapid Radiation Transfer Model) scheme was used [66], while for the short-wave radiations the Goddard scheme [67]. In addition the above, were also used the schemes of Mellor-Yamada-Janjic [68] for the boundary layer and Noah land surface model [69].

The microphysical scheme utilized was the Thompson [70] a well known double-moment scheme widely tested especially in high-resolution simulations. In the Nesting Two Way simulations for the parent-domains, the Kain Fritsch convective scheme [71] was used, while for the subdomains the resolution of convective processes was explicit.

A number of 65 vertical levels with higher resolution for the levels close to the surface and to the top of the air column using a vertical distribution with hyperbolic tangent were employed using the WRF software DOMAIN WIZARD distributed by NOAA.

The determination of the configuration with horizontal grid spacing of 10km came out by a single-run that covered a wide area with extension from latitude 30.03 DEG to 44.35 DEG and longitude from 2.67 DEG to 25.64 DEG.

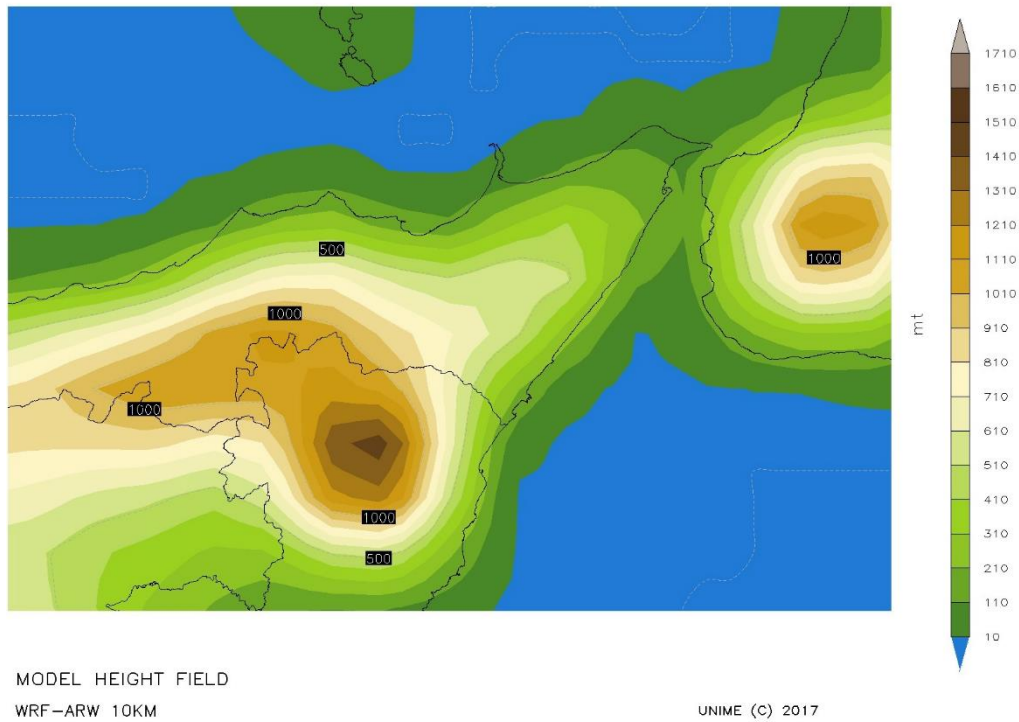


Fig. 27: Topography obtained by WRF with spatial resolution of 10 km. Heights are in meters.

For a LAM with a horizontal grid spacing of 10km, the actual topography cannot be clearly represented because of the grid sizes (Fig. 27)

With this grid spacing, the complex orography of S-E Sicily representation that includes Mount Etna, Nebrodi and Peloritani looks alike as a single mountainous relief, with heights far lower than the real ones [72-73]. The error that this topographic modeling generates, among others, affects two aspects of considerable importance for the formulation of weather forecasts: the estimation of vertical speeds and the flow divergence, and the latter affect, in a considerable way, the genesis and the development of heavy rainfalls with the results of a non-realistic simulation (Fig. 28).

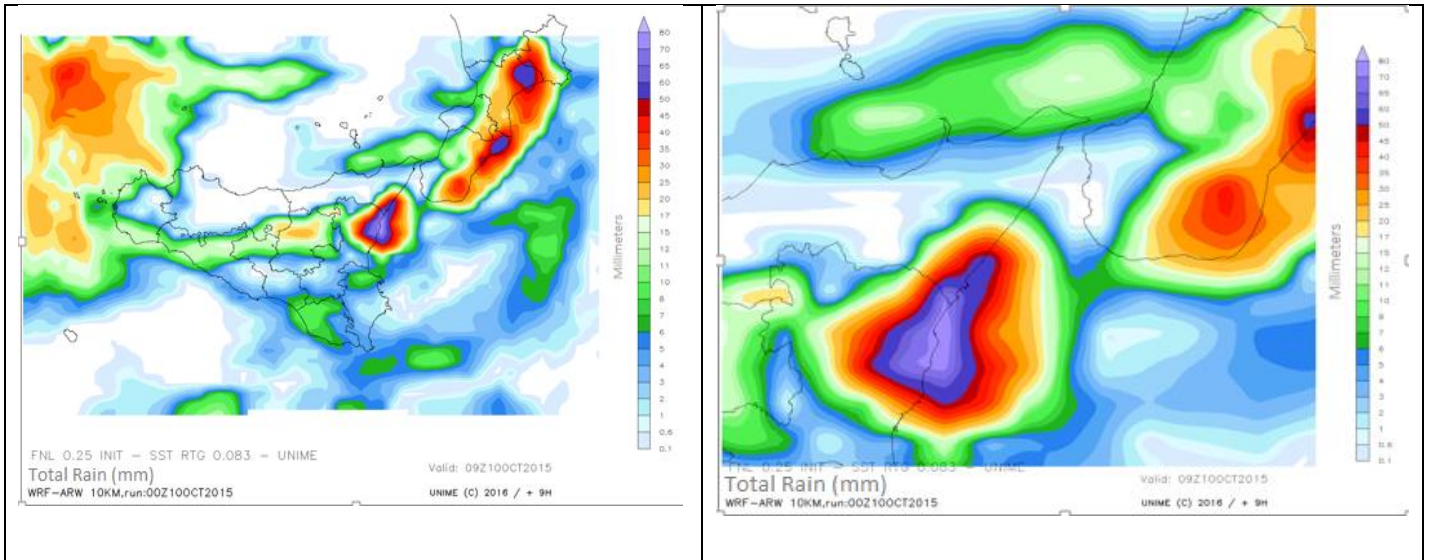


Fig. 28: Accumulated precipitations forecast by WRF with resolution at 10 km(left) and zoomed detail over North-Eastern Sicily (right) from 00 to 09 UTC.

Nesting configuration

Regarding nesting configurations, there are two possible options to select at the launch of each simulation:

- One-Way Nesting where the exchange of information between the father domain (parent domain) and the subdomain is unidirectional, since the subdomain uses the boundary conditions of the already processed parent domain, without performing a feedback procedure of the parent domain, which is coarser. The sub-domain receives the Lateral Boundary Conditions (LBC)(parent domain) on a 3-hr basis.
- Two-Way Nesting where the exchange of information between the parent domain and the subdomain is bidirectional. In such cases the feedback procedure influences the performance of the parent domain. The LBC of the subdomain includes microphysical variables and vertical movement and the subdomain uses the LBC of the parent domain at each time step ($T + nestT$).

The relevant factor to obtain good precipitation prediction has been attributed to the utilization of the Two-Way Nesting technique instead of a single-run configuration. While single-run uses Global Model data as boundary conditions, with lower resolution and, in the case of FNL, three-hours of input frequency, in the Nesting approach, the subdomain with a higher resolution uses as LBC the father domain (parent domain), which has a better vertical and horizontal resolution than the Global Models conditions. In addition, the parent domain provides the subdomain LBC at each timestep ($T + nestT$).

$$T = \text{Timestep (Parent Domain)} / \text{nest} T = \text{Timestep subdomain (T / ratio)}$$

In order to develop and refine the forecast's effectiveness, we increased the horizontal spatial resolution for a more correct treatment of the altimetry, improving the mountain systems localization [74-76]. The setup used for the analysis of the event is defined by Two Way Nesting with a horizontal grid spacing of 4km (parent domain) extended to the entire area of Sicily, surrounding seas, and a sub-domain with a horizontal grid spacing of 800 m. (ratio 1:5), limited to an area including Mt. Etna, Messina and the Calabrian coastline (Fig. 29).

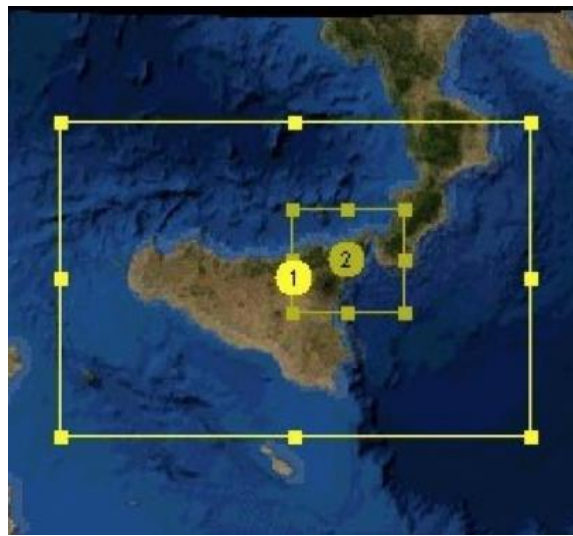


Fig. 29: Nesting Two Way: parent domain with horizontal grid spacing of 4km and subdomain with horizontal grid spacing of 800 m.

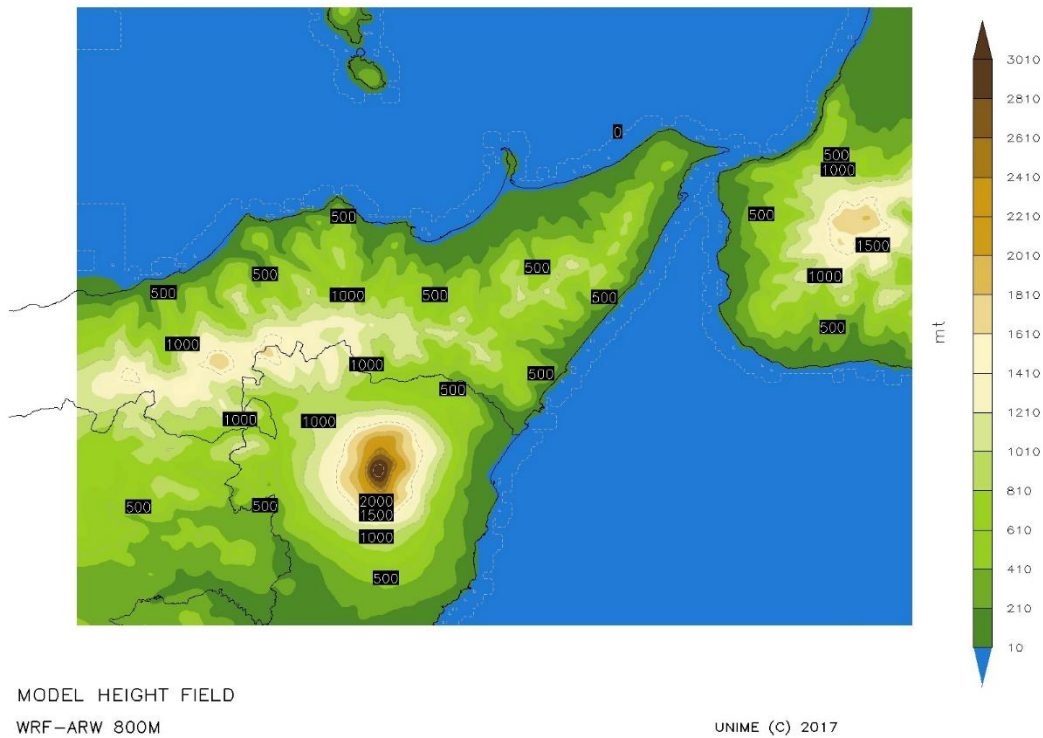


Fig. 30: Orography of WRF at 800 m of horizontal grid spacing.

Although the adopted procedure required remarkable computational resources, the obtained results fully justify such procedure. The new simulation obtained at this grid spacing, shows the SE flow in the lower layers, to impact against the massive mountain system constituted by the Eastern side of Mt. Etna triggering a remarkable Stau effect by adiabatic expansion of the mass air rising the mountain slope. On another note, with 800 m of grid spacing, the altitude of Mt. Etna reach 3010m ASL, vice 1500m ASL with 10 km of grid spacing. The Peloritani mountains, poorly represented in the version with 10 km of grid spacing, now constitute a mountain set very close to the sea of about 1000 m. height (Fig. 30). In the Two Way Nesting simulation with a sub-domain at 800 m. of grid spacing, the phenomena result strongly enhanced by orography, revealing a great foresight performance of the V-Shape thunderstorm that affected Messina on the night of 10 October 2015 (not shown).

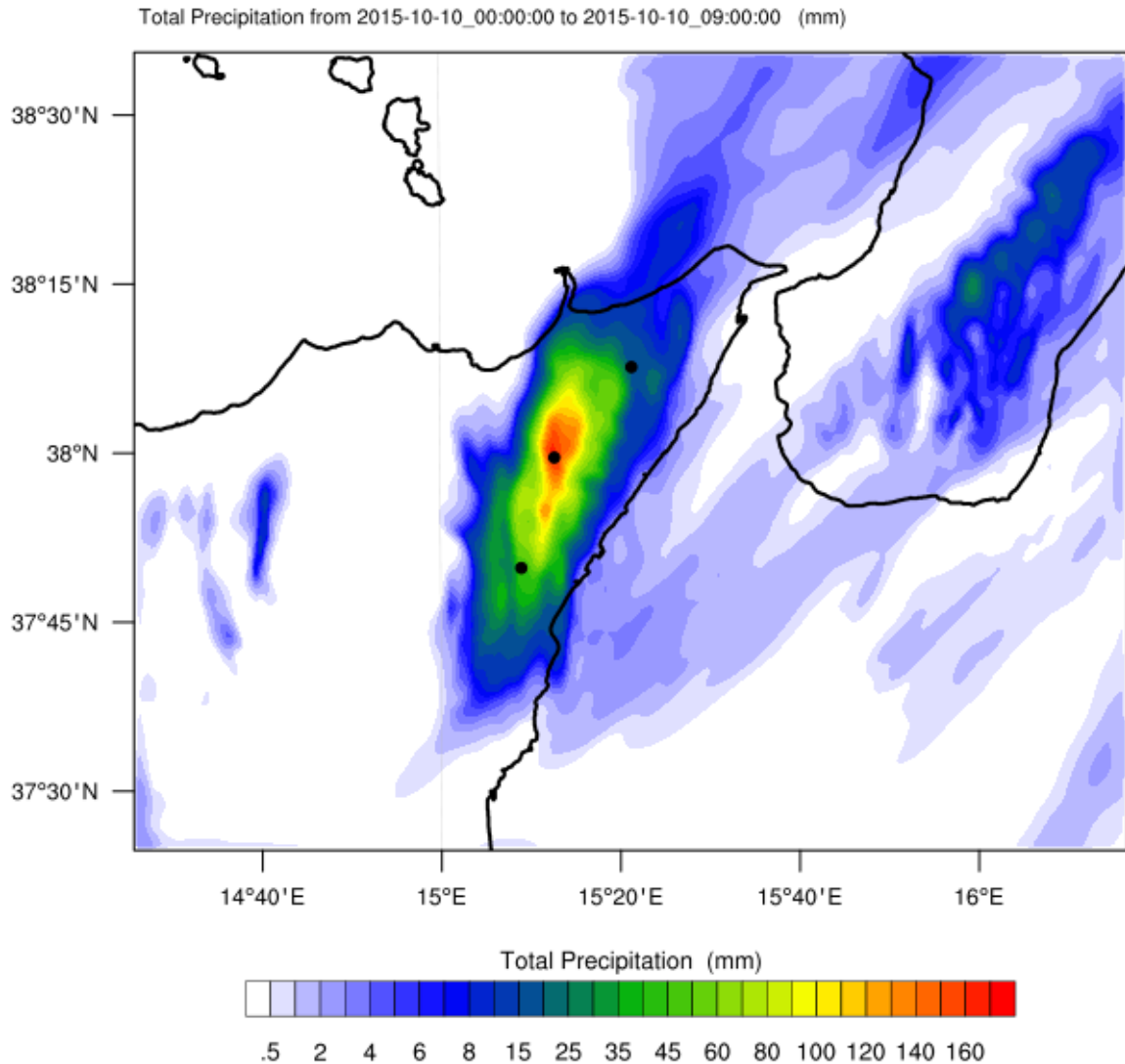


Fig. 31: Precipitation provided by WRF in NESTING TWO WAY configuration with a horizontal grid spacing of 800 m. The black dots show the position of the weather stations of San Pier Niceto, Antillo and Linguaglossa (from North to South).

As mentioned above, the improvement of the rainfall forecast (Fig. 31), in this case is due to a higher resolution of the orography, i.e. by a better representation of Mt. Etna, Peloritani and Nebrodi mountains and combined wind field effects (Fig. 32).

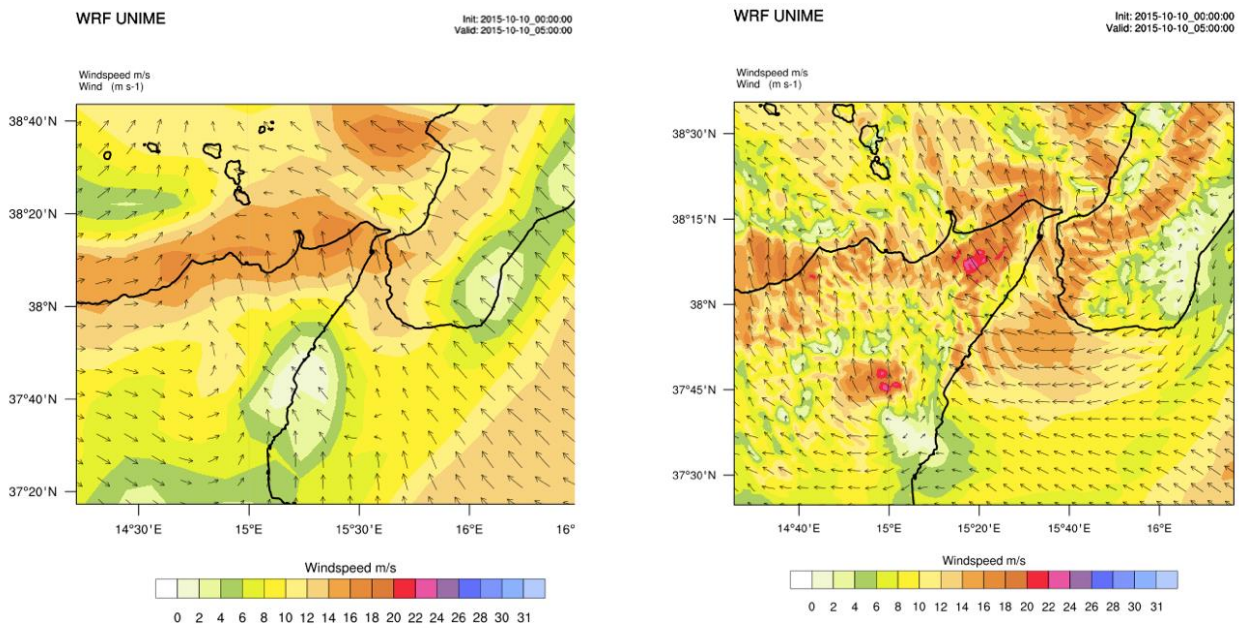


Fig. 32: 10 m. wind field forecast at 05:00 UTC by the WRF 10 km (left) and 0.8 km (right).

During the whole process, the differences in the wind fields at 10 m played a key role. With the 10 km model, there is a small area of convergence only; Mt. Etna induces it in the lower layers, generating a rainy core on the Ionian Sea. With the 800 m model, 10 m height winds with a mean velocity of about 90 km/h generate a strong Stau effect on the Eastern side of the Peloritani Mountains, while the Tyrrhenian side received only a few mm of accumulation (rain shadow effect). It is also evident the "turbulent friction" caused by Mt. Etna, producing a deviation to east of the low-level jet and the genesis of an area of convergence. The tests performed on the 10th of October 2015 episode shows that the WRF model configured via Two Way Nesting with subdomain centered in the area affected by the heavy precipitation provides good results in Peloritani area. In particular, they regard the position as well as the amount of the occurred precipitations. The verification has been extended to 3 weather stations: Antillo, Linguaglossa and San Pier Niceto. The position of each weather station is visible in Fig. 1, Fig. 4 and Fig. 9. The model performance is excellent at Antillo (rainfall peak). The total precipitation amount is significantly underestimated in Linguaglossa and San Pier Niceto, but the 4km-0.8km configurations improve the simulated precipitation relative to the 10km grid.

The forecast data from WRF output are visible in Fig. 33, compared with observed data.

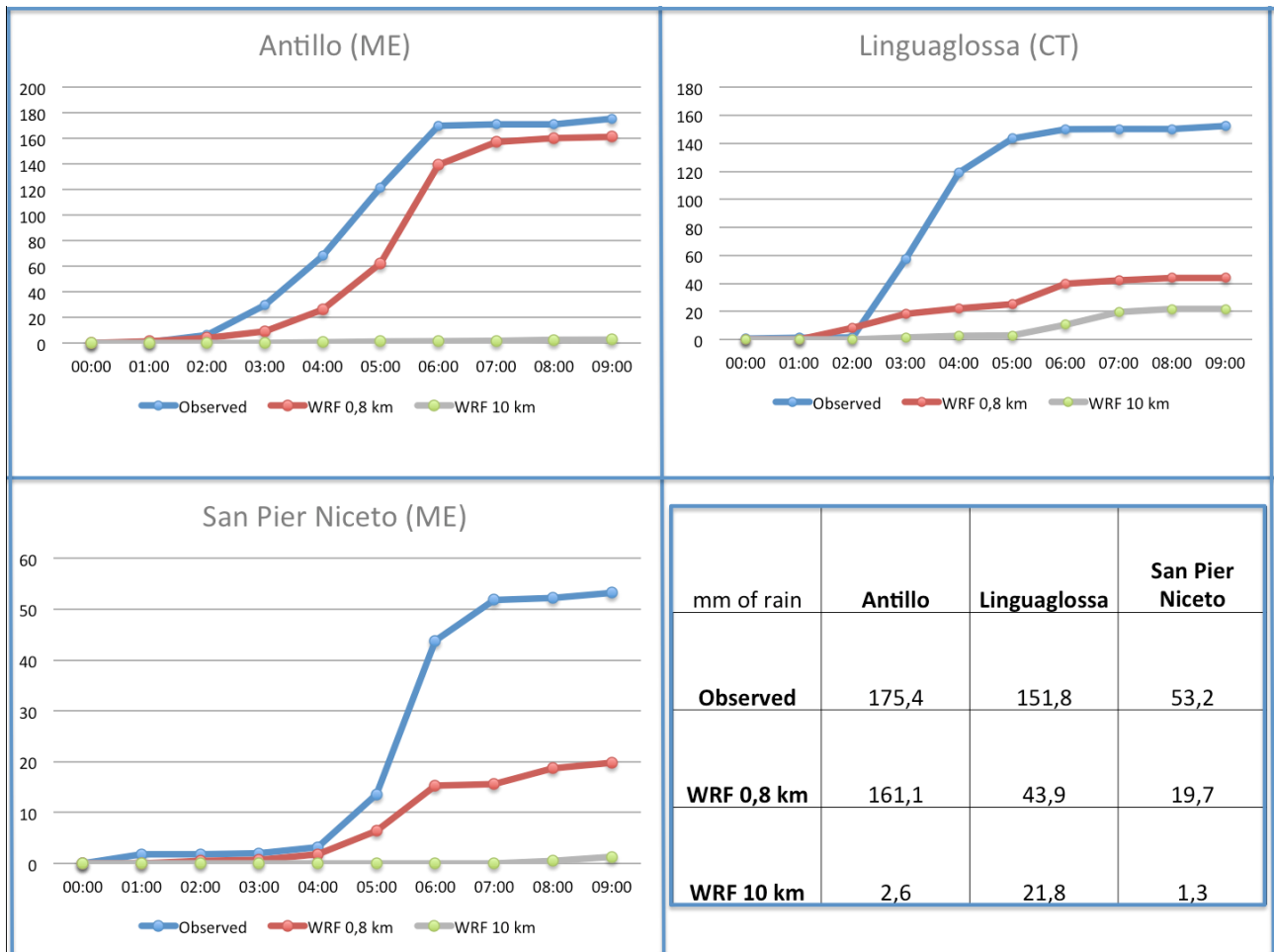


Fig. 33: Antillo, Linguaglossa and San Pier Niceto weather stations: observed rain (blue), WRF 0,8 km forecast (red) and WRF 10 km forecast (grey) versus time. Bottom right: Total accumulated precipitations observed and forecast.

The comparison between the GOES 12 Sat Imagery Simulation generated by UPP software and the MSG satellite picture is very impressive (Fig. 34).

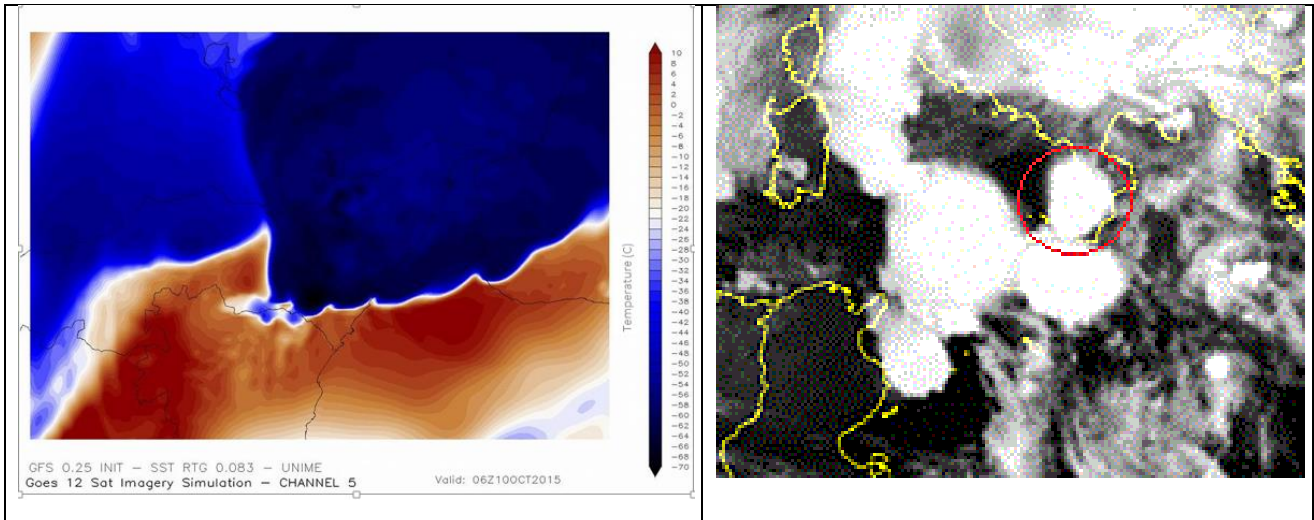


Fig. 34 Comparison of WRF simulation and satellite observation Sat MSG at 06:00 UTC

Impact of alternative geographic data for the mesoscale forecasting of rain events

In this case study, the definition of different geographic data utilization impact study is reached by performing a new run through the Two Way Nesting approach. The parameterizations used are identical to that described in the previous paragraph, with the replacement of alternative geographic data with those distributed along with the standard model WRF (Table 4).

	DEM	LAND-USE
Standard data	GTOPO 30	USGS30
HD data	ASTER	CORINE

Table4: Composition of Standard and HD Geographic data

The following image describes the orographic differences attributable [77-80] to the use of ASTER GDEM V2 data rather than GTOPO30 data (Fig. 35).

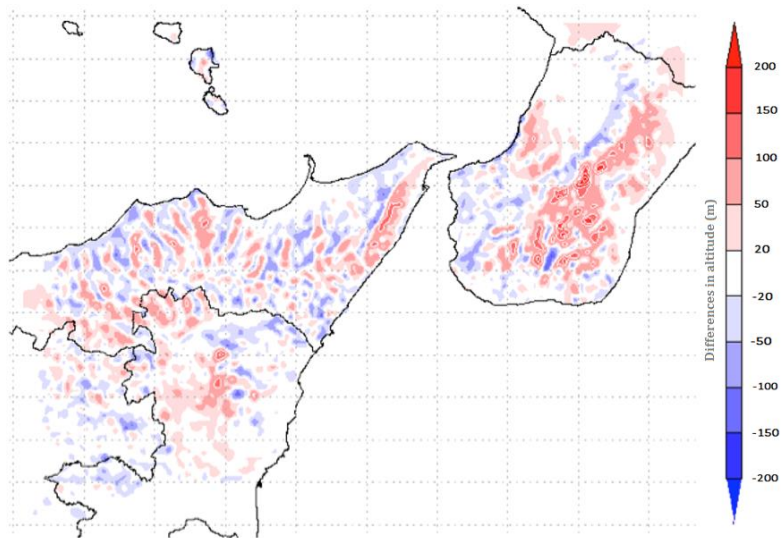


Fig. 35: Differences in altitude between ASTER V2 DEM (res: 30m) and GTOPO30 (res: 1km) on a 800m domain

Although both forecasts do not show many differences, with regard to the spatial location of the event, a better representation of the terrain obtained with the utilization of finer DEM and Land-se data (Fig. 36), had a positive impact on the precipitation amount forecast. Different types of Land use have different physical properties that can change the radiation and energy balances and hence vertical fluxes of moisture, heat and momentum, which also lead to changes in temperature, and moisture fields near the surface [81]. For example in presence of vegetative cover we have to consider the “evapo-transpiration” process. The surface energy and moisture budgets for bare and vegetated soils is crucial during typical thunderstorm weather conditions. Changes in land-surface properties are shown to influence the heat and moisture fluxes within the planetary boundary layer, convective available potential energy and other measures of the deep cumulus cloud activity.

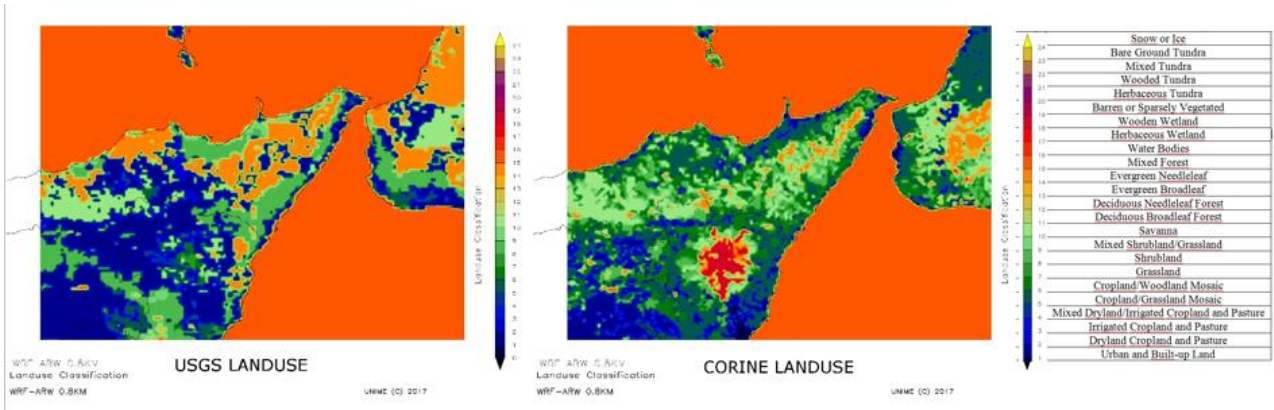


Fig. 36: USGS land-use and CORINE land-use on model domain

Hence, the change of Land-use data has a strong impact on the precipitation field, especially in presence of complex orography and with grid spacing smaller than 1 km.

In Table 5 and in detail, in Fig. 37, it is possible to highlight how the resulting differences obtained reaches in some areas also 60 mm.

	Antillo OBS	800m HD	800m SD	Linguagl. OBS	800m HD	800m SD	SP Niceto OBS	800m HD	800m SD
10/10/2015 00:00	0	0	0	0	0	0	0	0	0
10/10/2015 01:00	0,6	1,3	0,4	0,6	0	0	1,8	0	0
10/10/2015 02:00	6,2	3,9	3,6	0,8	8,3	9	1,8	0,5	0,5
10/10/2015 03:00	29,6	9,1	8,8	56,8	18,3	17,7	2	0,7	0,8
10/10/2015 04:00	68,1	26,1	32,7	118,6	22,2	21,5	3,2	1,8	2,3
10/10/2015 05:00	121,7	62,4	63,7	142,8	25,2	28,9	13,6	6,4	3,6
10/10/2015 06:00	169,9	139,3	86,2	149,4	39,8	34,3	43,8	15,3	12,9
10/10/2015 07:00	171	157,2	113,4	149,6	42,2	36,4	51,8	15,6	13,1
10/10/2015 08:00	171	160,2	116,1	149,6	43,9	39,5	52,2	18,7	15,4
10/10/2015 09:00	175,4	161,2	117,2	151,8	43,9	39,5	53,2	19,8	15,9

Table 5: Accumulated precipitation observed in Antillo, Linguaglossa and San Pier Niceto and forecast by WRF with 800m of grid spacing using Standard and HD geographic data

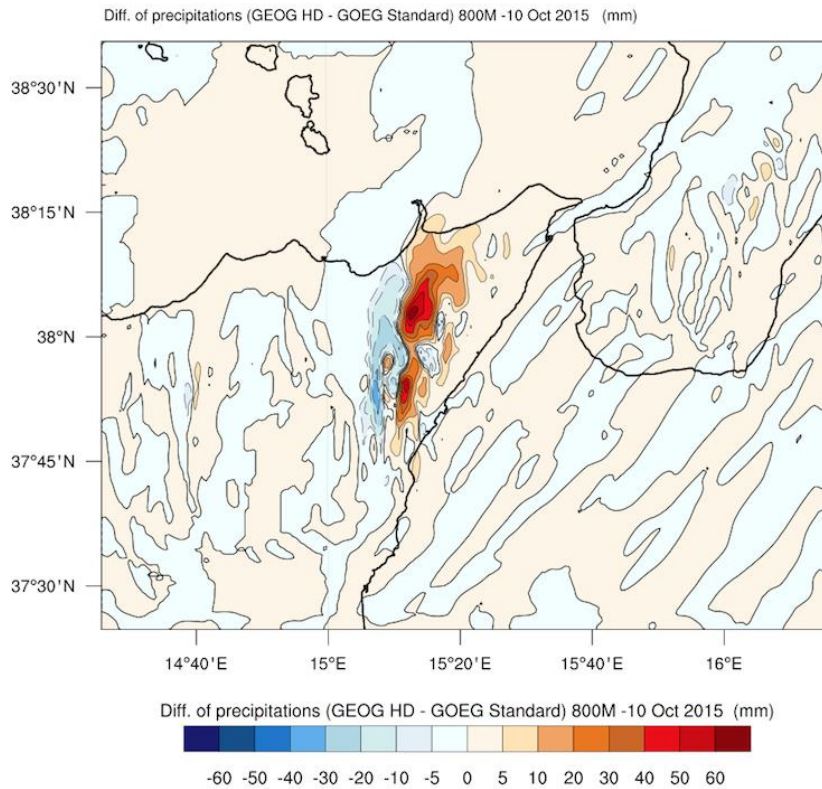


Fig. 37: Run 800m - final accumulations differences (GEOG STANDARD - GEOG HD)

The increase of the spatial resolution from 10 km to 4 km and then to 800 m, besides to substantially improve the territory representation, has allowed a larger detail for the main meteorological fields investigated, facilitating the understanding of the phenomenon itself. For example, looking at the synoptic analysis only, it is unclear if the air stream disturbance induced by Mt. Etna, has or has not played a decisive role. The image of the “stream” air flows (Fig. 38), rebuilt starting from the output of the model at 800m resolution through the Visualization and Analysis Platform for Ocean, Atmosphere, and Solar Researchers (VAPOR) software, highlights and clarifies many relevant aspects:

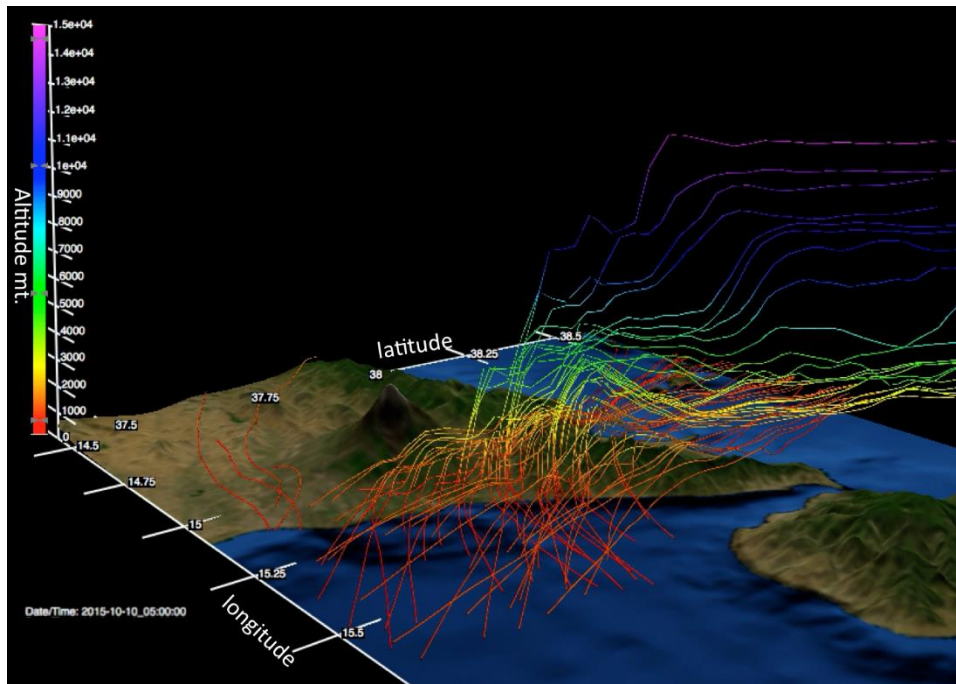


Fig. 38: 3D representation of the air flows of 10th October 2015, 05:00 UTC colored by altitude obtained by WRF 800m on domain 2.

- The Southeastern surface flow, as soon as it starts to rise, is immediately "caught" by the Southwestern one, predominant at 500 hPa level;
- The initial lift, finds a preferential path in Alcantara Valley allowing the warm and humid currents to climb the course of the valley for several tens of kilometers, before being raised;
- After an initial lift, a new pulse, stronger than the first one and generated by Mt. Etna, leads the air particles to rise up to quotes next to tropopause (Fig. 38).

A cross-section taken parallel to the coastline shows the vertical speed and the flows in the lower layers (Fig. 39) that lead the thunderstorm development. The model forecast of vertical wind component (w) shows extreme values till 24 m/s.

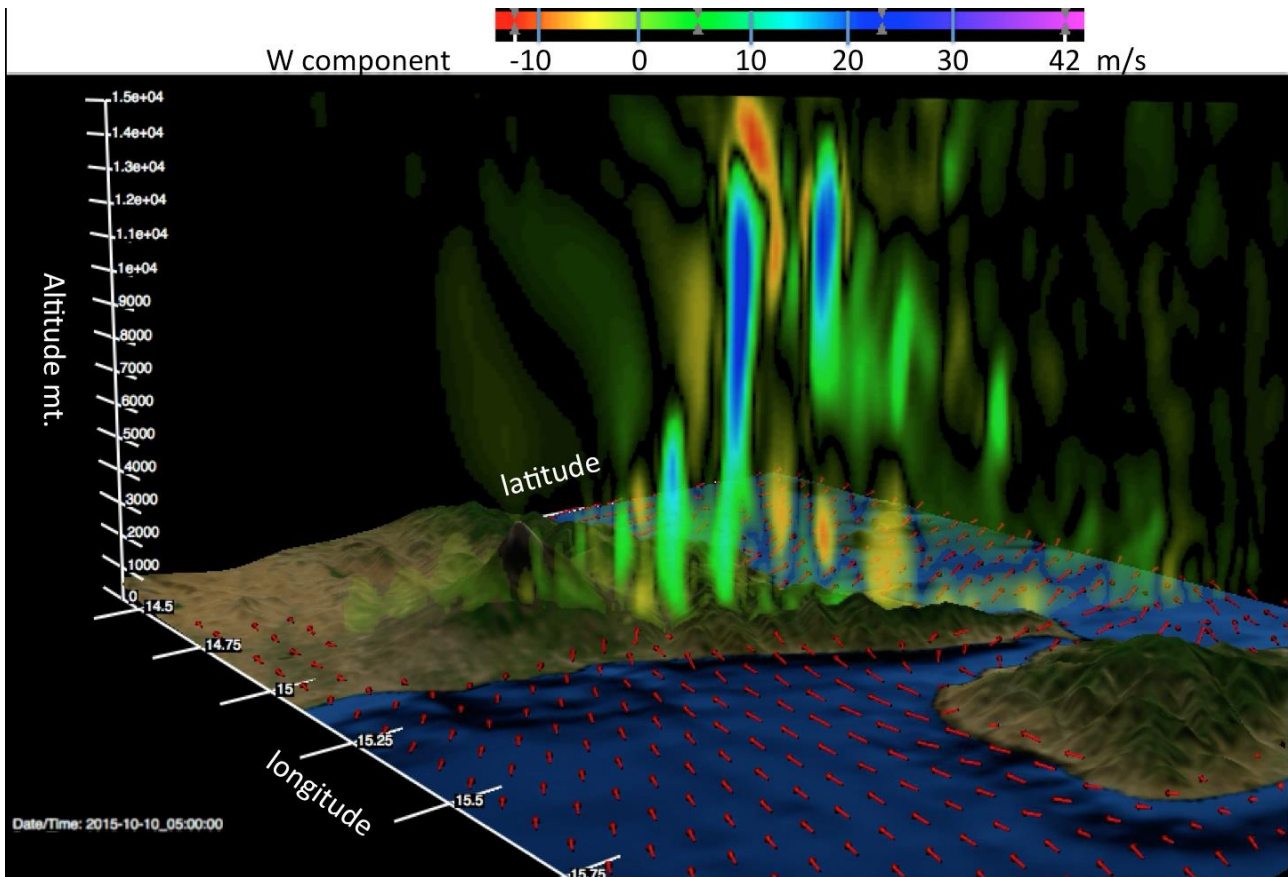


Fig. 37 Vertical component of the wind velocity (m/s) at 05:00 UTC on a coastline parallel cross-section on domain 2

Another aspect that the model with a 800 m of resolution allows to understand is the so called "Alcantara effect." Such "effect" is related to the role of the Alcantara Valley, which in the case of ground flows, coming from southeast would facilitate the entrance into the hinterland of huge volumes of moisture for several tens of kilometers. Air is forced to rise along the highest part of the Alcantara basin facilitating the condensation of water vapor and the subsequent development of convective clouds. This situation occurred in the early hours of October 10th and has been fully rebuilt by this simulation. The map in Fig.18 shows the water vapor mixing ratio field in g/kg in the lower portion of the atmosphere (500 meters ASL) as obtained by WRF 800 m. where is clearly visible the Alcantara effect.

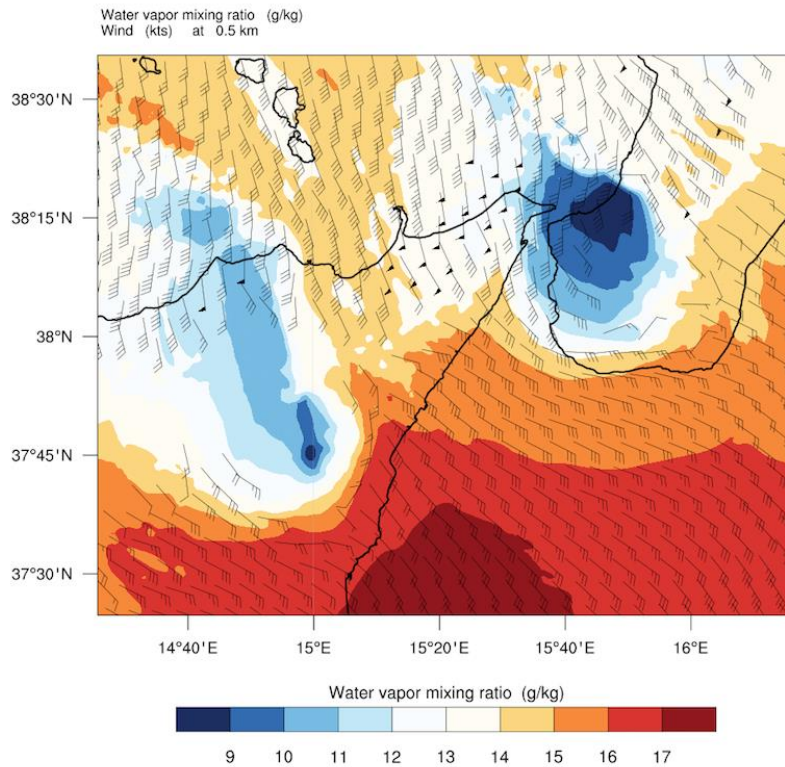


Fig. 38 Amount of vapor (g/kg) in the lower atmosphere (500 m ASL) and wind flows in kts at 05:00 UTC on domain 2

The 800 m resolution has also allowed for the rebuilding of the thundercloud structure, visually noticeable in Fig. 39. The highlighted portion is not only the morphological structure of the thunderstorm cell, but also the top altitude reached by cumulonimbus. The image is obtained by plotting the cloud fraction (CLDFRA) field of WRF by VAPOR software using the Direct Volume Rendering option.

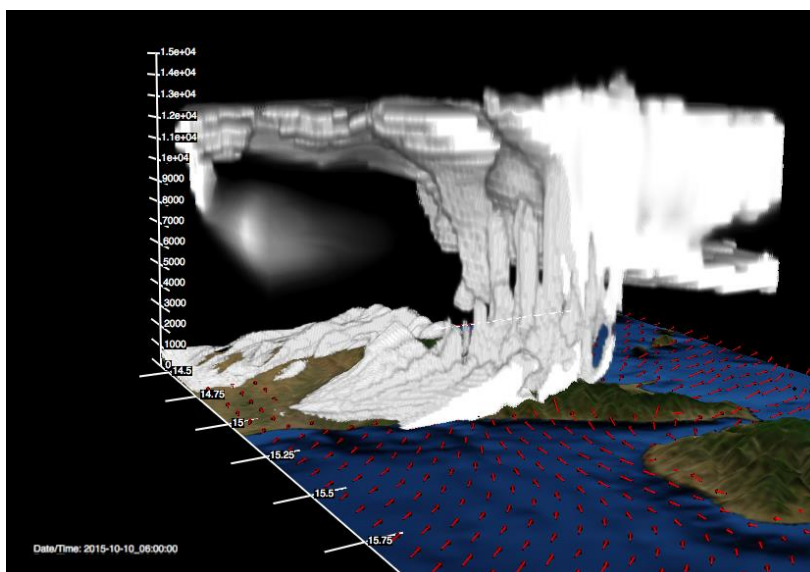


Fig. 39: Structure of the thunderstorm cell at 06:00 UTC obtained plotting a Direct Volume Rendering of CLDFRA field with isosurface = 1 and surface wind (red arrow) of WRF 800 m on domain 2

Conclusions

The purpose of the numerical simulations carried-out with the use of WRF-ARW model, properly set and configured for Sicily, was to find out the best compromise between the finest spatial resolution and the available calculation capacities to obtain the best timely forecast possible. To pursue these results, tests were conducted using different configurations. The stormy event of 10 October 2015 was used as a "case study" and has allowed us to compare the data collected from weather station networks available in Sicily with the model outputs. In particular, we have compared the amount and distribution of rainfall, using two WRF configurations. The first one employed a run with 10 km grid-spacing, while the other one used two two-way nested domains with 4 km and 0.8km grid-spacing.

Similar tests were performed using ASTER GDEM V2 data rather than GTOPO30 data, as well as replacing the USGS Landuse data with Corine Land Cover 2006 data.

A direct comparison between the observed and forecast data has also been performed using Antillo, Linguaglossa and San Pier Niceto weather stations record and focus on the Nebrodi range.

The obtained results consented to clearly show that the improvement of the model grid spacing, together with the use of more accurate geographic data and the land use data, more suitable for the description of the territory, are the key elements for the prediction accuracy. This is especially true for geographic areas like Sicily that are characterized by the presence of complex orographic structures.

- **9th June 2016**

The case study analyzed concerns a typical summer situation characterized by high instability as a result of infiltration of cold air at altitude. In particular, during the course of the previous day, the afternoon thunderstorms had developed on the northeastern part of the island between Etna and the chain of the Peloritani. On 9th June, after a morning with sky mostly clear, between 11 and 12 UTC, storm cells begin to develop both on the Ionian coast of Messina and on the central Sicily, between the provinces of Agrigento and Palermo (Fig. 40).

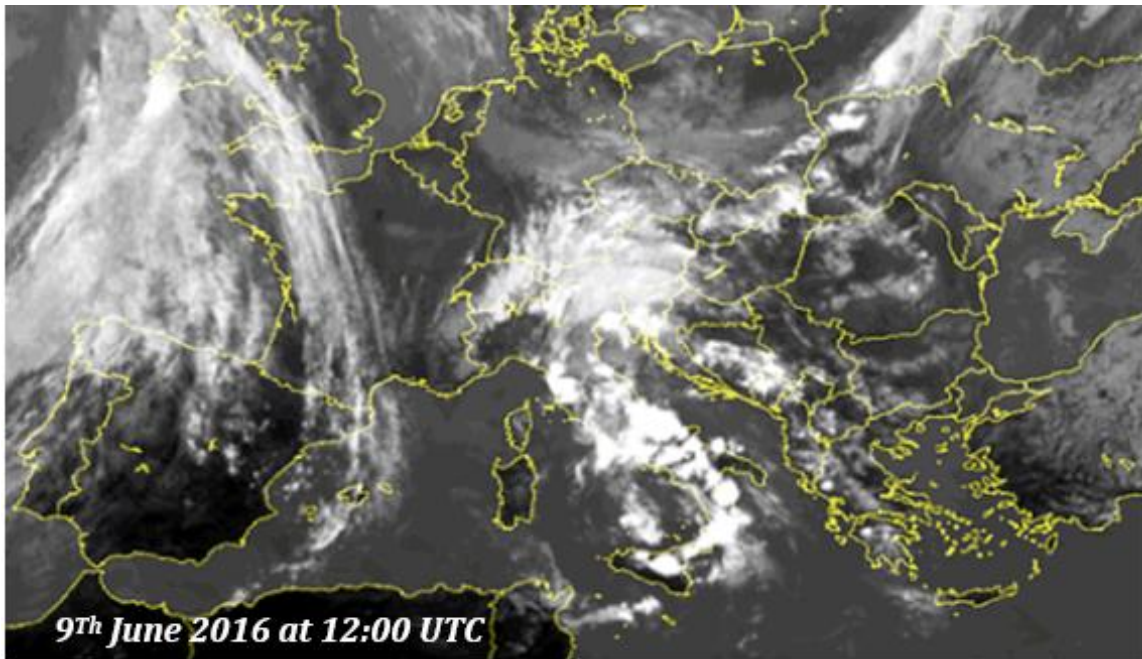


Fig. 40: MSG thermal infrared image at 12.00 UTC on June 9th 2016. The storm convection cell under development at the center of the Sicily region is clearly visible.

Between the hours 13 and 14 UTC the thunderstorm are fully developed and then begin to dissolve starting at 15 UTC. The total duration of the phenomenon can be estimated in 6 hours and the maximum accumulations of rain in the 24 hours were a little more than 30 millimeters with peaks of 31.2 in Mussomeli, 30.4 in Maletto, 27.2 in Cesarò (Fig. 41). From the map of the total rain accumulated in the 24 hours it is interesting to note that the southern and western sections of the island have not been affected by rain, and that only the internal areas have been subject to precipitations with two clearly visible maxima at Agrigento and in the northern part of Etna.

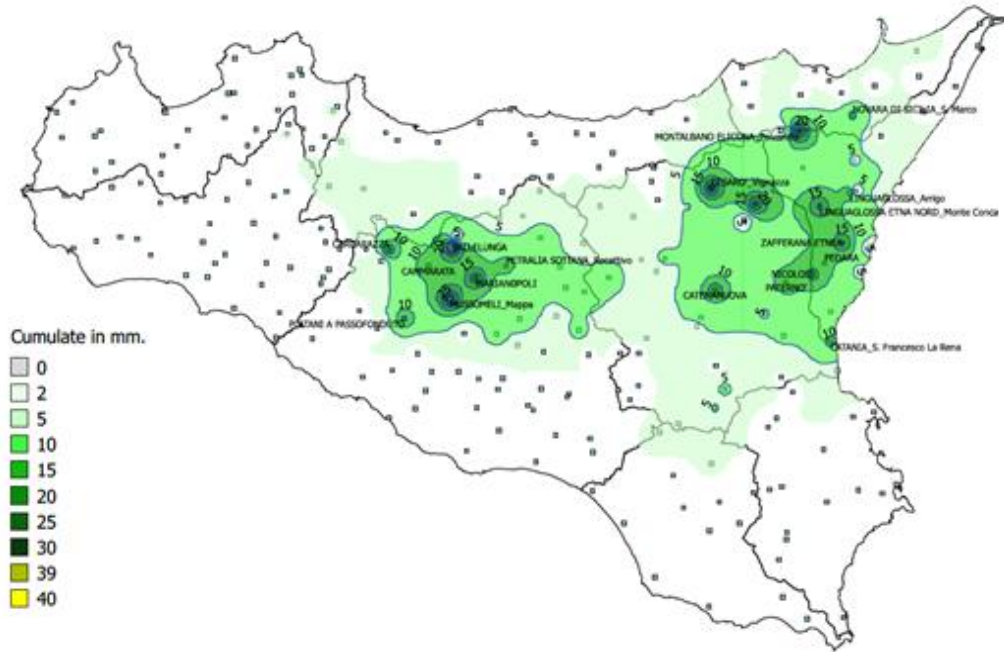


Fig. 41: Map of the total rains recorded by the meteorological stations of the Regional Civil Protection Department of the Sicilia region. The total rains accumulated data refer from the hours 00 UTC to the 24 UTC on 09 June 2016. It is possible to notice that the south and west areas of the island were not affected by rain. Only internal areas have recorded rainfall accumulations. In particular, the province of Agrigento and the northern part of Etna recorded the highest rainfall accumulations.

The evaluations carried out in the present case study regard the performances of the WRF model when the different physics parameterization of the convective schemes are applied.



Fig. 42: Map of the spatial domain used by the WRF model. The domain is centered on Sicily. The model is configured with horizontal grid spacing of 5km and a time interval resolution of 1h

In particular both the forecasts of CAPE (convective available potential energy) at Trapani and the amount and the spatial distribution of rain during the event are compared. The physics parameterizations of the convective schemes analyzed are shown in the Table 6:

Cu physics = 0	Explicit convection	No Cumulus scheme
Cu physics = 1	Kain-Fritsch scheme	Deep and shallow convection sub-grid scheme using a mass flux approach with downdrafts and CAPE removal time scale
Cu physics = 2	Betts-Miller-Janjic scheme	Operational Eta scheme. Column moist adjustment scheme relaxing towards a well-mixed profile
Cu physics = 3	Grell-Devenyi (GD) ensemble scheme	Multi-closure, multi-parameter, ensemble method with typically 144 sub-grid members
Cu physics = 4	Simplified Arakawa-Schubert	Simple mass-flux scheme with quasi-equilibrium closure with shallow mixing scheme.
Cu physics = 5	Grell 3D scheme	It is an improved version of the GD scheme that may also be used on high resolution (in addition to coarser resolutions) if subsidence spreading is turned on).

Cu physics = 6	Tiedtke scheme	Mass-flux type scheme with CAPE removal time scale, shallow component and momentum transport.
Cu physics = 14	New Simplified Arakawa-Schubert	New mass-flux scheme with deep and shallow components and momentum transport

Table 6: Physics parameterizations of the convective schemes analyzed

CAPE analysis:

The Convective Available Potential Energy (CAPE) is a thermodynamic index that represents the potential convective energy, defined by the following equation:

$$CAPE = g \int_{z_f}^{z_n} \left(\frac{T_{part} - T_{env}}{T_{env}} \right) dz \quad 58)$$

where is:

g: gravitational acceleration;

z_f = free convection level height;

z_n = equilibrium level (neutral buoyancy);

T_{part} : Virtual temperature of the particle;

T_{env} : Virtual environment temperature.

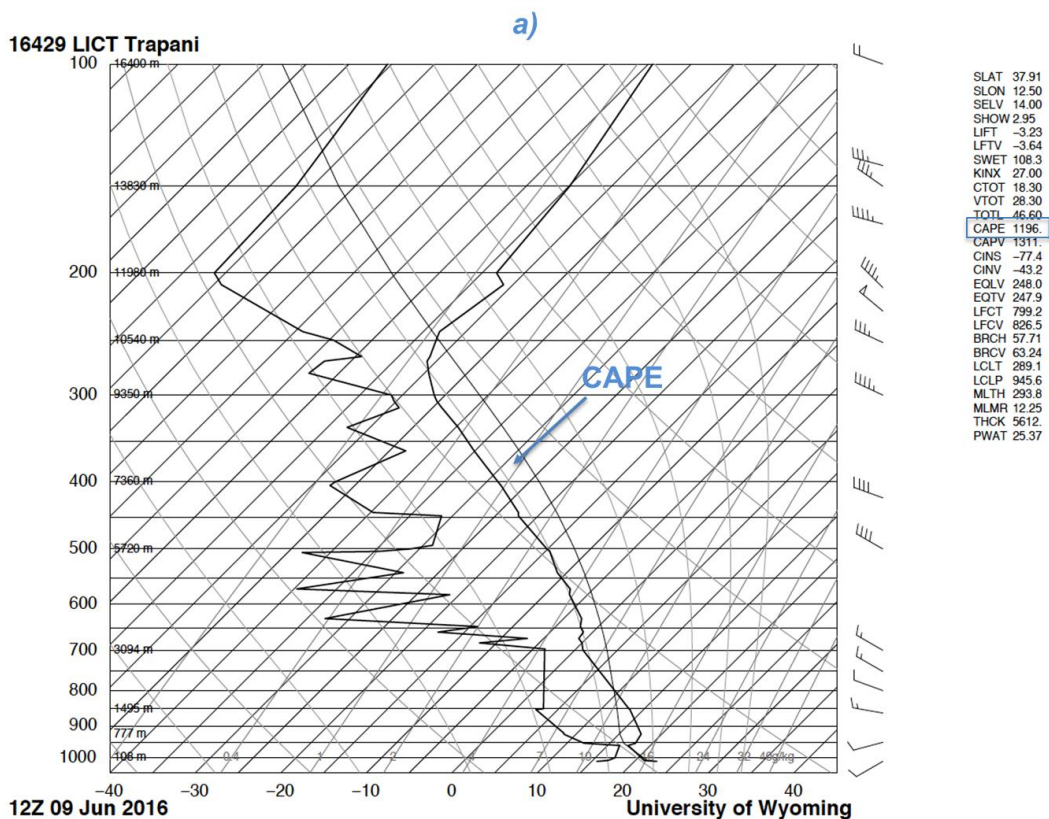
It is a necessary parameter, but not sufficient, to understand the degree of instability of the air column. In other words, it gives information on the probability that there will be thunderstorms and their intensity. CAPE parameter depends on the temperature and moisture of the air column between the ground and the upper troposphere; its unit is [J / kg]. High values indicate that the column of air has considerable convective energy and therefore, under an initial push, the convection will develop in a

considerable way giving rise to strong storms. In particular, according to the numerical value which assumes the CAPE, one has that:

CAPE < 500	absence of thunderstorms
500 < CAPE < 1000	possibility of thunderstorms isolates
1000 < CAPE < 2000	thunderstorms probable enough
CAPE > 2000	strong enough probable storms

Fig. 43: Numerical interval of the CAPE. High values indicate that the air column has a considerable convective energy. The convection will develop considerably, giving rise to strong storms.

As far as the CAPE predictions are concerned, obtained by varying convective parameterizations, as location for the forecasting the airport of Trapani has been chosen, since being the site of a radiosonde station, lends itself to a direct comparison between the observed data and the forecast data. As shown in the Fig. 44, the numerical CAPE value is defined by the area enclosed between the temperature status curve and the adiabatic curve.



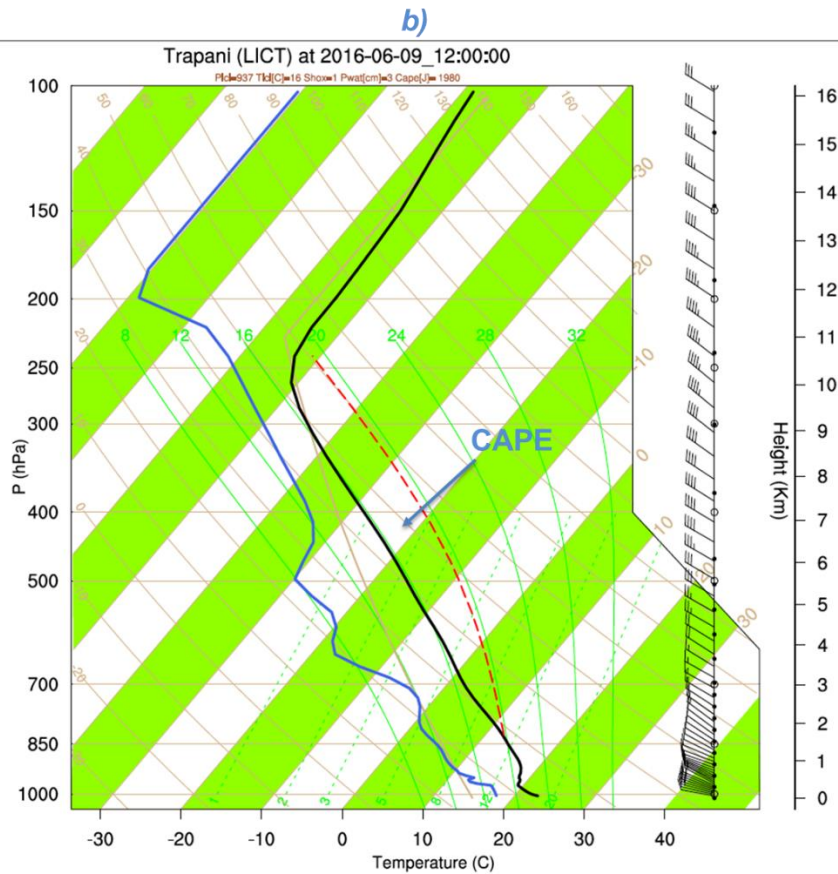


Fig. 44: Comparison between Skew T graph observed (a) and forecast (b) at 12:00 UTC of the 09th June 2016

From the analysis of the collected data (Fig. 45) it emerges that all the convective schemes underestimate the CAPE forecast for 12:00 UTC on 09th June 2016. Infact, the value observed from the radiosonde was 1196 J / Kg, while the values obtained by the models oscillate between 787 and 867 J / Kg. The graph of the 00:00 UTC of the 10th June instead shows an observed value of 266 J / kg, caught by the 3D Grell scheme (Cu-physics = 5).

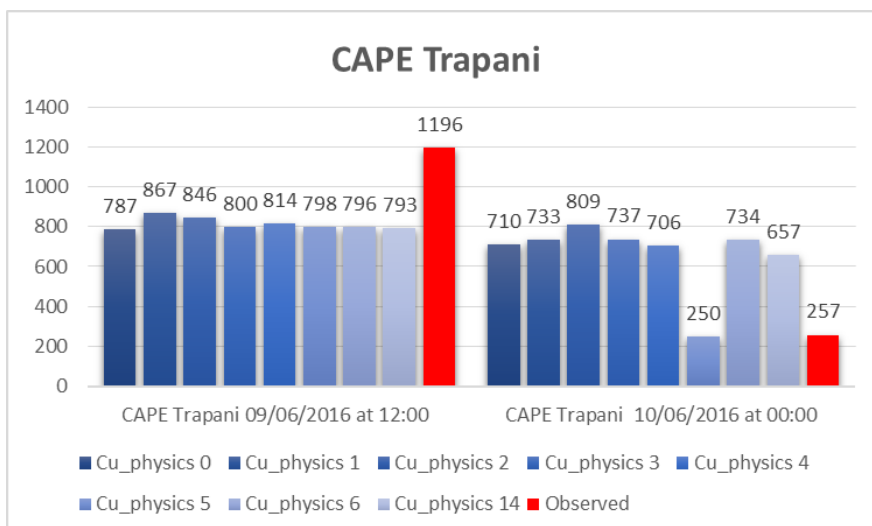


Fig. 45: Comparison between forecasts and observed (red) CAPE. The value of forecast CAPE it is obtained by a WRF model with different physics parameterizations of the convective schemes

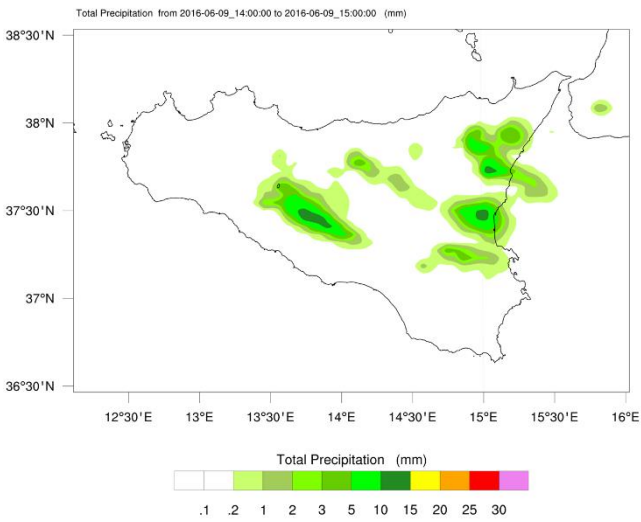
Rain analysis

The analysis of the field of hourly rainfalls observed between the hours 12:00 and 18:00 of the 9th June 2016 in Sicily (Fig 41), shows how the meteorological conditions has produced a convective thunderstorm on the Agrigento's area, and a minor cell between the northern slope of Etna and Siracusa.

The analysis of hourly precipitation maps produced by the WRF and centered at the same hours (14:00 to 15:00 UTC), shows, by varying the convective patterns, results in some cases very discordant. In particular in the case of the Betts-Miller-Janjic (Cu-Physic = 2) convective schema, which in this specific situation underestimates in an excessive way the precipitation to the ground, providing hour maximum values that do not exceed 2 mm on the entire region. They allow to locate the thunderstorm cell in a very precise way the 3D Grell schemes (Cu-Physic = 5) and the New Simplified Arakawa-Schubert (Cu_Physics = 14). The latter in particular, in addition to a perfect spatial and time localization, provides in an optimal way the hourly rain quantities (Fig. 46) .

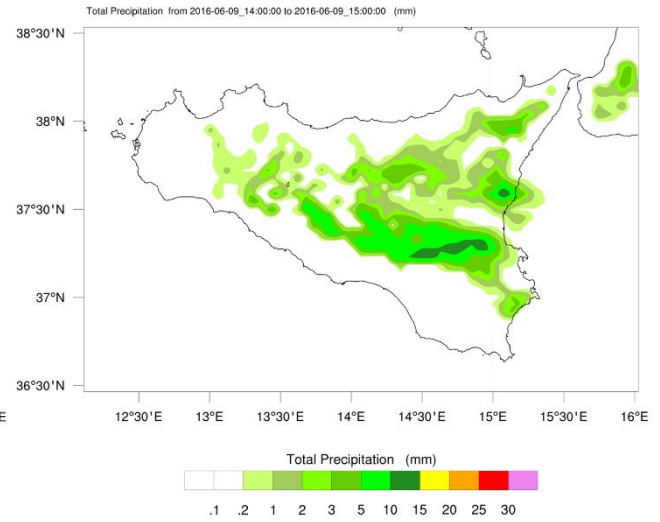
WRF Sicilia - Cu-Physic = 0

Init: 2016-06-08_00:00:00
Valid: 2016-06-09_15:00:00



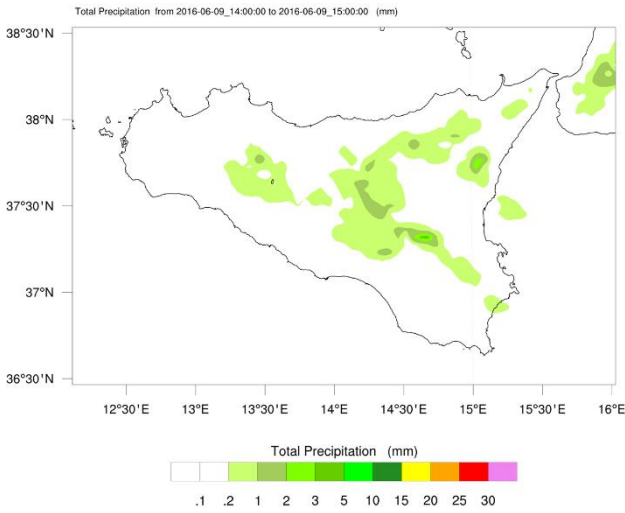
WRF Sicilia - Cu-Physic = 1

Init: 2016-06-08_07:00:00
Valid: 2016-06-09_15:00:00



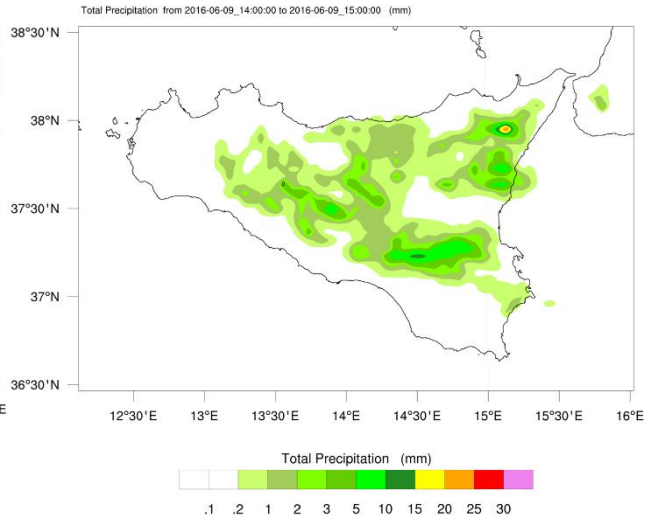
WRF Sicilia - Cu-Physic = 2

Init: 2016-06-08_07:00:00
Valid: 2016-06-09_15:00:00



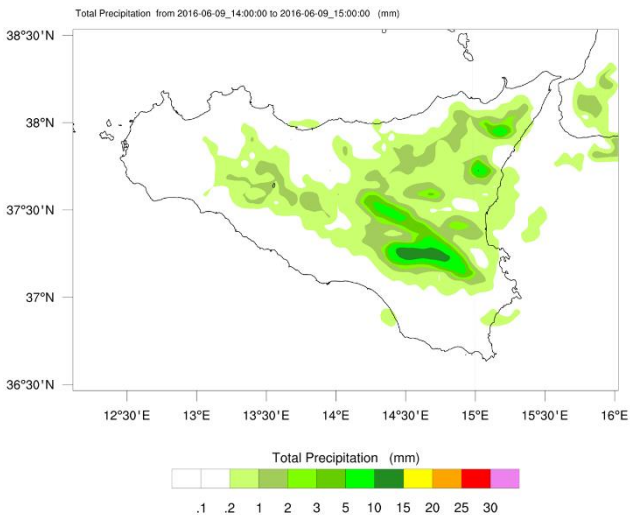
WRF Sicilia - Cu-Physic = 3

Init: 2016-06-08_00:00:00
Valid: 2016-06-09_15:00:00



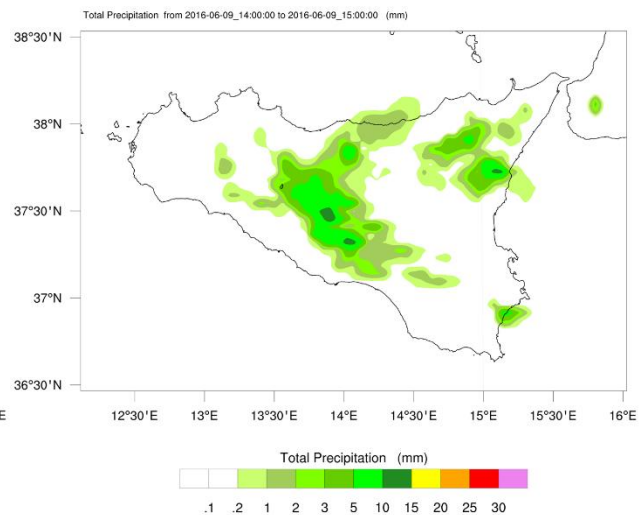
WRF Sicilia - Cu-Physic = 4

Init: 2016-06-08_00:00:00
Valid: 2016-06-09_15:00:00



WRF Sicilia - Cu-Physic = 5

Init: 2016-06-08_00:00:00
Valid: 2016-06-09_15:00:00



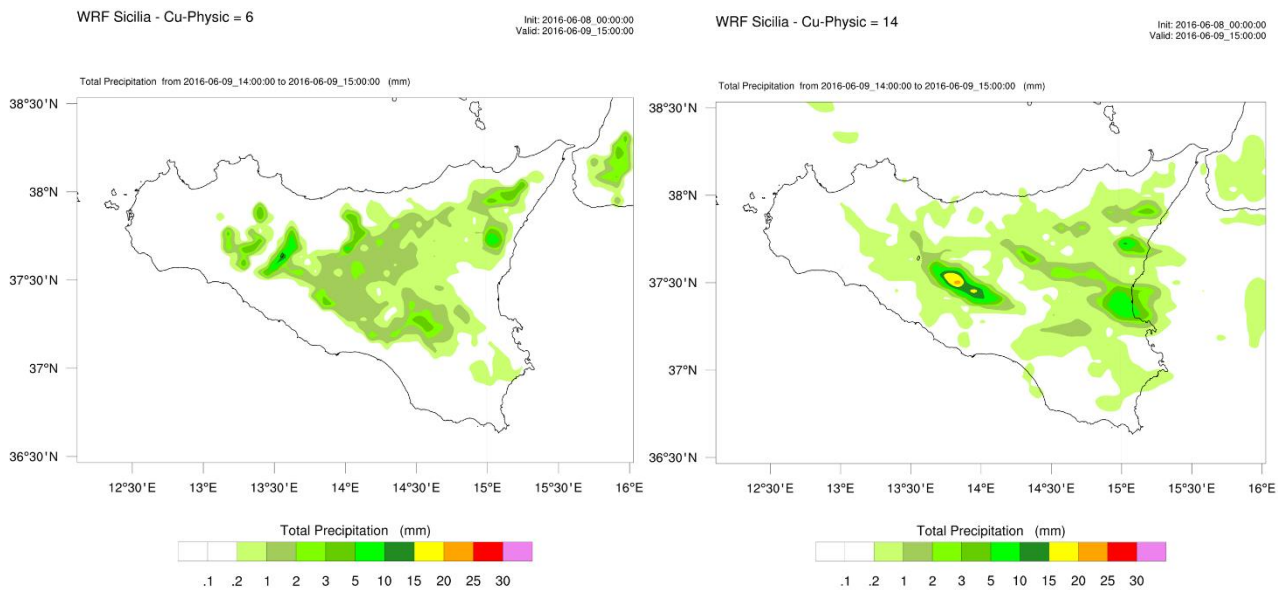
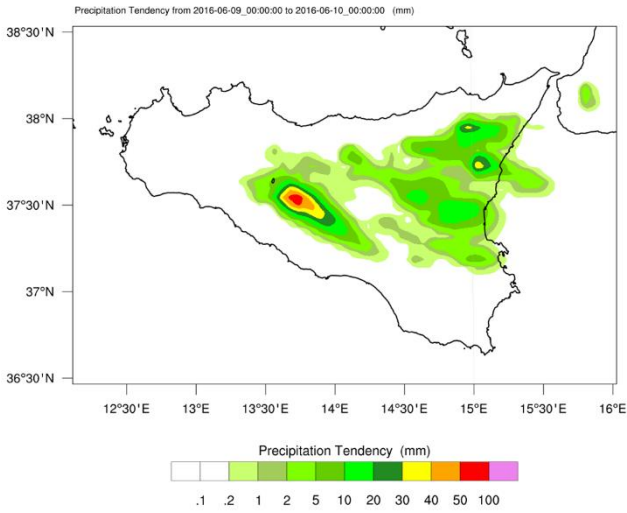


Fig. 46: Comparison of different output in hourly rain forecast between 00 and 15 UTC for different Cu-physics parametrization.

Analyzing the performances obtained on the total rainfall in 24 hours (Fig. 47), should be noted that explicit convection (Cu-Physics = 0) and the New Simplified Arakawa-Schubert (Cu_Physics = 14) overestimate the amount of rainfall. In fact, they forecast rainfall values above 50 millimeters. However, they are able to provide an excellent performance on the time and spatial location of the meteorological event under examination.

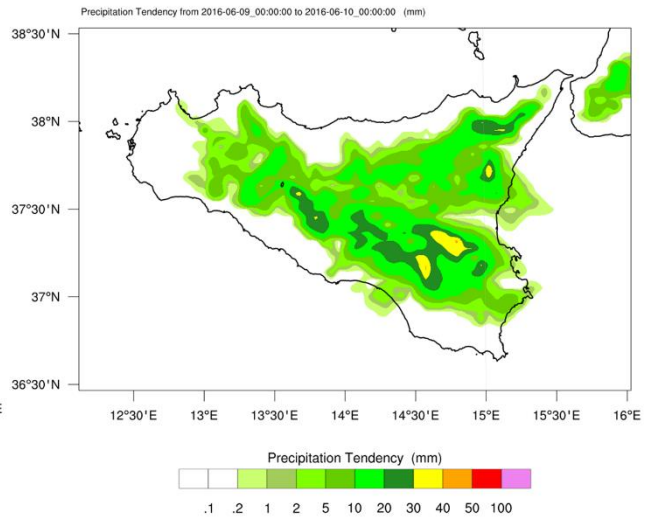
WRF Sicilia-UNIME - Cu-Physics=0

Init: 2016-06-08_00:00:00
Valid: 2016-06-10_00:00:00



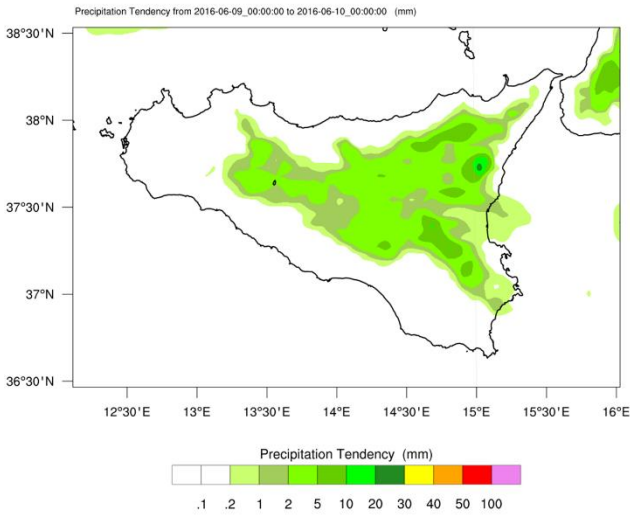
WRF Sicilia-UNIME - Cu-Physics=1

Init: 2016-06-08_07:00:00
Valid: 2016-06-10_00:00:00



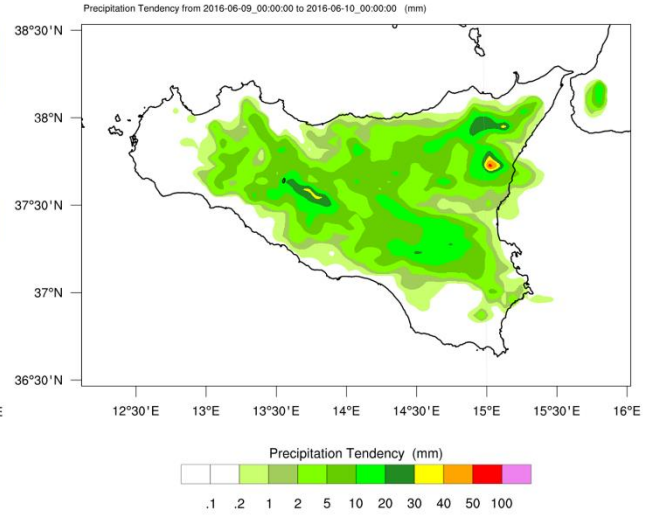
WRF Sicilia-UNIME - Cu-Physics=2

Init: 2016-06-08_07:00:00
Valid: 2016-06-10_00:00:00



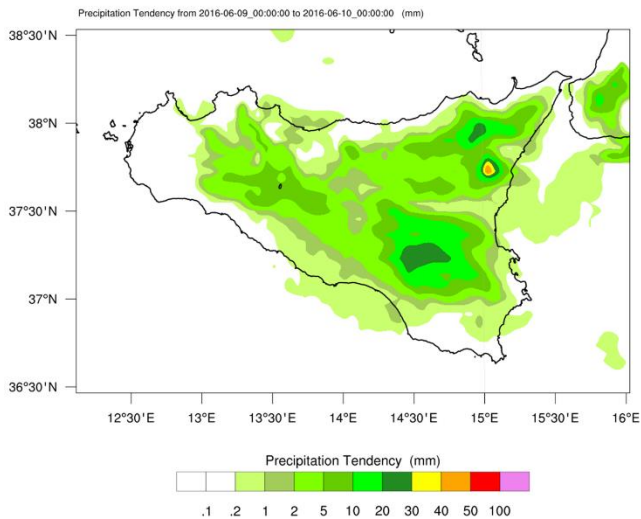
WRF Sicilia-UNIME - Cu-Physics=3

Init: 2016-06-08_00:00:00
Valid: 2016-06-10_00:00:00



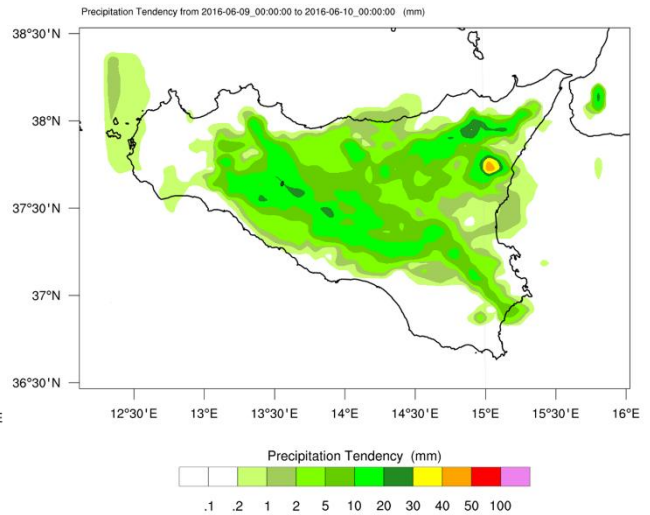
WRF Sicilia-UNIME - Cu-Physics=4

Init: 2016-06-08_00:00:00
Valid: 2016-06-10_00:00:00



WRF Sicilia-UNIME - Cu-Physics=5

Init: 2016-06-08_00:00:00
Valid: 2016-06-10_00:00:00



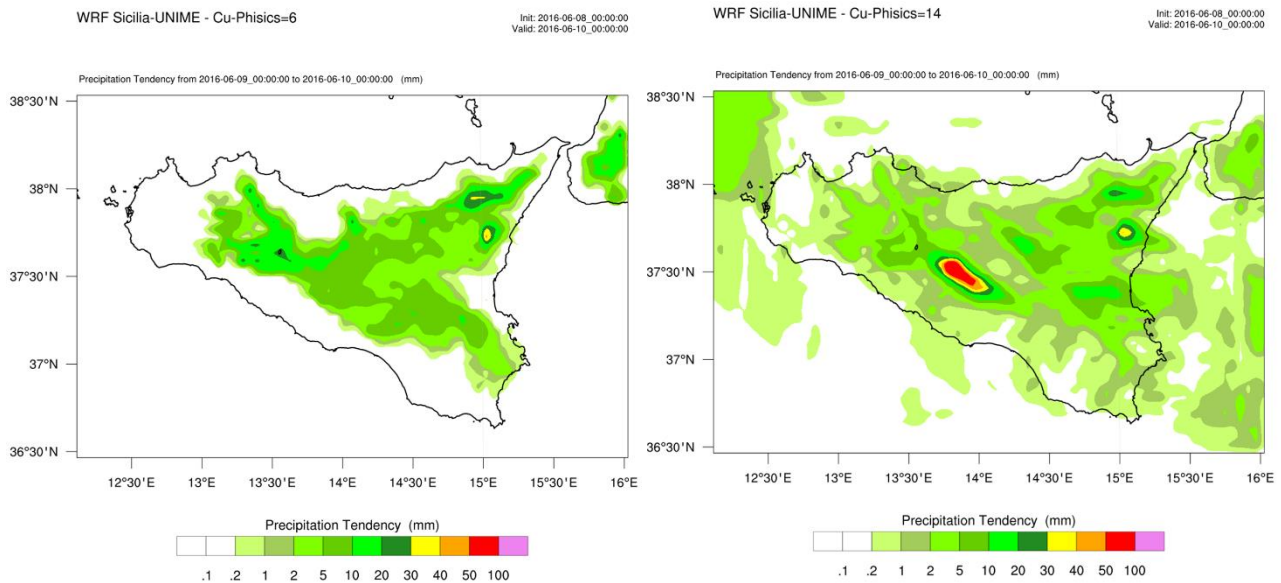


Fig. 47: 24 hours total precipitation forecast for compared Cu-physics parametrizations.

Further investigations carried out on the study case involved the selection of a predictor Storm parameter, able to provide useful information about the spatial and time localization of convective storm cells. The forecast of thunderstorms is in fact of great interest especially for meteorological forecasting for civil protection purposes and in the preservation and safeguarding of the territory. In addition to the CAPE they were taken into account the Cross-Total Index, the Total-Totals Index and the S Index. To complete the comparison, it took also into account the Absolute Vorticity 500 Hpa and the Storm Relative Helicity (SRH), a mathematical quantity derived from:

1. shear speed (how much wind speed increases with height) between the surface and 3 km above,
2. directional shear (how much wind speed direction changes with height) between the surface and 3 km above,
3. The strength of the low level wind directly into the speed and directional wind shear.

The stronger each of these components is the higher the helicity. 150-300: supercell development possible with large CAPE, 300-450: supercell development possible with small CAPE, > 450: large risk for supercell development, risk for violent tornadoes.

The comparison between the various indices shows how the only CAPE index is inappropriate to make a forecast of thunderstorms. Among the other indices used, only the S Index can give useful indications on the area of a probable storm cell development. A different discussion holds for the two diagnostic variables Absolute Vorticity and Helicity. In this case, the simultaneous analysis of the two variables would allow to give some useful guidance both on site and on the time when the thunderstorm cell would develop, as evidenced by the panels in Fig. 48.

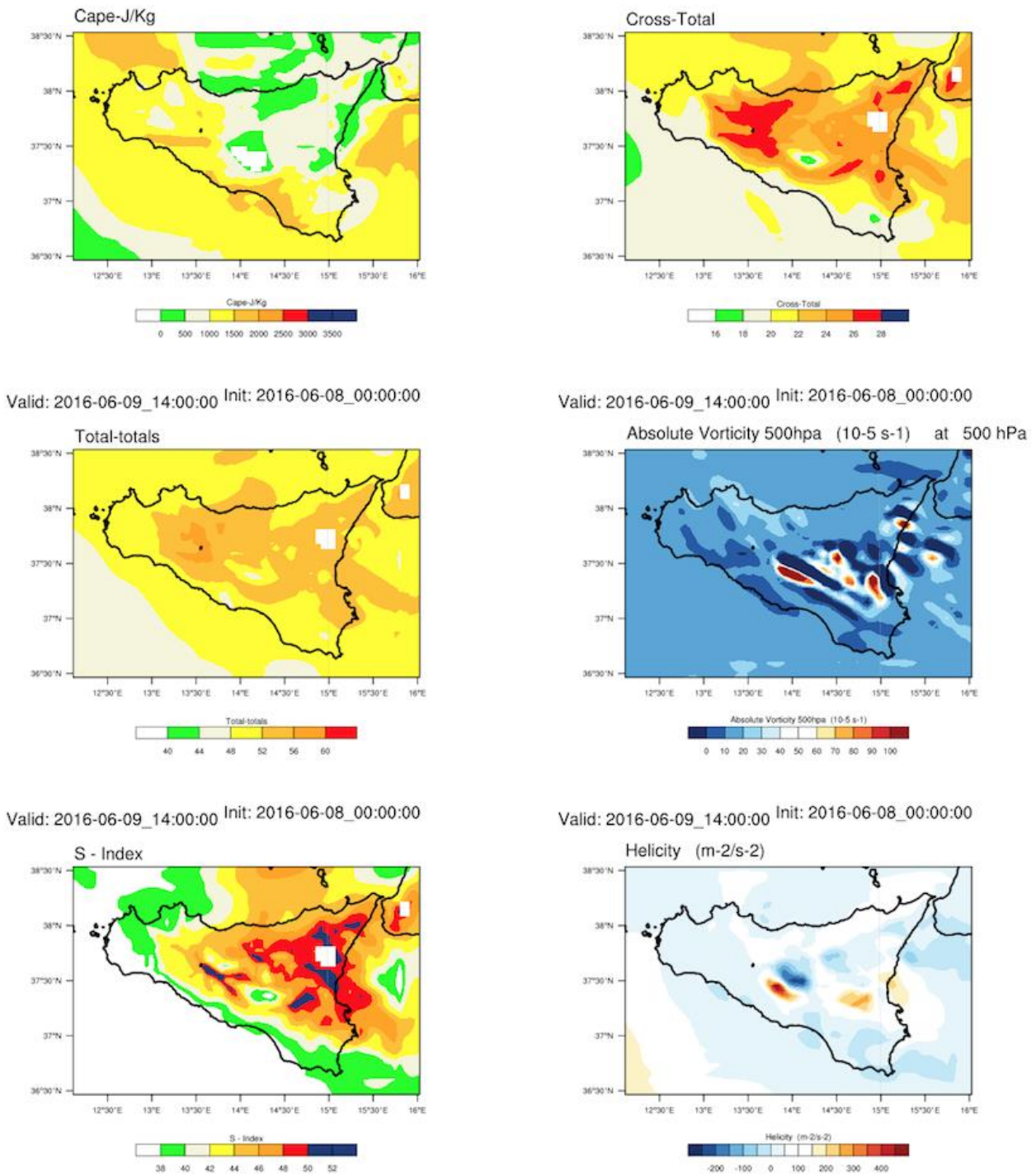


Fig. 48: Comparison between the various indices. The CAPE index is necessary but not sufficient to make a forecast of the storms. The S index can provide useful guidance on the area of a probable storm cell development. The two diagnostic variables Absolute Vorticity and Helicity would allow to give indication both on the site and on the moment in which the time cell would develop

Conclusion

The study undertaken wants to point out as the choice of convective parameterization determines the goodness of the prediction obtained by the WRF model. This study allowed to evaluate the performance on a particular territory, namely Sicily in which, the complex orography and to the presence of seas with bathymetric and thermodynamic characteristics often very different, can play a decisive role in the development or not of convective storm cells. The case study of the June 9th represents was the typical thermo-convective cell of summer storms, which developed because of excessive heating of the soil and favored in his ascension by the presence of unstable air. Some convective parameterizations in the model are able to grasp and adequately reproduce what then in reality occurred, others were deficient both concerning the time and spatial location, as well as for the estimation of forecast precipitation amounts. This study has allowed to define the parameter settings that allow the model to have the best performance.

- **25th November 2016**

The month of November 2016, was characterized by a long and prolonged phase of bad weather which affected the whole Sicily. One of the most significant because of its intensity, was the event occurred on 25 November which caused spread floods both on the southern coast and on the Ionian coast between the town of Catania and Messina.

The 500 hPa chart analysis (Fig. 49), shows an upper vortex centred over the Iberian, which caused a presence of intense vertical streams. The cyclonic bending support the surface convergence and the consequent presence of vertical streams over Sicily with values around 0,2 m/sec. This configuration allows the simultaneous presence of the three components able to generate the initial development of a convective system: the presence of high level of humidity in the lower atmosphere supported by sea surface temperature still relatively high able to provide latent heat during the processes of condensation and finally an instability of the troposphere.

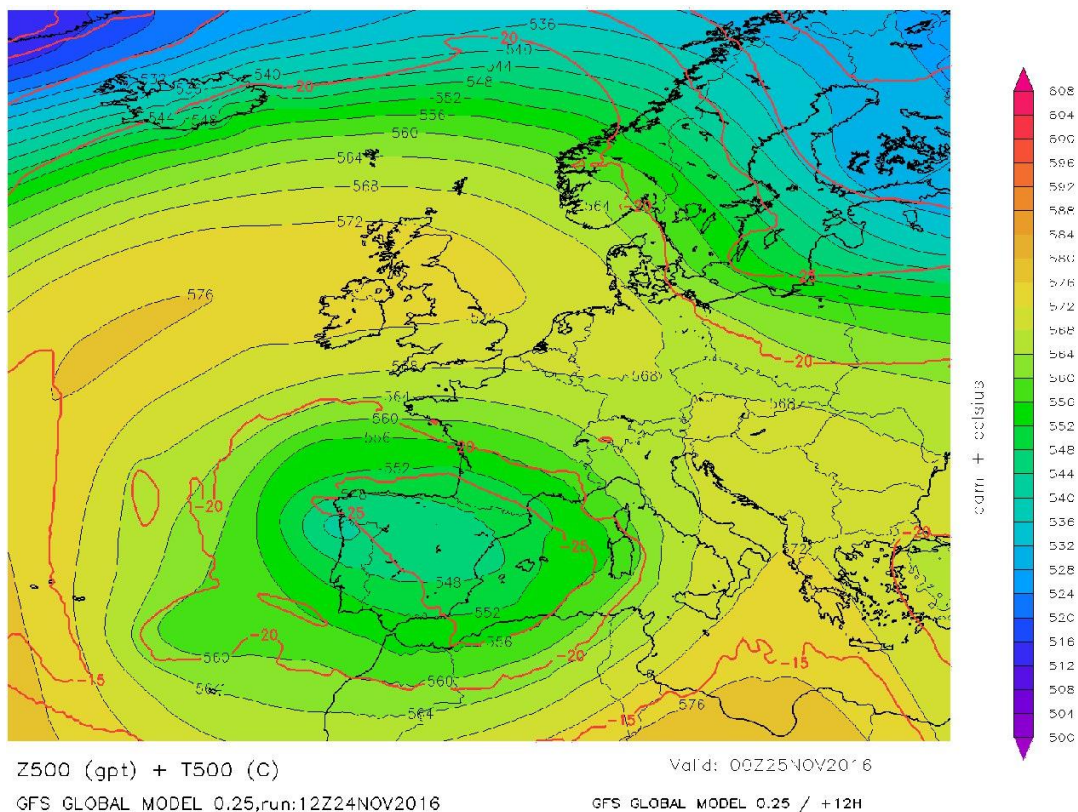


Fig. 49. Analysis of 500hPa. It shows the upper vortex centred over the Iberian, which caused a presence of intense vertical streams.

The relative high temperature of sea surface, allowed the development of high level of humidity in the lower atmosphere (Fig. 50) where is visible the huge reservoir of heat along the coast of Libyan Sea.

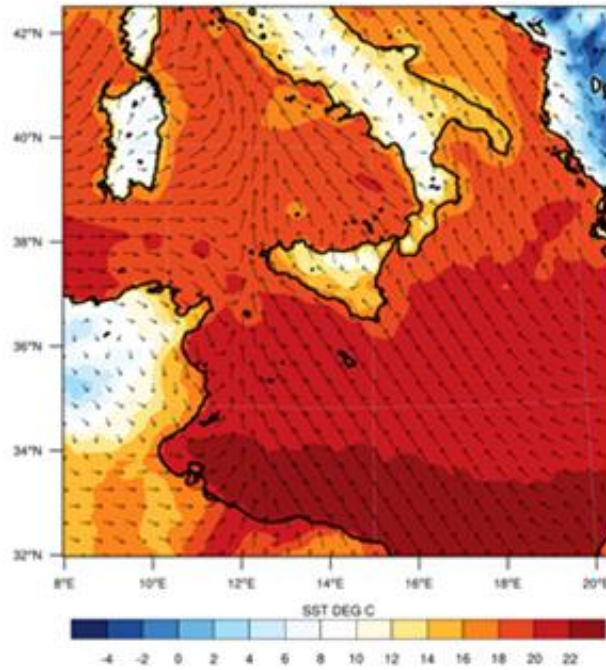


Fig. 50 Analysis of SST and surface wind streams. The figure shows the high level of humidity in the lower atmosphere, and the huge reservoir of heat along the coast of Libyan Sea.

After 00:00 UTC, the cold air mass reached the western coast of Sicily, causing scattered thunderstorms over the area. The air rising caused by the cold front, found an environment ready to generate a strong convective storm, which generate a V-shaped Storm in the northern portion of Pantelleria Island. The heaviest precipitations occurred along the southern coast of Sicily between the town of Ribera and Sciacca (Fig. 51).

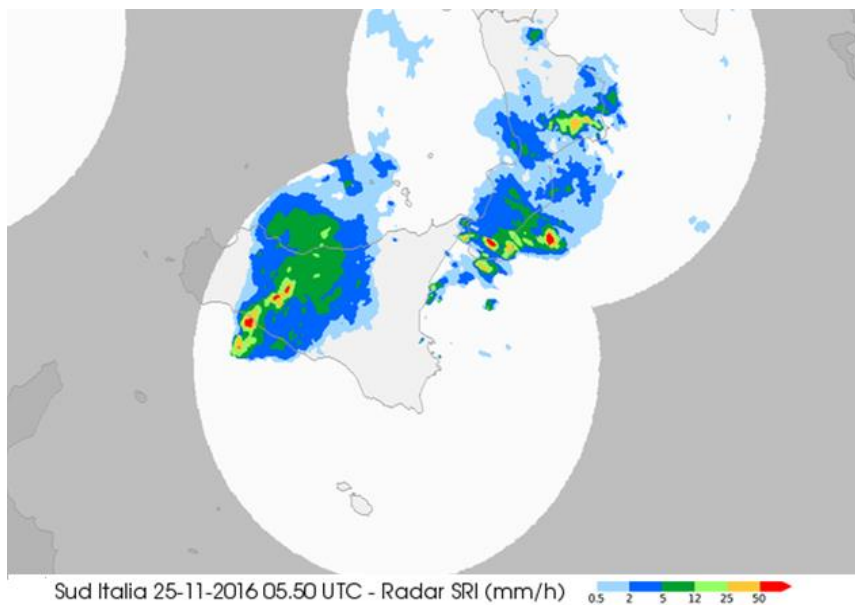


Fig. 51: RADAR picture taken at 05.50 UTC showing the high precipitation rate along the southern coast. The chromatic scale shows the millimetres/hours of rain observed.

This thunderstorm, called V-Shaped, are mesoscale storm systems, with the characteristic of produce intense precipitations in the southern portion of the V point where super cellular elements could be active. About 200 mm of rain were recorded by the weather station of Bivona between 05:30 and 11:00 UTC, with maxima values of 51,4 mm in 30 minutes. The weather station of Giuliana, few kilometres west of Bivona, recorded 163,2 mm. In the some hours, severe precipitation affected also the eastern coast producing the flood of the town of Giardini Naxos and a victim.

Description of the case study

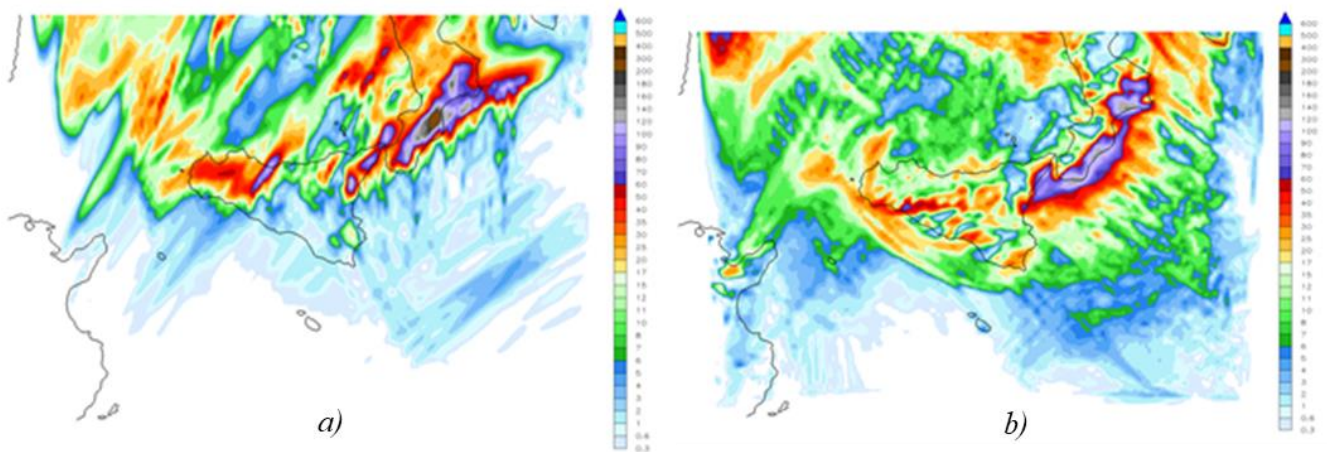
The model is configured with horizontal grid spacing of 5km came out by a single-run . The model configuration uses 65 vertical levels with a maximum height of 50 hPa. The global model GFS at 0.25 degrees with a time interval resolution of 1h, processed for the 00Z run relative to the 24 November 2016 have generated the initial and boundary conditions. RTG sea surface temperature data with a resolution of 0.083 degrees were used. For long-wave and short-wave radiations the RRTMG scheme was used. In addition the above, were also used the schemes of Mellor-Yamada-Janjic for the boundary layer and Noah land surface model. The microphysical scheme utilized was the Thompson, a well known double-moment scheme widely tested especially in high-resolution simulations.



Fig 52. Map of the spatial domain used by the WRF model. The domain is centered on Sicily. The model is configured with horizontal grid spacing of 5km and a time interval resolution of 1h

The evaluations carried out in the present study regard the performances of the model when changes in different convective parameterization are applied. In particular the forecasts the amount and the spatial distribution of rain during the event were compared. The parameterizations compared are as follows. CU0 represent the explicit convection. CU1 is the Kain-Fritsch scheme, it is a deep and shallow convection sub-grid scheme using a mass flux approach with downdrafts and CAPE removal time scale. CU2 is the Betts-Miller-Janjic schem and it is operational Eta scheme. It is a column moist adjustment scheme relaxing towards a well-mixed profile. CU3 is the Grell-Devenyi (GD) scheme. It is a ensemble scheme: Multi-closure, multi-parameter, ensemble method with typically 144 sub-grid members. CU5 is the Grell 3D scheme. Is an improved version of the GD scheme that may also be used on high resolution (in addition to coarser resolutions) if subsidence spreading (option `cugd_avedx`) is turned on. CU6 is the Tiedtke scheme. It is a mass-flux type scheme with CAPE removal time scale, shallow component and momentum transport. CU14 is the New Simplified Arakawa-Schubert scheme. It is a new mass-flux scheme with deep and shallow components and momentum transport.

Fig. 53 shows the simulations of the pluviometric accumulations, obtained using the various physical parametrizations of the convective schemes. The results can be compared with the map of the data observed by the network of meteorological stations of the Regional Department of Civil Protection (DRPC)



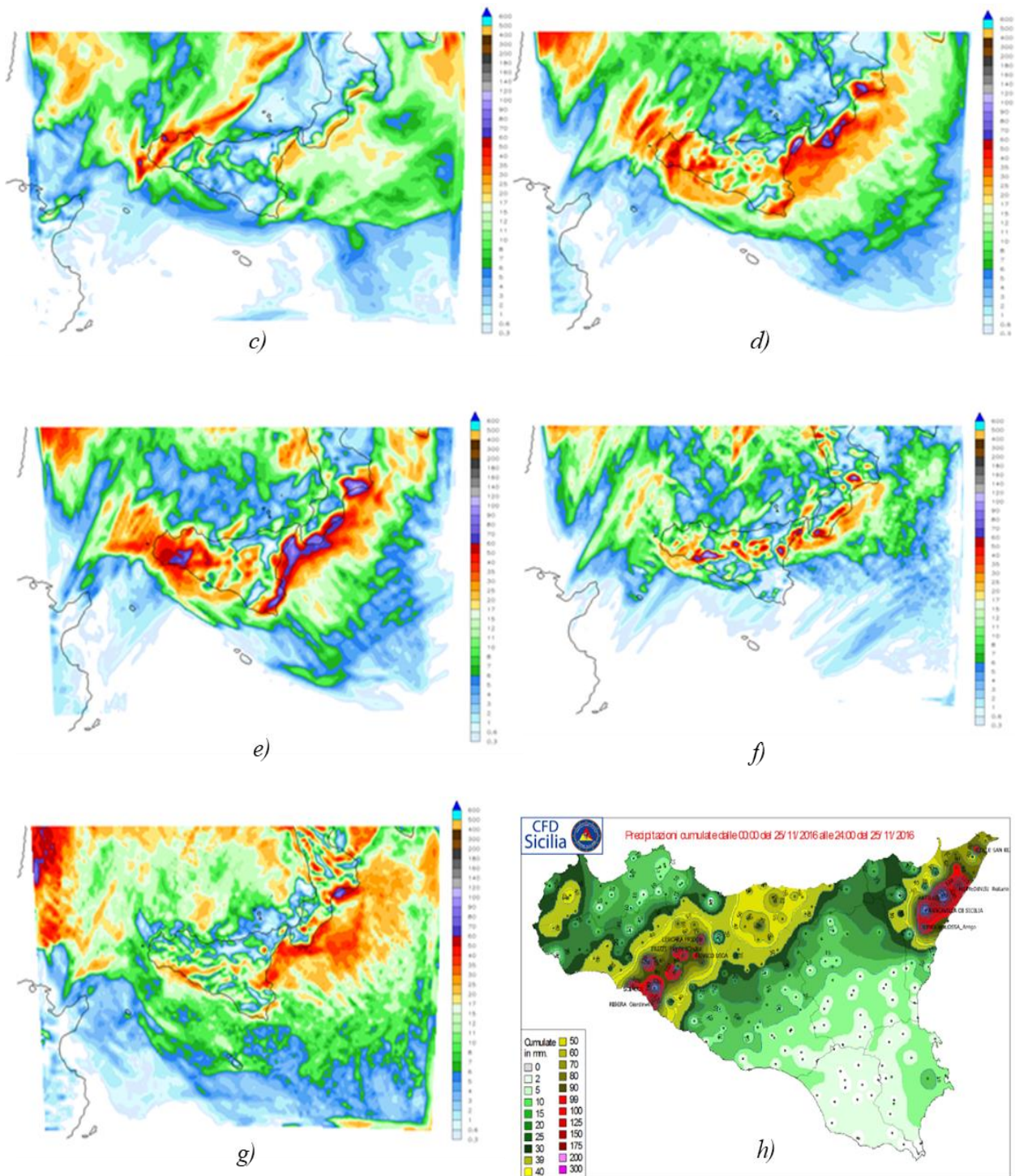


Fig. 53: Total rainfall maps (Accumulate + Convective) obtained through the WRF model using different physical parametrizations of convective schemes and map of data observed by the DRPC meteorological station network. a) is the CU0 convective parameterization; b) is the CU1 convective parameterization; c) is the CU2 convective parameterization; d) is the CU3 convective parameterization; e) is the CU5 convective parameterization; f) is the CU6 convective parameterization; g) is the CU14 convective parameterization; h) is the map of a pluviometric data observation

Visual analysis, however, fails to show what physical parameterization of convective schemes has provided the best performance. It is necessary to choose a set of meteorological stations in the area of interest, as shown in Fig. 54.



Fig. 54: Map of weather stations used in this case study: 5 stations in the north of Sicily (Castelbuono, Lascari, Pettineo, Polizzi and Cefalù), 4 in the northeast sector (Antillo, Fiumedinisi, Linguaglossa and San Pier Niceto) and 4 in the south - west (Bivona, Giuliana, Ribera and Sciacca).

In the first analysis, the extrapolation of the rainfall accumulations recorded by the 13 weather stations examined was carried out. The choice of meteorological stations has been done accounting for the spatial localization of the extreme recorded meteorological event. In particular, the following stations have been chosen as reference: 5 stations in the north of Sicily (Castelbuono, Lascari, Pettineo, Polizzi and Cefalù), 4 in the northeast sector (Antillo, Fiumedinisi, Linguaglossa and San Pier Niceto) and 4 in the south - west (Bivona, Giuliana, Ribera and Sciacca).

Subsequently, the rainfall data were extrapolated for each simulation in which the physical parametrizations of the convective phenomena were modified. The forecasted rainfall data and observed data by the 13 weather stations are shown in Table 6, 7 and 8

Station name	24 H Rain mm	24 H Rain mm CU0	24 H Rain mm CU1	24 H Rain mm CU2	24 H Rain mm CU3	24 H Rain mm CU5	24 H Rain mm CU6	24 H Rain mm CU14
<i>Castelbuono (N)</i>	74,1	2,3	12,2	3	1,7	8,5	18,5	7,6
<i>Lascari (N)</i>	53,6	15,7	14,5	3,6	11,1	12,6	7,5	5,3
<i>Pettineo (N)</i>	46,2	10,5	17,9	2,5	3,7	2,8	8,8	7,2
<i>Polizzi (N)</i>	89,4	8,2	7,5	1,1	7,1	7,3	8,2	0,8
<i>Cefalù (N)</i>	34,1	8,1	19,1	3	23,6	25,7	16,3	6,2

Table 6: The forecasted rainfall data and observed data by the 5 stations in the north of Sicily

Station name	24 H Rain mm	24 H Rain mm CU0	24 H Rain mm CU1	24 H Rain mm CU2	24 H Rain mm CU3	24 H Rain mm CU5	24 H Rain mm CU6	24 H Rain mm CU14
<i>Antillo (NE)</i>	159,5	40,1	10,8	5,2	22,1	19,8	9,6	1,5
<i>Fiumedinisi (NE)</i>	153,8	71,3	26,5	10,8	40	15,3	18,1	2,1
<i>Linguaglossa (NE)</i>	92,1	50,1	1,4	0	2,1	0,5	0,4	1,2
<i>San Pier Niceto (NE)</i>	98,6	22	18,6	2,9	9,4	10,6	4,5	6,6

Table 7: The forecasted rainfall data and observed data by the 5 stations in the north of Sicily

Station name	24 H Rain mm	24 H Rain mm CU0	24 H Rain mm CU1	24 H Rain mm CU2	24 H Rain mm CU3	24 H Rain mm CU5	24 H Rain mm CU6	24 H Rain mm CU14
<i>Bivona (SW)</i>	64,3	29,1	52,5	6,6	53	39,3	102,6	53
<i>Giuliana (SW)</i>	163,2	33,3	39,0	9,8	41,3	29,3	53,6	53,6
<i>Ribera (SW)</i>	198,4	7,5	52,4	5	28,5	29,2	74,5	12,9
<i>Sciacca (SW)</i>	132,3	13,2	50,8	9,9	37,8	46,2	46,6	21

Table 8: The forecasted rainfall data and observed data by the 4 stations in the south - west of Sicily

The hour time series of the pluviometric data forecast and observed for the meteorological stations of Bivona, Sciacca, Pettineo and Fiumedinisi are shown in the following graphs (Fig. 55):

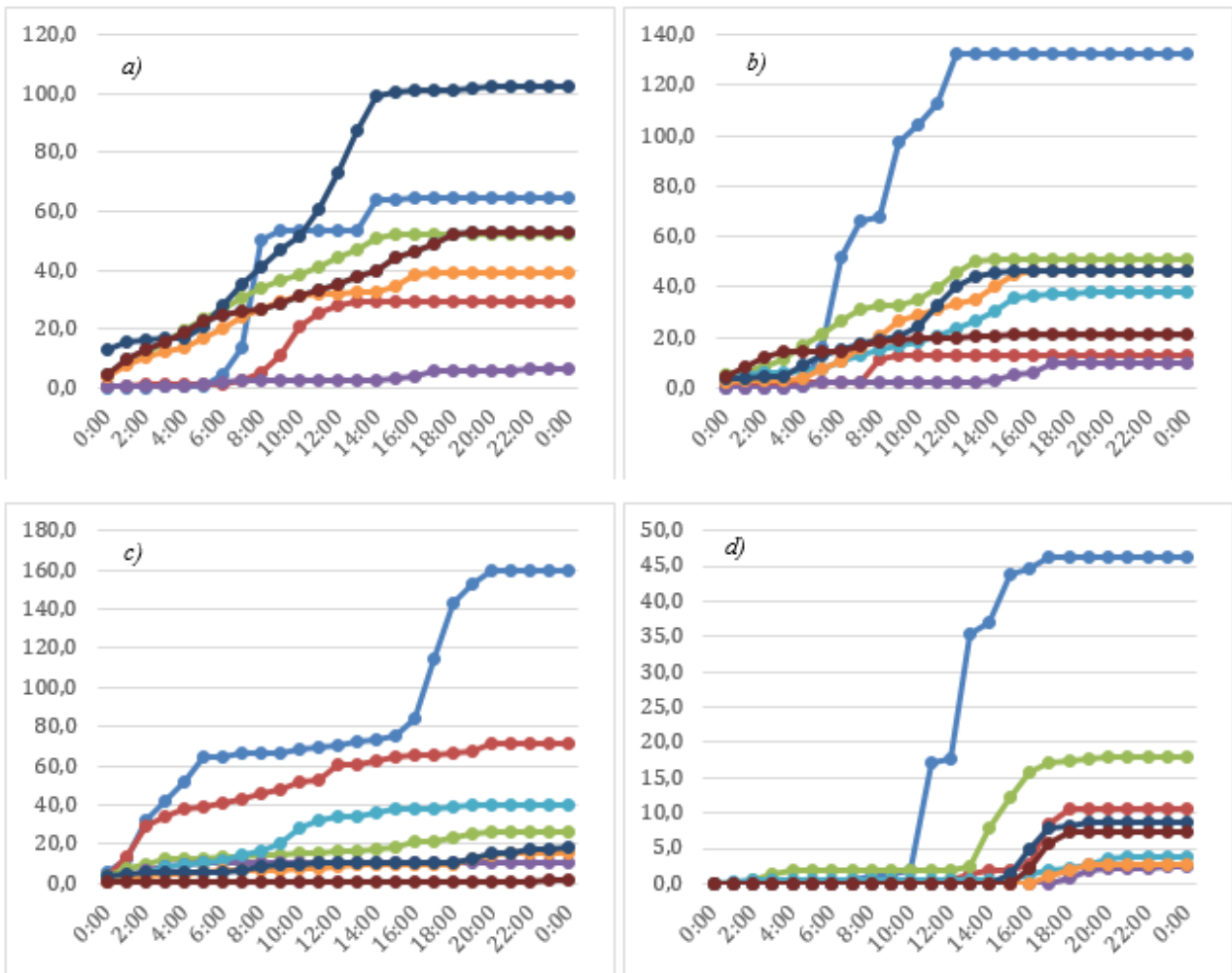


Fig. 55: The hour time series of the pluviometric data forecast and observed for the meteorological stations. a) is the time series of Bivona meteorological station; b) is the time series of Sciacca meteorological station; c) is the time series of Fiumedinisi meteorological station; d) is the time series of Pettineo meteorological station. In the graphs, the blue line represents the data observed by the weather station; the red line represents the simulation of the CU0 scheme; the green line represents the simulation of the CU1 scheme; the violet line represents the simulation of the CU2 scheme; the light blue line represents the simulation of the CU3 scheme; the orange line represents the simulation of the CU5 scheme; the dark blue line represents the simulation of the CU6 scheme; the bordeaux line represents the simulation of the CU14 scheme.

Performance testing of WRF model simulations

In order to establish which of the simulations provided the best performance, it is necessary to use statistical methods. The performance of a forecast model can be calculated using one or more scalar verification indices. A possible method to obtaining these indices is provided by the dicotomic predictions, yes / no. In order to calculate these indices you need to place the data in a table of $I \times J$ elements, called "contingency table", which contains the absolute frequencies of all possible combinations of the observed and predicted data pairs. Considering the case $I = J = 2$, as shown in Fig. 56, "a" indicates the number of cases in which the event was expected to occur and its actually happening, "b" is the number of cases in which the event was expected to happens but it did not occur, "c" represents the number of cases in which the event occurred but was not expected and finally "d" represents the number of cases in which the absence of the event was properly scheduled.

		<i>Observed</i>		
		yes	no	
<i>Forecast</i>	yes	a	b	a + b
	no	c	d	c + d
		a + c	b + d	N

Fig. 56: Contingency Table Schedule. The term $a + b$ represents the forecast meteorological events by the model. The term $c + d$ represents not forecast meteorological events by the model. The term $a + c$ represents the observed rainy weather events. The term $a + d$ represents the not observed rainy weather events

Dividing by $N = a + b + c + d$, we obtain the combined distribution of prediction relative frequencies and the observed data; a perfect forecast have zero values only for the elements on the diagonal of the table.

From the contingency table it is possible to define the categorical indexes used to quantify the yield of the simulations performed with this model, in particular:

- **Hit rate:** defined as the ratio between the number of cases in which the event was correctly predicted and the total number of cases considered, n. The value 0 indicates a bad forecast, on, the value 1 indicates a perfect forecast.

- **Threat score:** is an alternative to the hit rate, useful when the event considered has a substantially lower occurrence frequency than non-occurrence. If the threat score assumes the value 0, the forecast will be bad, otherwise, if it assumes the value 1, the forecast will be perfect.
- **Bias:** It represents the ratio between the predicted and observed data average.
 $B = 1 \rightarrow$ the event was predicted the same number of times that it was observed
 $B > 1 \rightarrow$ overforecasting, the model predicts events with greater frequency than real
 $B < 1 \rightarrow$ underforecasting, the model predicts events with a lower frequency than real
- **False Alarms Rate:** is designed to highlight the tendency to predict events that will not happen. It is especially useful to verify the prediction ability of extreme events. If it assumes the value 0, the forecast will be perfect, if it assumes value 1 there will be the prediction of events that will not happen.
- **Equitable Threat Score:** is based on TS. By definition ranging from -1/3 to 1 (perfect prediction)
- **Hanssen-Kuipers Discriminant:** is given by the ratio between the events correctly predicted and those actually occurred less the probability of having a false alarm. By definition ranging from -1 to 1 (perfect prediction,)

In the Table 9 and in the Fig. 57 are shows the indexes values obtained for the case study considered.

	<i>CU0</i>	<i>CU1</i>	<i>CU2</i>	<i>CU3</i>	<i>CU5</i>	<i>CU6</i>	<i>CU14</i>
Accuracy	0,68	0,53	0,45	0,54	0,53	0,51	0,52
TS	0,49	0,43	0,12	0,38	0,35	0,30	0,26
Bias	0,95	1,47	0,49	1,13	1,07	0,91	0,73
ETS	0,22	0,04	-0,06	0,05	0,03	0,01	0,01
POD	0,64	0,74	0,16	0,58	0,54	0,44	0,36
FAR	0,33	0,50	0,67	0,48	0,50	0,51	0,51

Table 9: Numeric values of indexes calculated for each simulation performed by modifying the physical parameterization of the convective processes of the WRF model



Fig 57: Graphic of indexes calculated for each simulation performed by modifying the physical parameterization of the convective processes of the WRF model. It shows that the CU0 (blue line) is the most reliable and accurate solution. The CU2 (green line) is the worst. CU1 (red line), CU3 (violet line) and CU5 (light blue line) show only small differences and they are the only ones that tend to overestimate the rain. The CU14 and the CU6 (orange line) schemes are only slightly better than the CU2

The analysis shows that the explicit resolution of convective processes (CU0) is the most reliable and accurate solution with the highest accuracy in term of Threat Score and Equitable Threat score.

The Betts-Miller-Janic scheme (CU2) is the worst and is the one that also generates the highest number of false alarms (FARs). The New Simplified Arakawa-Schubert (CU14) and Tiedtke (CU 6) schemes are only slightly better than the BMJ (CU2). New Kain Fritsch schemes (CU1), Grell-Devenyi (CU3) and Grell 3D (CU 5) show only small differences and they are the only ones that tend to overestimate the rain. The New Kain Fritsch scheme (CU1), excluding an excessive BIAS overlapping, has good overall behavior and is the one that shows the maximum POD (Probability Of Detection).

Conclusions

The physical parametrization of convective schemes plays a fundamental role in optimizing the performance of limited area meteorological models. This case study analyzed the alluvial event recorded in Sicily on 25 November 2016, the results showed that the explicit parameterization of convective schemes provided the best simulation of the extreme meteorological event. This result was expected from the literature. Most of the convective clouds have horizontal dimensions ranging from 0.1 to 10 km, typically smaller than those the spatial grid of the limited area model (5 km) used in this case study. It is a sub-grid phenomenon, which must be parameterized in terms of prognostic variables.

- **6th January 2017**

A center of low pressure that, between the days of 5th and 7th January 2017, moved from the central south of the Italian peninsula to the coast of Greece, pushed cold air masses from Siberia causing the temperatures to collapse throughout Italy. The marked atmospheric instability and the strong icy winds coming from the northern quadrants, on 6th January 2017, recorded heavy snowfalls throughout the Sicilian regional territory. Snowfalls at very low altitudes have also been recorded in the province of Messina. In particular, snowfalls were recorded on the Ionian coast of Messina. In the present case study, the numerical simulations of the WRF limited area model are analyzed. The performances of the WRF model, appropriately optimized for Sicily (territory characterized by a complex orography) provide considerable support in various multidisciplinary fields [82-85].

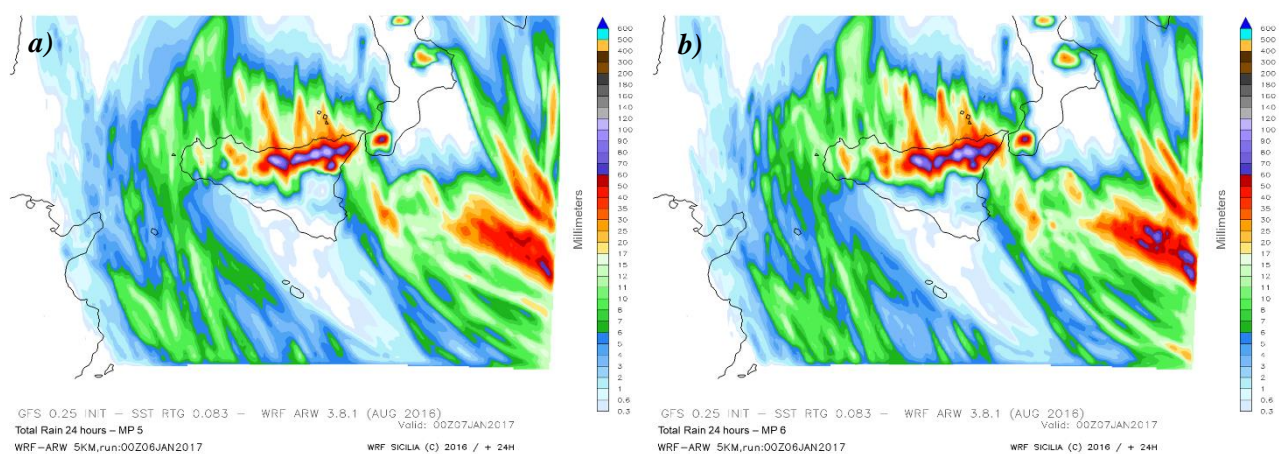
The model is configured with horizontal grid spacing of 5km (Fig. 58) came out by a single-run. The model configuration uses 65 vertical levels with a maximum height of 50 hPa. The global model GFS at 0.25 degrees with a time interval resolution of 1h, processed for the 00Z run relative to the 24 November 2016 have generated the initial and boundary conditions. RTG sea surface temperature data with a resolution of 0.083 degrees were used. For long-wave and short-wave radiations the RRTMG scheme was used. In addition the above, were also used the schemes of Mellor-Yamada-Janjic for the boundary layer and Noah land surface model.



Fig 58. Map of the spatial domain used by the WRF model. The domain is centered on Sicily. The model is configured with horizontal grid spacing of 5km and a time interval resolution of 1h

In the specific case, it is wanted to evaluate the performance of the model at the varies of a microphysicals parameterizations. The parametric schemes for the ETA Ferrier microphysics (MP5), WSM6 (MP 6) and Thompson (MP8) were examined. In both cases there are single moment schemes in which six classes of hydrometeors are considered. Specifically, the ETA Ferrier scheme considers the size of the hydrometeors as a function of temperature following Ryan's observations [38]. Processes between one phase and another of water for temperatures above 243 K are possible, while for lower temperatures only the solid phase is considered. The density of the various particles is considered a function of the growth processes to which the particles themselves are subjected. The WSM6 scheme pays particular attention to the concentration of ice crystals in relation to the temperature [31] and to the total mass of ice present in the volume considered. The distribution of the diameters is assumed exponentially and, during the precipitation of the particles, the melting / freezing processes are also calculated to increase the accuracy of the vertical profile relative to the release / absorption of heat [41]. Finally, in the Thompson scheme the snow size distribution is assumed to be a function both of the ice content of the volume considered, and of the temperature and is represented as a combination of the gamma and exponential distributions [37], while for the distribution of the diameters of the other hydrometeors a generalized gamma distribution is used [32]. The density of the snow is supposed to vary inversely proportional to the diameter, unlike what is assumed by many schemes, where it is considered constant.

The Fig. 59 show the simulations in which only the microphysics parameterization scheme has been modified. To highlight the differences, the total rain recorded in the 24 hours and the Snow Water Equivalent (i.e. the international unit to measure the amount of snowpack expressed in kg/m^2) are shown.



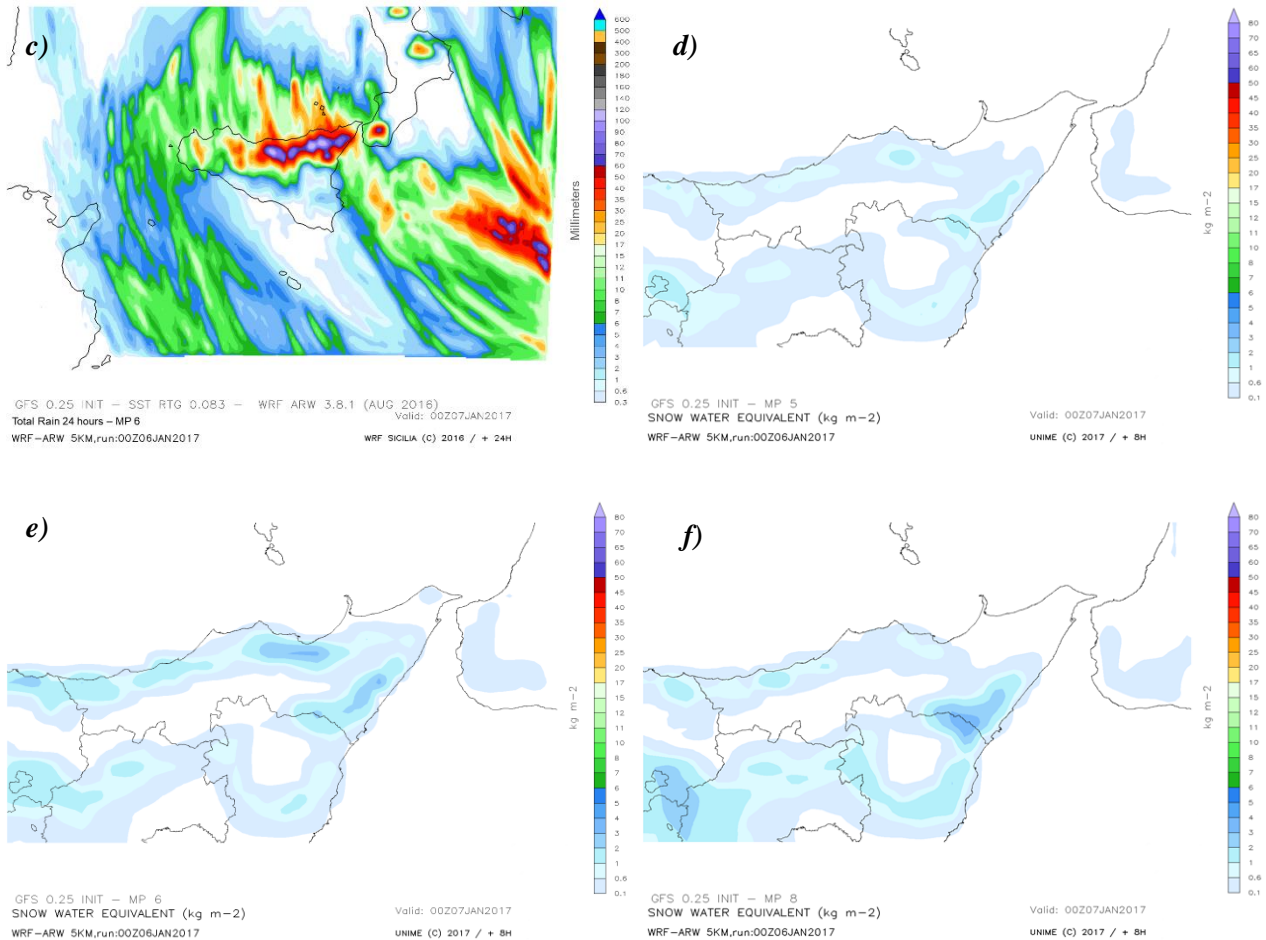


Fig 59. Simulations in which only the microphysics parameterization scheme has been modified.. a) Total rain recorded in the 24 hours through MP5, b) Total rain recorded in the 24 hours through MP6, c) Total rain recorded in the 24 hours through MP8, d) Snow Water Equivalent through MP5, e) Snow Water Equivalent through MP6, f) Snow Water Equivalent through MP8.

The visual analysis of the forecast maps shown in Fig. 59 shows a substantial agreement in the total precipitation accumulated over the 24 hours. The MP6 microphysical scheme provided slightly higher pluviometric accumulations than the remaining schemes (MP5 and MP8). A substantial difference, however, is highlighted in the Snow Water Equivalent. The MP6 microphysical scheme, unlike the MP5 and MP8 schemes, was the only one to forecast, with 24 hours in advance, the snowfalls recorded on the Ionian coast of the province of Messina.

Conclusions

Systems of nonlinear equations, such as the generalized Navier-Stokes equations, and the parametrizations of physical processes, form the basis of numerical models for meteorological analysis. The purpose of this case study is to evaluate the performance of the meteorological model presented to the variation of the microphysical parameters, each of which takes into consideration

different processes of nucleation of the hydrometeor. Between the days of 6 and 7 January 2017, frigid air masses from Siberia, caused a significant drop in temperatures throughout the Sicilian territory, making intense snowfalls recorded at very low altitudes. The analysis of the forecast maps shows how the WSM6 microphysical scheme (MP6), unlike the ETA Ferrier microphysics (MP5), and Thompson (MP8), was the only one to forecast, with 24 hours in advance, the snowfalls recorded on the Ionian coast of the province of Messina.

References

- [1] R. Benzi, G. Parisi, A. Suter, A. Vulpiani: Stochastic resonance in climatic change. *Tellus* (1982) 34, 10-16.
- [2] Davies-Jones, R., Burgess, D., Foster, M., 1990. Test of helicity as a tornado forecast parameter. *Amer. Meteor. Soc.*, 588–592.
- [3] Showalter, A. K., 1953. A stability index for thunderstorm forecasting. *Bull. Amer. Meteor. Soc.*, 34, 250–252.
- [4] Nebeker, F., 1995. *Calculating the Weather: Meteorology in the 20th Century*. New York: Academic Press. <https://doi.org/10.2307/3106892>
- [5] Curry, J.A., Webster, P. 1998. *Thermodynamics of Atmospheres and Oceans*. Academic press. [https://doi.org/10.1016/s0074-6142\(99\)x8020-x](https://doi.org/10.1016/s0074-6142(99)x8020-x)
- [6] Gill, A.E. 1982. *Atmosphere-Ocean Dynamics*. Academic Press. [https://doi.org/10.1016/s0074-6142\(08\)x6002-4](https://doi.org/10.1016/s0074-6142(08)x6002-4)
- [7] Scoccimarro, E., Gualdi, S., Bellucci, A. et al, 2013. Heavy Precipitation Events in a Warmer Climate: Results from CMIP5 Models. *J. Climate*, 26, 7902–7911. <https://doi.org/10.1175/jcli-d-12-00850.1>
- [8] Galway, J. G., 1956. The lifted index as a predictor of latent instability. *Bull. Amer. Meteor. Soc.*, 37, 528–529.
- [9] Altinbilek, D., Barret, E.C., Oweis, T., Salameh, E., Siccardi, F., 1997. Rainfall climatology on the Mediterranean in EU-AVI 080 Project ACROSS — analyzed climatology rainfall obtained from satellite and surface data in the Mediterranean basin. <http://www.diam.unige.it/idromet/avi080/altinb.html>
- [10] Fiori, E., Comellas, A., Molini, L., Rebora, N., Siccardi, F., Gochis, D.J., Tanelli, S., Parodi, A., 2014. Analysis and hindcast simulation of an extreme rainfall event in the Mediterranean area: the Genoa 2011 case. *Atmos. Res.* 138, 13–29.
- [11] Chen C., Lin Y. 2005. Orographic effects on a conditionally unstable flow over an idealized three-dimensional mesoscale mountain. *Meteorol. Atmos. Phys.* 88, 1 – 21.
- [12] Chen, S.H., Sun, W.Y., 2002. A one dimensional time dependent cloud model. *J. Meteorol. Soc. Jpn.* 80, 99–118.
- [13] Cassola, F., Ferrari, F. & Mazzino, A. 2015. Numerical simulations of Mediterranean heavy precipitation events with the WRF model: a verification exercise using different approaches. *Atmospheric Research*, 164-165, 210-225.

- [14] Chu C, Lin Y. 2000. Effects of orography on the generation and propagation of mesoscale convective systems in a two-dimensional unstable flow. *J. Atmos. Sci.* 57: 3817 – 3837.
- [15] Randall, D., 2001. An introduction to Atmospheric Modelling, Department of Atmospheric Science, Colorado State university, Boulder.
- [16] Giuffrida, A., Sansosti, G., 2007. Manuale di meteorologia; Gremese editore.
- [17] Salby, M.L., 1996. Fundamentals of Atmospheric Physics, Academic Press.
- [18] A. Drago: Sette anni di piogge abbondanti: in Sicilia un lungo periodo in controtendenza. I dati e le elaborazioni del Sias. Palermo (2010)
- [19] M.T. Caccamo, A. Cannuli, G. Castorina, F. Colombo, V. Insinga, E. Maiorana, S. Magazù, Highlights on Extreme Meteorological Events in Sicily, SCIREA Journal of Geosciences, 2017
- [20] Banacos, P. C., Schultz, D. M., 2005. The use of moisture flux convergence in forecasting convective initiation: Historical and operational perspectives. *Wea. Forecasting*, 20, 351-366 <https://doi.org/10.1175/waf858.1>
- [21] Budkyo, M.I., 1982. The Earth's Climate: Past and Future. Academic Press. [https://doi.org/10.1016/s0074-6142\(08\)x6016-4](https://doi.org/10.1016/s0074-6142(08)x6016-4)
- [22] Miller, D.H., 1981. Energy at the Surface of the Earth: An Introduction to the Energetics of Ecosystems. Academic Press. [https://doi.org/10.1016/s0074-6142\(08\)x6022-x](https://doi.org/10.1016/s0074-6142(08)x6022-x)
- [23] Banacos, P. C., Schultz, D. M., 2005. The use of moisture flux convergence in forecasting convective initiation: Historical and operational perspectives. *Wea. Forecasting*, 20, 351-366 <https://doi.org/10.1175/waf858.1>
- [24] Budkyo, M.I., 1982. The Earth's Climate: Past and Future. Academic Press. [https://doi.org/10.1016/s0074-6142\(08\)x6016-4](https://doi.org/10.1016/s0074-6142(08)x6016-4)
- [25] Miller, D.H., 1981. Energy at the Surface of the Earth: An Introduction to the Energetics of Ecosystems. Academic Press.
- [26] M. Korologou, H. Flocas, H. Michalopoulou: Developing an index for heavy convective rainfall forecasting over a Mediterranean coastal area, *Nat. Hazards Earth Syst. Sci.*, 14, 2205–2214, 2014
- [27] Hoogenboom, D.D Gresham, “Auto weather station network “, Proceeding of the 1997 Georgia water resource Conference. Athens, vol.1 (1997) 483-486
- [28] Skamarock, W. C., A Description of the Advanced Research WRF Version 3 NCAR technical note (2008).

- [29] Laprise, R., The Euler equation of motion with hydrostatic pressure as independent variable. *Mon. Wea. Rev.*, 120:197-207 (1992).
- [30] Ooyama, K. V., A Thermodynamic foundation for modeling the moist atmosphere, *J. Atmos. Sci.*, 47:2580-2593 (1990).
- [31] Fletcher, N. H., *The Physics of Rain Clouds*. University Press (1962).
- [32] Walko, R. L., Cotton, W. R., Meyers, M. P. and Harrington, J. Y., New RAMS cloud microphysics parameterization. Part I: The single moment scheme. *Atmos. Research*, 38:29-62 (1995).
- [33] Morrison, H., Pinto, J. O., Mesoscale Modeling of Springtime Arctic Mixed-Phase Stratiform Clouds Using a New Two-Moment Bulk Microphysics Scheme. *J. Atmos. Sci.*, 62:3683-3704, (2005).
- [34] Lim, K.-S., Hong S.-Y., Development of an Effective Double-Moment Cloud Microphysics Scheme with Prognostic Cloud Condensation Nuclei (CCN) for Weather and Climate Models. *Mon. Wea. Rev.*,
- [35] 138:1587-1612, (2010).
- [36] Hong, S. Y., Lim, K. S., Kim, J.-H. and Lim, J.-O. J. Sensitivity Study of Cloud-Resolving Convective Simulation with WRF Using Two Bulk Microphysical Parameterization: Ice-Phase Microphysics versus sedimentation Effects. *J. of Appl. Meteor.*, 48:61-76, (2008).
- [37] Morrison, H., Thompson, G. and Tatarskii, V., Impact of cloud microphysics on the development of trailing stratiform precipitation in a simulated squall line: Comparison of one- and two-moment schemes. *Mon. Wea. Rev.*, 137:991-1007, (2009).
- [38] Ryan, B. F., On the global variation of precipitating layer clouds. *Bull. Am. Meteorol. soc.*, 77:53-70, (1996).
- [39] Hong, S. Y., Lim, J. O. J., Thw WRF Single-Moment 6-Class Microphysics Scheme (WSM6), *J. Korean Meteor. Soc.*, 42:129-151, (2006).
- [40] Lin, Y. L., Farley, R. D. and Orville H. D. Bulk parameterization of the snow field in a cloud model. *J. Appl. Meteor.*, 22:1065-1092, (1983).
- [41] Hong, S. Y., Dudhia, J. and Chen, S. H., A Revised Approach to Ice Microphysical Processes for the Bulk Parameterization of Clouds and Precipitation, *Mon. Wea. Rev.*, 132:103-120, (2004).
- [42] Morrison, H., Pinto, J. O., Mesoscale Modeling of Springtime Arctic Mixed-Phase Stratiform Clouds Using a New Two-Moment Bulk Microphysics Scheme. *J. Atmos. Sci.*, 62:3683-3704, (2005).

- [43] Holton, J. R., An introduction to dynamic meteorology. Academic Press, III edition, (1992).
- [44] Emanuel, K. A. and Raymond, D. J., \textit{The representation of cumulus convection in numerical models}. American Meteorological Society, (1993).
- [45] Arakawa, A. and Schubert, W. H., Interaction of a cumulus cloud ensemble with the large scale environment. Part I. J. Atmos. Sci., 31:674-701 (1974).
- [46] Betts, A. K., A new convective adjustment scheme. Part I. Observational and theoretical basis. Quart. J. Roy. Meteor. Soc., 112:693-709 (1986).
- [47] Betts, A. K. and Miller, M. J., A new convective adjustment scheme. Part II. Single column tests using GATE wave, BOMEX, ATEX and arctic air-mass data sets. Quart. J. Roy. Meteor. Soc., 112:693-709 (1986).
- [48] Kuo, H. L., Further studies of the parameterization of the effect of cumulus convection on large scale flow. J. Atmos. Sci., 31:1232-1240 (1974).
- [49] Anthes, R. A., A cumulus parameterization scheme utilizing a one dimensional cloud model. Mon. Wea. Rev., 105:270-286, (1977).
- [50] Fritsch, J. M. and Chappell, C. F., Numerical prediction of convectively driven mesoscale pressure system. Part I: Convective parameterization. J. Atmos. Sci., 37:1722-1733, (1980).
- [51] Kain, J. S. and Fritsch, J. M., The role of trigger function in numerical forecasts of mesoscale convective system. Meteorol. Atmos. Phys., 49:93-106 (1992).
- [52] A. Bejan. Heat Transfer. John Wiley & Sons, Inc. 1993
- [53] F.P. Incropera, D.P. De Witt. Fundamentals of Heat and Mass Transfer. Third Edition, John Wiley & Sons, Inc. 1990
- [54] H. Schlichting. Boundary Layer theory. 4th Edition- Mc Graw Hill, New York, 1960
- [55] R.B. Bird, W.E. Stewart, E.N. Lightfoot. Transport Phenomena. Wiley, New York, 1966
- [56] Bonacina, A. Cavallini, L. Mattarolo. Trasmissione del calore. CLEUP. Padova.
- [57] M. T. Caccamo, M.T., G. Castorina, F. Colombo, V. Insinga, E. Maiorana, S. Magazù, “Weather forecast performances for complex orographic areas: Impact of different grid resolutions and of geographic data on heavy rainfall event simulations in Sicily”, Atmospheric Research, 198, pp. 22-33, 2017, <http://dx.doi.org/10.1016/j.atmosres.2017.07.028>

- [59] Ray, P., 1986. *Mesoscale Meteorology and Forecasting*, American Meteorological Society.
- [60] Wallace J. M., Hobbs, P. V., 2006. *Atmospheric science: an introductory survey*, Academic Press.
- [61] Morrison, H., Milbrandt, J., 2011. Comparison of two-moment bulk microphysics schemes in idealized supercell thunderstorm simulations. *Mon. Weather Rev.* 139, 1103–1130.
- [62] Reeves, H. D., and R. Rotunno, 2008. Orographic flow response to variations in upstream humidity. *J. Atmos. Sci.*, 66, 3557–3570.
- [63] Smith, R., 1979. The influence of mountains on the atmosphere. *Adv. Geophys.* 21: 87 – 230.
- [64] Buzzi, A., Tartaglione, N., Malguzzi, P. 1998. Numerical simulations of the 1994 Piedmont flood: Role of orography and moist processes. *Mon. Wea. Rev.*, 126, 2369 –2383.
- [65] Pineda, N., O. Jorba, J. Jorge, J. M. Baldasano, 2004: Using NOAA AVHRR and SPOT VGT data to estimate surface parameters: application to a mesoscale meteorological model, *International Journal of Remote Sensing*, 25:1, 129-143.
- [66] Mlawer, E.J., Taubman, S.J., Brown, P.D., Iacono, M.J., Clough, S.A., 1997. Radiative transfer for inhomogeneous atmosphere: RRTM, a validated correlated k-model for the long-wave. *J. Geophys. Res.* 102, 16663–16682.
- [67] Chou, M.D., Suarez, M.J., 1994. An efficient thermal infrared radiation parameterization for use in general circulation models. Technical Report. NASA/Goddard Space Flight Center.
- [68] Janjic, Z.I., 2002. Nonsingular implementation of the Mellor–Yamada level 2.5 scheme in the NCEP meso model. Technical Report 437. NOAA Science Center.
- [69] Chen, F., Dudhia, J., 2001. Coupling an advanced land-surface/hydrology model with the Penn state/NCAR MM5 modeling system. Part I: model description and implementation. *Mon. Weather Rev.* 129, 569–585.
- [70] Thompson, G., Rasmussen, R.M., Manning, K., 2004. Explicit forecasts of winter precipitation using an improved bulk microphysics scheme. Part I: description and sensitivity analysis. *Mon. Weather Rev.* 132, 519–542.
- [71] Kain, J.S., 2004. The Kain–Fritsch convective parameterization: an update. *J. Appl. Meteorol.* 43, 170–181.
- [72] Davolio S., Buzzi A., Malguzzi P. (2006) Orographic influence on deep convection: case study and sensitivity experiments, *Meteorologische Zeitschrift*, 15, 215-223.

- [73] Hoskins, B.J, James, I., N., 2014. Fluid Dynamics of the Mid Latitude Atmosphere, Wiley Blackwell.
- [74] Holton, J. R., 2004. An introduction to dynamic meteorology, Academic Press.
- [75] Markowski P., Richardson Y., 2010. Mesoscale Meteorology in Midlatitudes, Wiley.
- [76] Martin, J. E., 2006. Mid-Latitude Atmospheric Dynamics. A First Course, Wiley.
- [77] Stensrud, D.J., 2007. Parametrization Scheme, Cambridge.
- [78] Miglietta, M. M., and A. Buzzi, 2001: A numerical study of moist stratified flows over isolated topography. *Tellus*, 53A, 481–499.
- [79] Haltiner, G., Williams., H., 1983. Numerical prediction and dynamic meteorology; Wiley & Sons Ltd.
- [80] Lackman, G., 2011. Midlatitude Synoptic Meteorology, American Meteorological Society.
- [81] Esteve, B.J., 2014. Land use influence in WRF model. A high resolution mesoscale modeling over Oriental Pyrenees. Master de Meteorologia. Universitat de Barcelona
- [82] Caccamo MT, Castorina G, Colombo F, Insinga V, Maiorana E and Magazù S, Weather forecast performances for complex orographic areas: Impact of different grid resolutions and of geographic data on heavy rainfall event simulations in Sicily. *Atmos. Res.* 2017; (198): 22-33.
- [83] Castorina G, Colombo F, Caccamo M T, Cannuli A, Insinga V, Maiorana E, Magazù S. Cultural Heritage and Natural Hazard: How WRF Model Can Help to Protect and Safe Archaeological Sites. *International Journal of Research in Environmental Science*, 2017; vol. 3, no. 3: 37 - 42.
- [84] Colombo F, Castorina G, Caccamo M T, Insinga V, Maiorana E, Magazù S. IT Technologies for Science Application: using meteorological Local Area Model to contrast the hydrogeological risks. *Hydrol. Current. Res.* 2017; Volume 8, Issue 4, 1000284
- [85] Castorina G, Caccamo MT, Magazù S. Employment of a Weather Forecasting Model for Yield Photovoltaic Plants Optimization. *SF J Environ Earth Sci.* 2018; 1(1): 1002.

Acknowledgements

The first acknowledgement goes, without any doubt, to the supervisor Prof. Salvatore Magazù, who with availability, patience and kindness has advised me, helped and supported during the entire journey.

A special acknowledgement goes also to the colleagues of the research group with whom I worked in these years, always ready to lend a hand and, above all, lovingly close in moments of discouragement.

I would like to thank the Dipartimento Regionale di Protezione Civile della Regione Sicilia (DRPC) and the Servizio Informativo Agrometeorologico Siciliano (SIAS) for the material provided (maps and meteorological data)

Finally, a special acknowledgement goes to my family, my girlfriend and to true friends who, with their closeness and their immense love, have helped me to overcome the obstacles that life has reserved for me.